Universidade de Aveiro Departamento de Fisica
Ano 2010

MANDEFRO YEHULIE TEFERI

DESENVOLVIMENTOS DE ESTRUTURAS MULTIFERROICAS DE FILMES FINOS DE LIGAS Ni-Mn-Ga E PMN-PT

DEVELOPMENTS OF MULTIFERROIC HETEROSTRUCTURES OF THIN FILM OF Ni-Mn-Ga ALLOYS AND PMN-PT

Universidade de Aveiro Departamento de Física
Ano 2010

MANDEFRO YEHULIE TEFERI

DESENVOLVIMENTOS DE ESTRUTURAS MULTIFERROICAS DE FILMES FINOS DE LIGAS Ni-Mn-Ga E PMN-PT

DEVELOPMENTS OF MULTIFERROIC HETEROSTRUCTURES OF THIN FILMS OF Ni-Mn-Ga ALLOYS AND PMN-PT

A dissertation presented to the University of Aveiro to fulfill the formalities essential to obtain the Master degree in Material Science, carried out under the scientific supervision of Dr. Victor Amaral, Professor in Department of Physics University of Aveiro and co-supervisor Dr. Armando Lourenco, assistant professor in Department of Physics University of Aveiro

Dissertação apresentada à Universidade de Aveiro para cumprimento dos requisitos necessários à obtenção do grau de Mestre em Ciência e Engenharia de Materiais, realizada sob a orientação científica do Doutor Victor Amaral, Professor Catedrático do Departamento de Física da Universidade de Aveiro e co-orientação do Doutor Armando Lourenço, Professor Auxiliar do Departamento de Física da Universidade de Aveiro

Apoio financeiro no âmbito do Programa Erasmus Mundus (EU)

o júri

presidente

Prof. Doutor Florinda Mendes da Costa,
professora Associada do Departamento de Física da Universidade do Aveiro

Prof. Doutor Pedro Manuel de Melo Bandeira Tavares,
professor Associado do Departamento de Quimica da Universidade de Trás-os-Montes e Alto Douro, Vila Real

Prof. Doutor Victor Brás de Sequeira Amaral
professor catedrático do Departamento de Física da Universidade do Aveiro

Prof. Doutor Armando António Cardoso dos Santos Lourenço
professor auxiliar do Departamento de Física da Universidade do Aveiro

agradecimentos

I would like to express my deepest gratitude and appreciation to my supervisor Prof. Vitor Amaral, for allowing me to work in his group, excellent guidance, encouragement, and material support. I gratefully acknowledge him for the discussion we held and all those sparking suggestions and comments he made regarding my work, his patience in correcting my thesis and in every step of my work during my Master study. I benefited a lot from his scientific guidance in every aspect and I appreciate all these invaluable help. I would also like to express the same gratitude to my co-supervisor, Prof. Armando Lourenço, for all invaluable and exciting discussions we held from the beginning to the end the work, providing me materials and encouraging me to work very hard. It was a great honour to learn from him about thin film synthesis and magnetron sputtering deposition system

I would like to thank Dr. Soma Das and Dr. Joao Amaral who helped me a lot during VSM and SQUID measurement

I would like to thank Dr. Dzmitry Karpinski who helped me during MFM and PFM measurement and Dr. Rosario Soarer who helped me during XRD measurement.

I would like to thank Prof. Sobolev and his student Joao Vasco Silvestre Vidal for offering me the opportunity to use magnetoelectric measurement facility and their help during measurement.

My Sincere thanks goes to University of Aveiro.

I would like to thank European Commission (EU) for providing me financial support during my master study in the University of Aveiro.

Finally, I extend my thanks to those who helped me in one way or another to accomplish this work.

palavras-chave ligas ferromagneticas com memoria de forma, Ni-Ma-Ga, magnetoelectrico, multiferroico, filmes finos, pulverização catódica .

resumo

Ligas de forma ferromagnética em sistemas Ni-Mn-Ga são uma classe recente de materiais activos que podem gerar deformações de até 10% induzidas por um campo magnético por um rearranjo de maclas. Esta e outras propriedades físicas destas ligas têm importância tecnológica. Este trabalho investiga as propriedades de filmes finos de ligas de Ni-Mn-Ga sobre diferentes substratos, incluindo substratos activos (piezeléctricos). Para estudar as propriedades de filmes finos da liga, heteroestruturas sob a forma de Ni-Mn-Ga/substrato foram produzidas por RF sputtering com magnetrão utilizando temperaturas de deposição de 320^0C, 370^0C, 400^0C sobre substratos de Al_2O_3, MgO, $SrTiO_3$ e PMN-PT. A influência da temperatura do substrato durante a deposição nas propriedades estruturais e magnéticas de filmes finos foi estudada. Além disso, o acoplamento magnetoeléctrico entre Ni-Mn-Ga como filme fino material ferromagnético e PMN-PT como material piezoeléctrico foi investigada. O efeito magnetoeléctrico foi investigado apenas em filmes depositados a temperatura do substrato de 370^0C e 400^0C. As propriedades estruturais foram estudadas por difração de raios-X, as propriedades magnéticas foram investigadas por VSM, SQUID, e MFM, e o efeito magnetoeléctrico foi estudado por técnica lock-in. A medida estrutural mostrou que os filmes depositados são parcialmente cristalinos e o grau de cristalinidade aumenta como o aumento da temperatura do substrato. Fases austenita e martensita foram observadas nesses filmes. Os resultados da medição magnética mostram que todos os filmes depositados exibem comportamento ferromagnético e o comportamento ferromagnético é favorecido com o aumento da temperatura do substrato. Todos os filmes depositados na temperatura do substrato de 400ºC apresentam temperaturas dev Curie acima da temperatura ambiente: 337K para Ni-Mn-Ga/PMN-PT, 345K para Ni-Mn-Ga/STO e 348K para Ni-Mn-Ga/Al_2O_3. Nenhuma evidência separada de temperatura de transição estrutural foi observada para nos filmes. Os resultados das medições magnetoeléctricas mostram que as heteroestruturas multiferróicas Ni-Mn-Ga/PMN-PT apresentam efeito magnetoelétrico. O valor máximo medido para a tensão magnetoeléctrica induzida para filmes depositados à temperatura do substrato de 370^0C e 400^0C são 3.16mV/cmOe e 3.02mV/cmOe, respectivamente.

keywords

Ferromagnetic shape memory alloys(FMSAs), Ni-Mn-Ga, Magnetoelectric, multiferroic, thin film, sputtering.

abstract

Ferromagnetic shape memory alloys (FSMAs) in Ni-Mn-Ga systems are a recent class of active materials that can generate large magnetic field induced strains up to 10% by twin rearrangement. This and other physical properties these alloys have many technological importance. This work investigates the properties of Ni-Mn-Ga alloy thin films on different substrates including active substrate (piezoelectric). To study the properties of thin films of the alloy, the heterostructures in the form of Ni-Mn-Ga/substrate were produced by RF magnetron deposition system using substrate deposition temperatures of 320^0C, 370^0C, and 400^0C, where the substrates used were Al_2O_3, MgO, $SrTiO_3$ and PMN-PT. The influences of deposition substrate temperature on structural and magnetic properties of sputtered thin films on the aforementioned substrates were studied. Moreover, magnetoelectric coupling between Ni-Mn-Ga thin film as ferromagnetic material and PMN-PT as piezoelectric material was investigated. The magnetoelectric effect was investigated only on films deposited at substrate temperature of 370^0C and 400^0C. The structural properties were studied by x-ray diffraction, magnetic properties were investigated by VSM, SQUID, and MFM, and the magnetoelectric effect was studied by lock-in technique. The structural measurement has shown that as-deposited films are partially crystalline and degree of crystallinity increases as substrate temperature increase. Austenite and martensite phases have been observed in these films. The magnetic measurement results show that all films as-deposited display ferromagnetic behaviour and ferromagnetic behaviour improvements are observed as substrate temperature increases. All films deposited at substrate temperature of 400^0C exhibit Curie temperatures above room temperature which are 337K for Ni-Mn-Ga/PMN-PT, 345K for Ni-Mn-Ga/STO, 348K for Ni-Mn-Ga/Al_2O_3. No separate signature of structural transition temperature was observed for all these films. The magnetoelectric measurement results show that a heterostructure of Ni-Mn-Ga/PMN-PT multiferroic exhibit magnetoelectric effect. The measured maximum induced magnetoelectric voltage for films deposited at substrate temperature of 370^0C and 400^0C are 3.16mV/cmOe and 3.02mV/cmOe, respectively.

LIST OF FIGURES

LIST OF TABLES

1 Introduction

It is known that functional magnetic and electronic materials form an important part of modern technology. For instance, ferroelectric materials (materials with spontaneous electric polarization that can be switched by applied electric field) are widely used as tunable capacitors and ferroelectric random access memory (FRAM) in computers. On the other hand, ferromagnetic materials (materials with spontaneous magnetic polarization that can be switched by magnetic field) are used in hard disk drive, in data recording and storing. However, the current technological trend is towards device miniaturization, which led to an ever-increasing interest in combining of several order parameters (ferroelectric, ferromagnetic, and ferroelastic) in to multifunctional materials to produce a single device component that can perform more than one task. What is known as multiferroic materials are materials that possess at least two or more order parameters that can have potential applications in such multifunctional device. These materials not only have their parent compounds property but also they cross-interact between magnetic and electric order which leads to additional functionalities.

From the view point of constituent materials, multiferroics can be divided in to two types: single phase [1, 2] and composite [3, 4]. Single phase multiferroic materials are materials having at least two of the ferroic orders in a single phase while composite multiferroic are those materials having ferroic orders in multiphase. In a two phase composite multiferroics the order parameters exist separately in the two phase (e.g. ferromagnetic order in ferromagnetic phase and ferroelectric order in ferroelectric phase). The coupling interaction between different order parameters could produce a new effect. The magnetoelectric (ME) response is the appearance of electric polarization up on applying magnetic field (i.e. direct ME effect) and/or the appearance of magnetization by up on applying electric field (i.e. converse ME effect). Magnetoelectric effect may arise directly between two order parameters (ferroelectric and ferromagnetic) as in single phase multiferroic, or indirectly via stress/strain as in multiferroic composite heterostructures. It is known as a product tensor property in composite multiferroics. In the case of single phase for most materials, the magnetoelectric effect is observed far below room

temperature and the magnetoelectric output is low. This limits their application in practical devices. However, ferro/ferromagnetic and ferro/piezoelectric composite or nanostructured composites may reveal magnetoelectric coupling several hundred of mV/cm Oe [3, 5] stronger than single phase materials.

As outlined by Boomgaard et al. [6], high ME output can be obtained if the composite fulfils certain requirements. These requirements are: two phases should be in equilibrium, no chemical reaction between piezoelectric and magnetic phase, the Magnetostriction coefficient of magnetic phase and piezoelectric coefficient of piezoelectric phase must be high, and the resistivity of both phases should be high so as to avoid a leakage path of the accumulated charges during poling and proper poling strategy should be adopted to get a large ME effect in composite.

The search for combination of ferromagnetic and piezoelectric materials that can give high magnetoelectric output is a hot ongoing area of research. Various composites have been reported in literature Ni (Co, Mn) Fe_2O_4-$BaTiO_3$ [6], $Ni_{0.93}Co_{0.02}Mn_{0.05}Fe_{1.95}O_4$-$Na_{0.5}Bi_{0.5}TiO_3$ [7], $Ni_{0.98}Co_{0.02}Fe_2O_4$-PZT [8], Terfenol-D/lead magnesium niobate-lead titanate (PMN-PT) [9], and so on.

Ferromagnetic shape memory alloys (FSMAs) are known to have high magnetic field-induced strain. As a result they are promising candidates to be used as magnetic material in the multiferroic composite (ferromagnetic/piezoelectric structure). Since these alloys have ferromagnetic and structure orders, they can be changed from ferromagnetic state to paramagnetic state or from one phase to another phase by changing magnetic field and temperature. Among the known FSMAs, Ni-Mn-Ga alloys have received a considerable interest and they have high magnetostriction coefficient which is one of the requirement to be fulfilled in multiferroic composite [10]. The additional advantage of these alloys is their properties like magnetization, Curie temperature, and martensite structural transitions which are composition dependent opening a room to change their properties by changing their composition.

Many bulk ME composites have been found to exhibit such a stained mediated ME effect above room temperature. However, multiferroic ME structured films, in comparison with bulk ME composite, have some unique advantages. For example, piezoelectric phase and

magnetic phase could be tuned and controlled at the nanoscale, representing a new scale for exploring ME coupling mechanisms. The bond between the two phases at interface in bulk is usually loss while at nanoscale different phase can be combined at atomic level which leads to reduce interface loss significantly. Availability of new approaches or developments on thin film growth techniques provides the opportunity to produce high quality thin films in thin film ME composites. Moreover, the growth technique allows in producing ferroelectric oxides (or their solid solution) with large piezoelectric properties like PMN-PT. Thus, by combining different phases with similar crystal lattices, epitaxial composite thin films can be designed, which facilitates the understanding of ME coupling at the atomic scale. Multiferroic ME thin films are therefore promising candidates for use in integrated magnetic/electric devices, such as sensors, micro-electromechanical systems, high density memories and spintronics [2, 3, 11].

In this work, Ni-Mn-Ga alloy thin films as magnetic material and single crystal PMN-33PT as piezoelectric material for substrate were used. In addition, other substrates like Al_2O_3, $SrTiO_3$, and MgO were used for comparison purpose. These materials (the alloy and PMN-PT) were selected because of their good property to be used in ME composites: PMN-33PT because of its superior piezoelectric property and Ni-Mn-Ga alloy because of their large magnetic field-induced strain. Using sputtering deposition, the compositions of the alloys were tailored by using different deposition conditions to achieve the required properties to be used in ME composite. The required properties are high saturation magnetization value, structural, and ferromagnetic transition temperatures above room temperature so that the Ni-Mn-Ga alloys thin films are ferromagnetic martensite at room temperature.

This thesis is organized in to five chapters. A brief overview of general concepts of ferroelectric and ferromagnetic materials and their description is given in the first chapter of this thesis. Moreover, about properties of shape memory alloys and ferromagnetic shape memory alloys, compositional dependence of structural and magnetic properties of Ni-Mn-Ga alloys, and the interaction of ferroelectric and ferromagnetic materials in magnetoelectric multiferroic are discussed in this chapter. The second chapter of this thesis presents a brief discussion about the sputtering deposition technique. It also includes

experimental deposition conditions, type of substrates used to deposit Ni-Mn-Ga films. The third chapter includes a brief description of all the characterization techniques used in this work. These techniques are x-ray diffraction to study phase (or structure) of the Ni-Mn-Ga alloy thin films; Vibrating Sample Magnetometer (VSM), Super Conducting Quantum Interference (SQUID) Magnetometer, and Magnetic Force Microscopy (MFM) to study the magnetic property of the film; and Lock-in technique to study the magnetoelectric coupling. The fourth chapter presents the results and discussion part of the thesis. It includes the results of structural, magnetic, and magnetoelectric coupling and their discussions. Finally, the fifth chapter includes the conclusion of the work and outlook for further study.

1.1 Piezoelectricity

Piezoelectricity was first discovered by Jacques and Pierre Curie in certain crystals such as quartz, zinc blend, and Rochelle salt (Potassium-sodium tartrate-tetrahydrate, KNaC4H4O6.4H2O) [12]. Since then, it is a term used to describe the ability of materials to generate electricity (or electric charge) when mechanical stress is applied it. These materials can also exhibit the converse effect, produce deformation (strain) when electric field is applied. Figure 1.1 below shows the direct piezoelectric effect in the left, tensile or compression stress produce polarization and converse Piezo-effect in the right, electric field produce strain. For the occurrence of piezoelectric effect, the material should lack a center of symmetry.

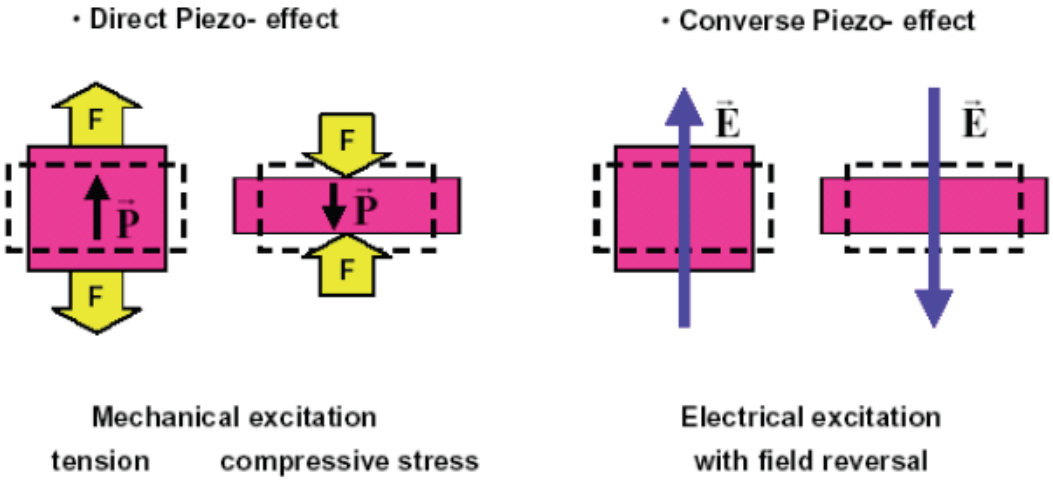

Figure 1. 1 Direct and converse Piezo-effect [13].

It is know that on basis of the symmetry of elements of translational position and orientation, there are 230 space groups. However, without considering translational repetition, these 230 space groups reduce to 32 space groups among which 21 of them are noncentrosymmetric point groups and 11 of them are centrosymmetric. Thus, 20 noncentrosymmetric groups possess piezoelectricity while centrosymmetric groups do not. As shown in the Figure 1.2 below, the 21 noncentrosymmetric classes can be further divided in to one class which posses other combined symmetry elements, 10 classes which can be polarized by mechanical stress and other 10 classes which possess spontaneous polarization, so they can be permanently polar and can thus have piezoelectric as well as pyroelectric (generation of electricity from heat or its converse, generation of heat from change of the state of polarization) effects. In other words, ferroelectric materials belong to pyroelectric family, which in addition has a spontaneous polarization that can be reversed by the external electric field, i.e. it has more than one equivalent direction for spontaneous polarization. Thus, it is clear that a ferroelectric material must be simultaneously Piezoelectric and Pyroelectric material.

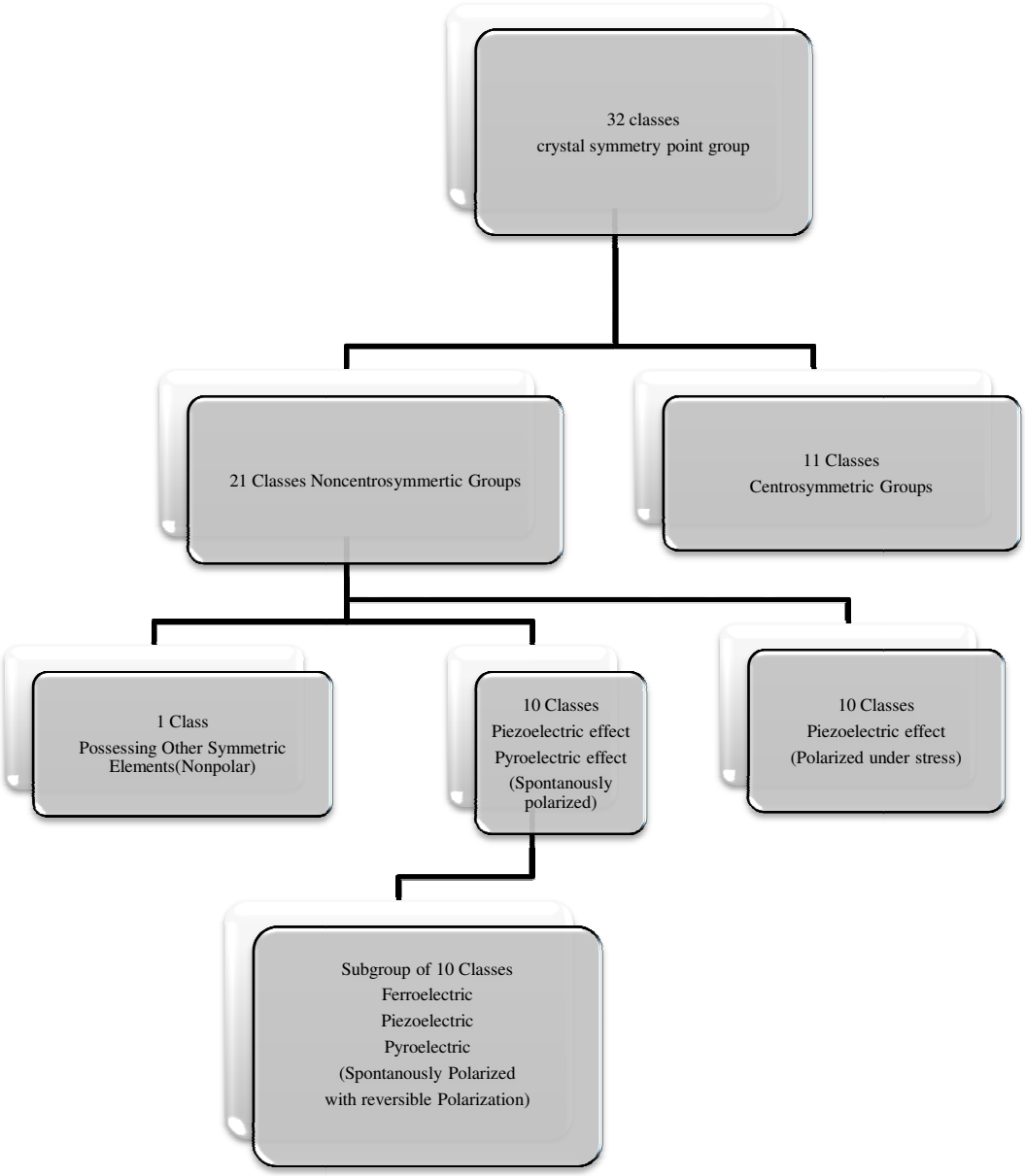

Figure 1. 2 Classification of crystals showing the class with piezoelectric, pyroelectric, and ferroelectric effects

When an electric field is applied on materials, there is a second order phenomenon which is known as Electrostriction that refers to the ability of these materials to deform under this electric field. In general, if an insulating crystal is subjected to both elastic stress and electric field [14], then its deformation is given by

$$x_{ij} = s_{ijkl}X_{kl} + d_{mij}E_m + M_{mnij}E_mE_n, \quad (1.1)$$

where x_{ij} are components of elastic strain tensor, s_{ijkl} is elastic compliance tensor, $X_{kl}$are the stress component, d_{mij} are piezoelectric tensor component, M_{mnij} is the electrostrictive tensor, E_m and E_n are the components of an external electric field. The Electrostriction effect for most practical cases is extremely small or negligibly thereby equation 1.1 can be reduced to

$$x_{ij} = s_{ijkl}X_{kl} + d_{mij}E_m. \quad (1.2)$$

Under zero stress, the converse piezoelectric effect deformation as shown in the right side of Figure 1.1 can be written as

$$x_{ij} = d_{mij}E_m. \quad (1.3)$$

On the other hand, the direct piezoelectric effect shown on the left side of Figure 1.1 can be written mathematically as

$$P_m = d_{mi}X_i, \quad (1.4)$$

where P_m is the component of electric polarization.

Since ferroelectricity is very fascinating properties of single or polycrystalline dielectric solids, it is good to discus at this point general features of ferroelectric phenomena. Ferroelectric crystals show a reversible spontaneous electric polarization and a hysteresis loop that can be observed in certain temperature regions, delimited by a transition point called Curie temperature, T_c. At temperature above T_c, the crystal is no longer ferroelectric, instead it exhibits normal dielectric or paraelectric behavior. These ferroelectric crystals have anomalously high dielectric constant especially near the Curie temperature. The dielectric constant increases very rapidly to a peak value at T_c. At any temperature greater than Curie temperature, the dielectric constant is given by Curie-Weiss relation

$$\varepsilon_r = \frac{C}{T - T_C}, \quad (1.5)$$

where C is Curie constant. Below and above T_c, the response of ferroelectric material to an applied electric field is not similar. Below T_c a typical non linear variation of polarization with electric field is found as shown in the Figure 1.3 below. As it is shown, in a typical hysteresis loop for small electric field, the polarization is nearly

linear (from 1 to 2). This is due to the fact that the field is not large enough to cause orientation of the polarization of domains.

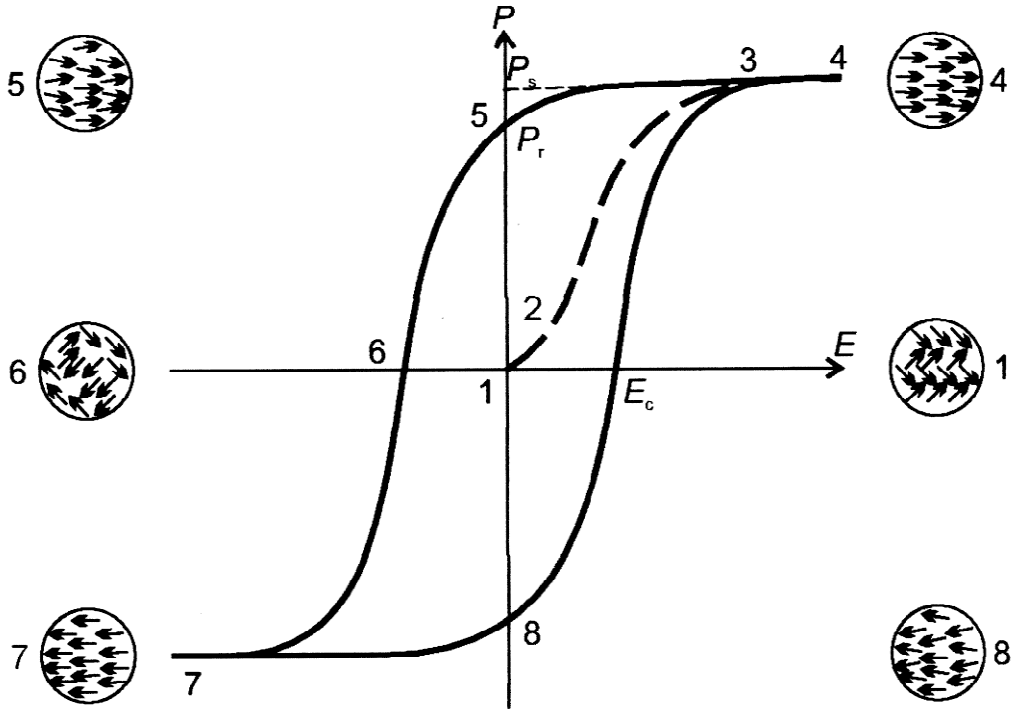

Figure 1. 3 Typical Hysteresis loop of ferroelectrics [15].

At higher fields, polarization increases nonlinearly as the field increases, since all domains, which have a polarization directed differently from field direction, start to orient toward the direction of the field (nearly from 2 to 3). Further increase of the field above coercive field, E_c, (from point 3 above), will lead to saturation value of polarization (P_s) and the sample will be mono domain. Now if the field starts to decrease, the polarization generally decreases but will not be zero or does not follow the same path. At zero electric field the material will have a polarization called remnant polarization, P_r. Usually P_r is smaller than P_s, since some domains may return to their original position or a direction different from their direction at point 4. This process, switching of all domains in to a single orientation, is called poling. To reverse the orientation of this polarization, an electric field in opposite (or negative) direction should be applied and the complete

hysteresis loop looks like as shown in the above figure. Indeed, the shape of the hysteresis and the values P_r, P_s and E_c for a given material depend on the temperature.

Ferroelectric materials

Among four possible types of structures of ferroelectric materials, the most extensively studied and widely used structure in practical application is the perovskite structure. A general formula for a perfect perovskite structure is ABO_3, where A is a divalent or trivalent metal cation and B is tetravalent or trivalent metal cation. The ideal structure of the perovskite structure is with a spacial group Pm-3m. The larger A cations occupy the corners of the cube while the smaller B cations occupy at the body center and oxygen ions occupy at the face center position. For example, $BaTiO_3$ is a well known ferroelectric and piezoelectric with distorted perovskite structures. The tetravalent Ti^{+4} ions occupy the B site of the $BaTiO_3$ perovskite structure and are surrounded by O^{-2} in octahedral configuration.

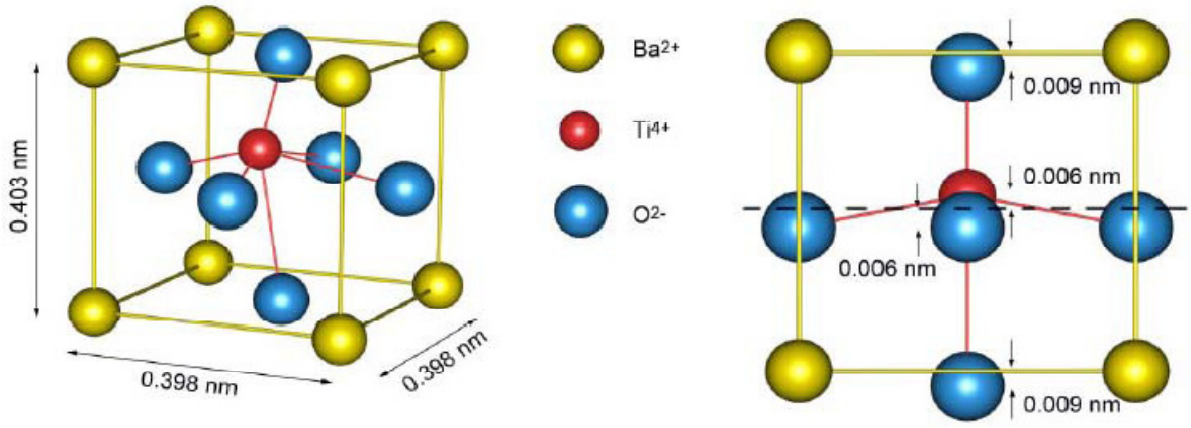

Figure 1. 4 $BaTiO_3$ unit cell showing displacement of Ti^{+4} and O^{-2} and viewing from one face [16].

At a temperature $T > T_c$, although the open octahedral structure allows Ti^{+4} ion to move from one position to another position, there is no net dipole moment. This is due to random thermal vibration of Ti^{+4}. In this cubic structure, the material is paraelectric. However, when the temperature $T < T_c$, the structure changes from cubic to tetragonal due to the displacement of Ba (A) and Ti (B) ions with respect to O ions as shown in the Figure 1.4. This gives a net dipole moment (spontaneous polarization). At lower temperature a sequence of phase transformation is found in $BaTiO_3$: from tetragonal to orthorhombic

with a <110> spontaneous polarization, and from orthorhombic to rhombohedral with spontaneous polarization <111>. The spontaneous polarization direction is coupled to lattice structure through electrostriction and the differential of electrostrictive strain over applied field gives rise to piezoelectricity. In Perovskite family, it is not only Titanium cation but a large number of cations can be accommodated in the cages created by oxygen anions which gives rise to wide varieties of materials. Moreover, substitution of A and B cation perovskite lattice sites is possible without drastically changing the perovskite structure. Thus, it is possible to manipulate properties of materials such as Curie temperature, piezoelectric constant, coercive field and so on which are much desired from technological point of view. Among many functional materials with perovskite structures, lead based and other materials such as Lead Titanate ($PbTiO_3$-PT), Lead Zirconate Titanate (PZT), Lead Lanthanum Zirconate Titanate (PLZ), Lead Magnesium Niobate (PMN), Strontium Titanate ($SiTiO_3$-ST), Potassium Niobate ($KNbO_3$-KN), Potassium sodium Niobate (K_xNa_{1-x} TiO_3-KNT), are some of technologically important materials [17]. It is also possible to produce solid solution of these compounds and control their macroscopic properties. PMN-PT is the solid solution of PMN and PT. The properties of PMN-PT can be tailored by varying the composition of the alloying compound (or value of x in (1-x)$Pb(Mg_{1/3}Nb_{2/3})O_3$-x$PbTiO_3$) [18]. M.H. Lente et al. have studied the effect of composition (or x) on PMN-PT material for instance on their structural and coercive electric fields [18]. This relaxor is known to have excellent ferroelectric properties. In this work, it was used as a single crystal substrate for ferromagnetic thin film of alloy of Ni-Mn-Ga.

1.2 Ferromagnetism

Ferromagnetism is a phenomenon used to describe materials which possess spontaneous magnetization. The Spin of electron together with Pauli principle is the physical origin of ferromagnetism. Atoms with partially filled shells and with unpaired electron can exhibit a net magnetic moment in the absence of external field. Ferromagnetic materials, unlike paramagnetic materials, have magnetic atoms which interact with each other due to molecular field or exchange interaction and, they try to align each other along the same

direction as shown in the Figure 1.5 a below. This interaction is dominant up to certain temperature

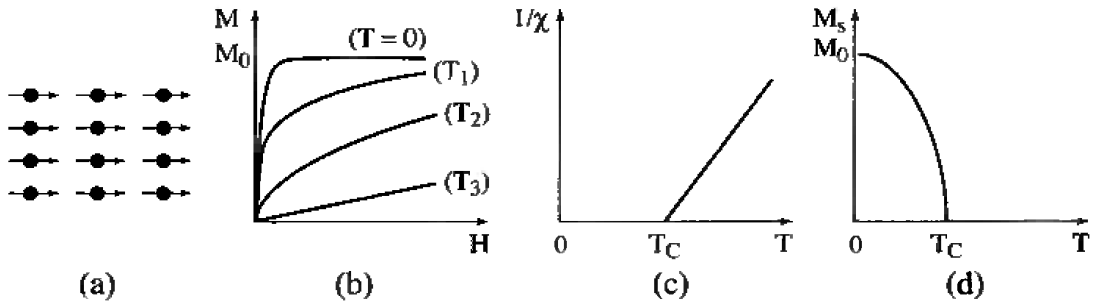

Figure 1. 5 Ferromagnetism (a) spin lattice , (b) Magnetization versus magnetic field, (c) temperature dependence of $^{1}/_{\chi}$, and (d) spontaneous magnetization versus temperature [19].

called Curie temperature, T_c. However, above Curie temperature the thermal agitation (or energy) overcomes this interaction and the magnetic moments orient in random fashion which results material to behave like paramagnetic materials. The susceptibility of ferromagnetic materials becomes infinity at Curie temperature instead of being infinity at temperature of 0 K and the inverse of susceptibility increases linearly for any temperature greater than Curie temperature as shown in Figure 1.5 (c). Because of parallel alignment of moments the material possesses spontaneous polarization (or magnetization) below the Curie temperature. As shown in Figure (b) and (d) the spontaneous polarization increases as the temperature decrease and it reaches maximum value at 0 K. At 0 K all moments align in the same direction.

Even though, ferromagnetic materials with Curie temperature above room temperature have spontaneous polarization at room temperature, they may not show up a magnetic moment with north and south poles (or they may not have global magnetization) at room temperature. If a ferromagnetic material is in such state, it is said to be in demagnetized state. This paradox was explained by Pierre Weiss through the formation of structures what he called domains which are separated by domain walls. Each domain contains large number of atoms with their atomic moments pointing in the same direction (along the easy axis of magnetization) which locally give spontaneous magnetization for each domain, for example, as shown in the Figure 1.6 (a). Since the directions of local spontaneous magnetization of domains are randomly oriented, the vector sum of the magnetizations of

all domains of the entire specimen is zero. However, it is possible to magnetize the material by applying an external magnetic field which modifies the distribution of domains. Consider a ferromagnetic material with a very simple domain structure as shown in Figure 1.6 (b). When an external magnetic field is applied to the material, the increases of total magnetization of the material occur in two stages. In the first stage when the applied magnetic field is small, domain whose magnetization vector is closest to the field direction grows at the expense of that with less favorably oriented. In the second stage (at large magnetic fields) the magnetization involves the rotation of domain magnetization vectors away from the easy axis of magnetization. After the two stages saturation magnetization will be maintained.

Figure 1.6 (c) shows the plot of magnetization versus magnetic field for ferromagnetic materials. As it can be seen from the figure after saturation magnetization has been maintained, the original magnetization curve is not retraced if the applied field decreases; instead the magnetization remains at higher value than expected for a particular field value give rise to the phenomenon of the magnetic hysteresis. At the value of zero field, the material has a magnetization value, called remnant magnetization (M_r), which is lower than that of the saturation magnetization value. To return the magnetization of the material to zero, a field H_c has to be applied in opposite direction to the initial applied field. This field, called coercive field, causes the domains to return back to their original position and the material to its demagnetized state.

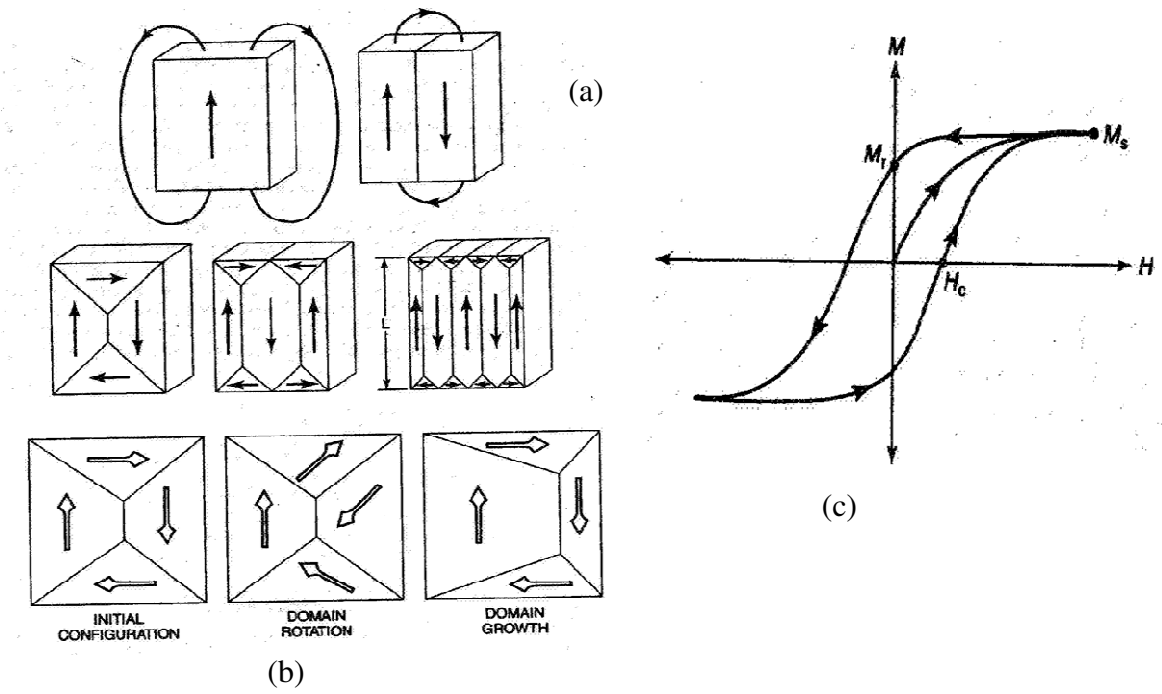

Figure 1. 6 (a) some example of domain structure, (b) change in domain structure with applied field, and (c) plot of the magnetization versus applied field [20].

1.2.1 Magnetostriction

Magnetostrictive materials are a class of smart materials that can convert between magnetic and elastic states. Magnetostrictive materials are similar to ferromagnetic shape memory alloys (FMSAs) in that both of them show stain when they are exposed to magnetic fields and produce magnetization when stress is applied. However, the straining mechanisms for both materials are not the same. In the case of Magnetostriction materials, straining mechanisms occurs due to spin-orbital coupling or the interaction between the spin and the orbital motion of each electron. When external field is applied to Magnetostrictive materials, the spin tries to orient to the direction of the field and the orbit of that electron also tends to be reoriented. As a result, there will be considerable distortion of crystal lattice which produces large macroscopic stain [21]. To illustrate the straining mechanism clearly, consider a Magnetostrictive material which is pre-compressed in order to magnetize as shown in the Figure 1.7 below. When voltage is applied to the coils to produce magnetic field, the produced magnetic field along the longitudinal

direction changes the orientation of the dipole moments along the field. This re-orientation of the moments generates stain and the plot of

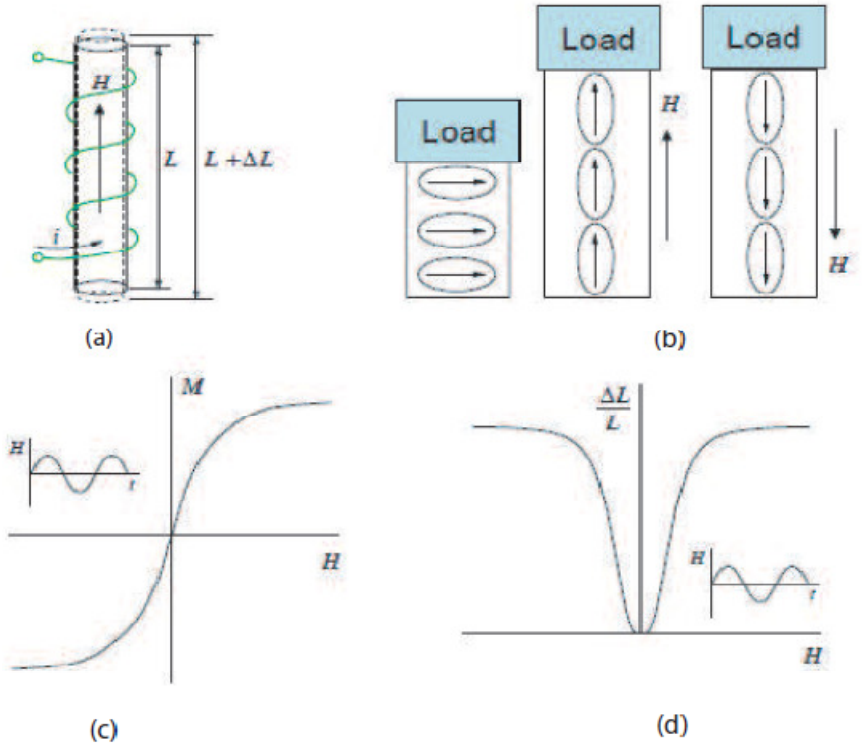

Figure 1. 7 Joule Magnetostriction produced by magnetic field. (a) Magnetic field (H) is proportional to the current in the solenoid when voltage is applied to it, (b) the rotation of magnetic dipoles change the length of the sample, (c) M versus H and (d) $\Delta L/L$ versus H [21].

stain $\Delta L/L$ versus the field looks like butterfly shaped which is proportional to the square of magnetization curve as shown in the bottom part of the figure. The magnetization direction can be changed to its original direction either by applying external magnetic field or stress. For instance, applying magnetic field perpendicular to the longitudinal direction can change the magnetization to its original direction. Moreover, such Magnetostrictive materials respond to an external stress by changing magnetization orientation which can be detected by measuring the induced voltage in a pickup coil. Some example of mgnetostrictive materials in addition to Ni-Mn-Ga alloys are Terfenol-D, Fe, Ni, Co and others. For kwon ferromagnetic materials for instance Fe and Ni, the strains associated to magnetostriction are of the order of $10^{-4}\%$ while exceptional large magnetostriction, for example Terfenol-D alloy, shows the strain of order of 0.1% [22].

1.2.2 Shape memory Alloys (SMAs)

Since behavior of Ferromagnetic shape memory alloys (FMSAs) such as Ni-Mn-Ga is similar to the behavior of shape memory alloys, it is relevant to review the properties or behaviors SMAs to understand the behavior of Ni-Mn-Ga FMSAs. The traditional shape memory alloy effect was originally discovered in a Au-Cd alloy in 1951. Later, in 1963, the effect was also observed in Ti-Ni alloys which exhibit a prominent shape-memory performance [23]. Since then because of interest in smart materials (used as sensors and actuators), research on shape memory alloys became very active.

It is known that SMAs have two phases each with different crystal structure and therefore they have different properties. One is high temperature phase called austenite (A) and the other is low temperature phase called martensite (M). Austenite has a cubic structure and martensite have tetragonal, orthorhombic or monoclinic structure. The transformation from one structure to the other does not occur by diffusion of atoms rather by shear lattice distortion. Such transformation is known as martensite transformation. Martenstic crystal structure can have structures with different orientation called variants and these variants can exist in two forms called twinned (left bottom) and detwinned (right bottom) as show in the Figure 1.8 below. When the material is cooled from high temperature austenite (called forward transformation) in the absence of applied load,

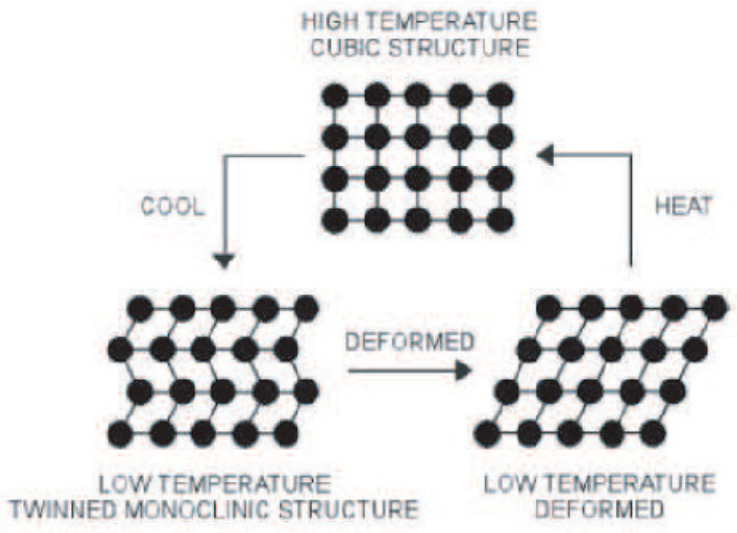

Figure 1. 8 SMA transformation between high and low temperature transformation [24].

the twinned Martenstic structure is formed. At low temperature when stress is applied to the material, the twins reorient so that they all lie in same direction and this process is called detwinning. When the material is heated from detwinned martensite phase, the crystal structure transforms back to austenite phase and this transformation is called reverse transformation. The material finally remembers its original shape for this reason the effect is known as shape memory effect.

The transformation from one phase to another follows hysteresis loop as shown in the Figure 1.9 below.

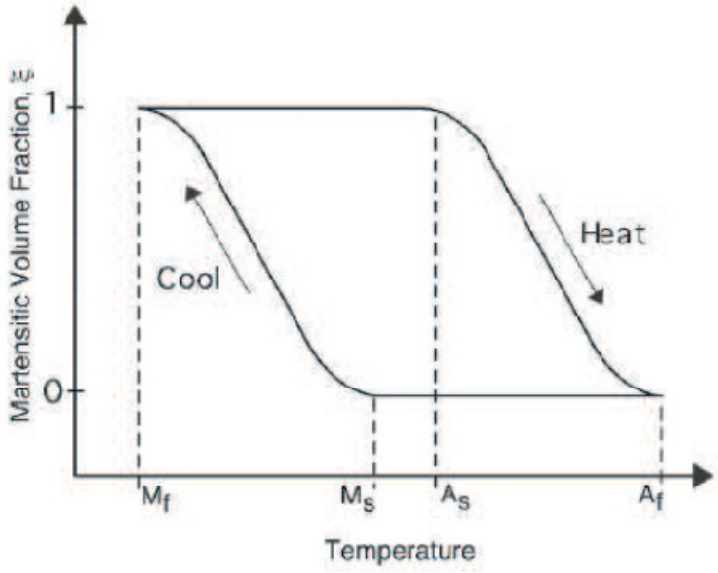

Figure 1. 9 Schematics of phase transformation [24].

Suppose that ξ is the amount of volume fraction of martenstic phase in the material. Then $1-\xi$ will be volume fraction of austenite phase. There are four characteristics temperature associated with phase transformation. During the forward transformation, without load the austenite begins to transform at Martenstic start temperature (M_s) and completes transformation to martensite at martensite finish temperature (M_f). Above M_s $\xi = 0$ and below M_f $\xi = 1$ and the transformation is complete and then the material is fully in the twinned structure. Similarly, during heating, the reveres transformation starts at austenite start temperature (A_s) and finishes at the austenite finish temperature (A_f). Below A_s $\xi = 1$ and above A_f $\xi = 0$.

Phase transformation can also be induced through applied loads. Figure 1.10 below shows the stress-strain curves at a temperature below M_f and at a temperature above A_f. Consider first for any temperature less than the martenstic finish temperature (M_f), the stress-strain curve is shown in Figure 1.10 (a). When the twinned structure is subjected to an external stress lower than the detwinning start stress (σ_s) (the minimum stress required for detwinning initiation), the material shows an elastic behavior (region from O to A). In the region between A and B, the reorientation process starts which will result in the growth of certain favorably oriented Martenstic variants that grow at the expense of other less favorable variants. The detwinning of martensite process completes at a stress level called detwinning finish stress (σ_f). After detwinning process is completed (in the region between B and C), the material again deforms elastically. Increasing the stress

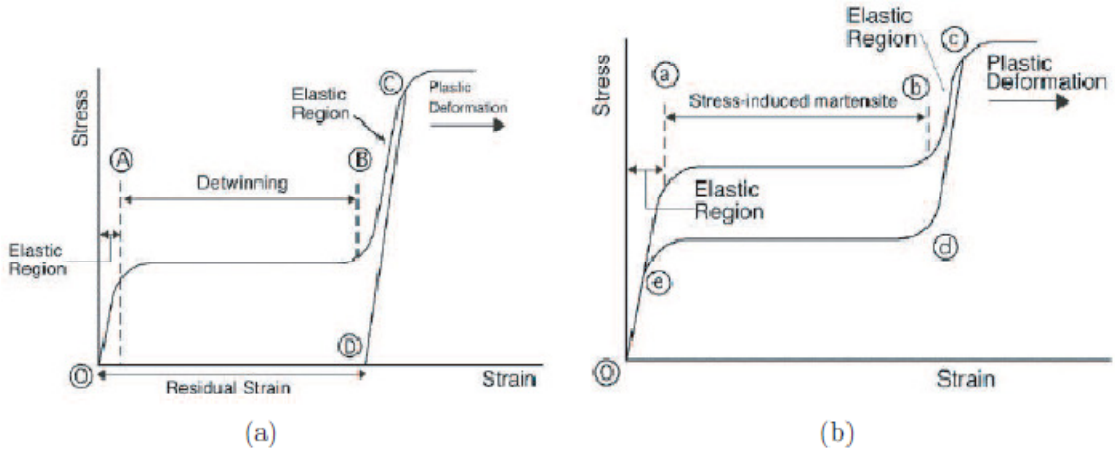

Figure 1. 10 Stress-strain behavior of shape memory alloys for (a) below M_f and (b) above A_f [24].

further above C deforms the material plastically. When the material is unloaded in the region between C and D, the material does not come back to its original shape rather there will be residual strain. Only the elastic deformation is recovered. However, the residual strain can be recovered by heating the material above A_f and allow it to cool.

For any temperature above the austenite finish temperature (A_f), the stress-strain curve is shown in Figure 1.10 (b). In the region between O and a, the material exhibits a linear stress-strain relation as the stress is increased until σ_M (the stress at which the detwinned martensite phase commences). In the region between a and b, stress-induced martensite is formed and this region is followed by elastic region (region b and c). Further increasing

the stress beyond c deforms the material plastically. Up on Unloading (from c to e), the stress-induced martensite goes through elastic unloading, which is followed by the transformation to the austenite phase. Finally the material returns to its original phase and shape. This behavior is known as supperelasticity. For shape memory alloy effect, temperature and stress are responsible for the phase transformation. The order of magnitude of this effect is 10^{-1} [25].

1.2.3 Ferromagnetic Shape Memory Alloys (FMSAs)

Ferromagnetic shape memory alloys (FSMAs) was first discovered by Ullakko et al. in 1996 [26] as a hypothetical new class of active materials up on the observation of a 0.2% magnetic field-induced strain in a single crystal of Ni_2MnGa. This class of materials shows up to 10% magnetic field- induced strain [27] which is higher than the strain that can be obtained from magnetostrictive materials. Not only the values of strains obtained are different from magnetostrictive materials but also the straining mechanisms.

Various alloys such as Nickel-manganese-gallium (Ni-Mn-Ga), iron-palladium (Fe-Pd), Co-Ni-Ga, La-Sr-CuO_4 and cobalt-nickel-aluminum (Co-Ni-Al) show ferromagnetic shape memory effect. Among these alloys Ni-Mn-Ga is the most studied FSMA, which is also commercially available. Many studies have been conducted on off-stoichiometric Ni-Mn-Ga that demonstrated larger strains at higher temperatures. Studies conducted by Tickel and James on $Ni_{51.3}Mn_{24.0}Ga_{24.7}$ [28] at temperature of -15^0C which was exposed to fields of less than 10Oe showed strains of up to 0.2% due to cyclic application of an axial field magnetic field and strains 1.3% when fields were applied transverse to rod shape of sample that started from a stress biased state. For Ni-Mn-Ga alloys, theoretically strains up to 6% for tetragonal martensitic structure with five-layered (5M) and 10% for seven-layered (7M) can be obtained which of course makes these materials as attractive materials.

The basic requirements for the appearance of the ferromagnetic shape memory effect are the material should be (ferro) magnetic and exhibit martensite transformation and the magnetic anisotropy energy must be higher than the energy required to move a twin boundary. Moreover, from the point of view of practical applications the material should be in the martensitic phase at room temperature. Since Ni-Mn-Ga alloys have shown these properties, they are the most promising materials for practical application. This work is

concerned on thin film of Ni-Mn-Ga alloys; most of the discussions will be on these alloys, even though most of the discussions are also valid for other alloys too.

1.2.4 Ni-Mn-Ga Crystal structure

The stoichiometric Ni_2MnGa alloy is an intermetallic compound that displays Heusler structure. At high temperature, Ni_2MnGa in particular or Heusler alloys in general exhibit cubic austenite structure ($L2_1$, $Fm\bar{3}3$) as shown in the Figure 1.11 (a) below. The eight Ni atoms are located at the center of each of the eight cubic sub-units while Ga and Mn atoms are located on the remaining sites. At low temperature, it exhibits a martensite tetragonal (l4/mmm) structure as shown in the Figure 1.11 (b) below. This compound not only show martensite transformation but also shows paramagnetic/ferromagnetic transition with Curie temperature of 373K [29, 30]. The martensite structure is usually described as a face centered tetragonal cell related to austenite cubic $Fm\bar{3}3$ by a simple contraction along the c-axis forming a tetragonal structure with a relation $\frac{c}{a} < 1$. In this case the maximum theoretical strain that can be obtained is then given by

$$\varepsilon_{max} = 1 - \frac{c}{a}. \tag{1.6}$$

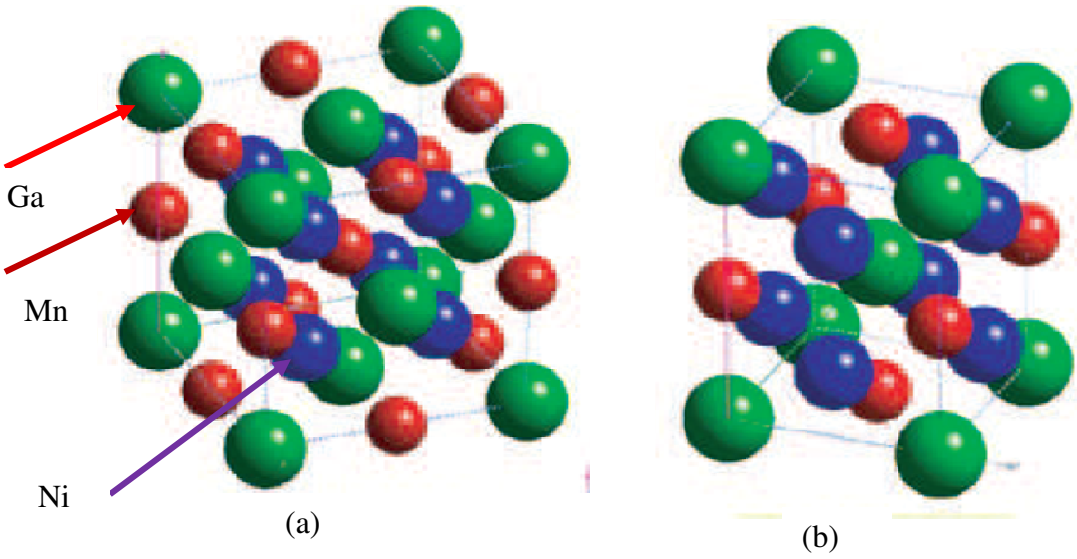

Figure 1. 11 Ni-Mn-Ga crystal structure (a) Cubic Heusler structure, (b) tetragonal structure under martensite finish temperature. Blue: Ni, Red: Mn, Green: Ga.

Most commonly observed value of $\frac{c}{a}$ ratio is 0.94 in which maximum strain of 6% can be obtained. However, as the composition deviates from the stoichiometric the martensite structure begins to change as well. For example, tetragonal and orthorhombic have been found for Ni-rich compositions [31]. In other way round, the ratio $\frac{c}{a}$ is also composition sensitive.

In martensite phase with tetragonal structure, there are three possible variants in which two of them are identical with respect to the axis of the samples. For convenience a simple representation of these crystal structures are show in the Figure 1.12 below. The undeformed austenite phase has cubic edge length of a_0 whereas the tetragonal structure has a short and two long edge length of c and a_0, respectively.

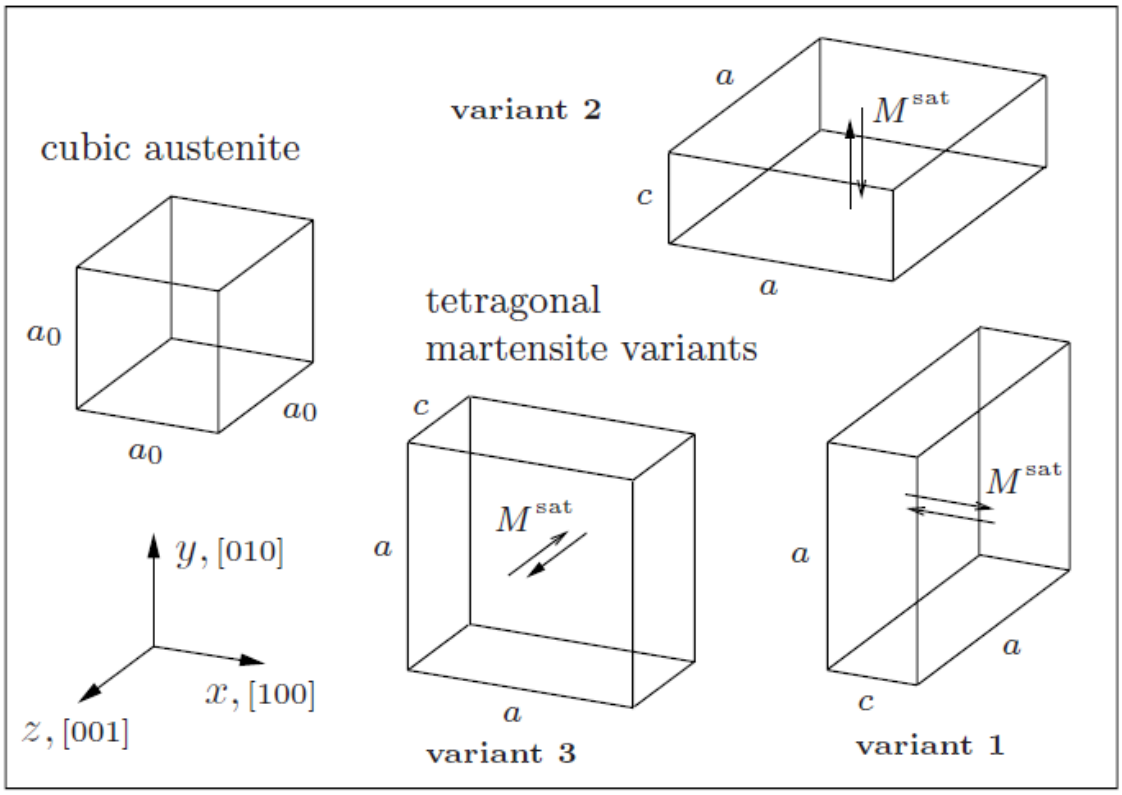

Figure 1. 12 The crystal structure of austenite and tetragonal variants. The arrows in the variants are used to show the magnetization direction along the easy axis of the variants [32].

1.2.5 Straining Mechanisms of FSMAs

One of the requirements for Ni-Mn-Ga alloys in particular and ferromagnetic shape memory alloys in general to show ferromagnetic shape memory effect is the material should have large magnetic anisotropy. Martensite structure of off-stoichiometric Ni-Mn-Ga typically shows strong magnetocrystalline anisotropy. The simplest and most commonly observed magnetic anisotropy is uniaxial anisotropy in which magnetization vector align along the easy axis of magnetization in the absence of magnetic field as shown in the Figure 1.12 for different variants. In this case the magnetic anisotropy energy for the tetragonal martensite is given by

$$U_a = K_{u0} + K_{u1} sin^2\theta + K_{u2} sin^4\theta + \cdots \quad , \tag{1.7}$$

where θ is the angle between the easy axis of magnetization and magnetization vector, and K_{ui} are the magnetic anisotropy coefficients (measure of energy required to rotate the magnetization to align with the field direction away from the easy axis). If this energy is large enough to align the magnetization vector along the magnetic field, then the physical orientation of the unit cell changes thereby creating strain in the material. One can summarize the energy requirement for a general case as

$$U_a > M_s H > \sigma_{ex}\varepsilon_0 > \sigma_0\varepsilon_0, \tag{1.8}$$

where $M_s H$ is the magnetic input energy due to applied field H , $\sigma_{ex}\varepsilon_0$ is the input mechanical energy due to external applied stress σ_{ex}, $\sigma_0\varepsilon_0$ is the required energy to move twin boundary, σ_0 is called the twinning stress (the stress level at which deformation by twin boundary motion initiates), and ε_0 is the residual or twinning strain. This phenomenon is the primarily straining mechanism in FMSAs. The mechanical properties of FMSAs in martensite phase are the same as SMAs, see Figure 1.10 (a).

The local crystallographic structure controls the easy axis of magnetization, so that each variant has different direction of easy axis of magnetization. To understand straining mechanisms, consider that the martensitic structure has two variants with different easy axis of magnetization in absence of magnetic field as shown in the Figure 1.13 (a) below. When

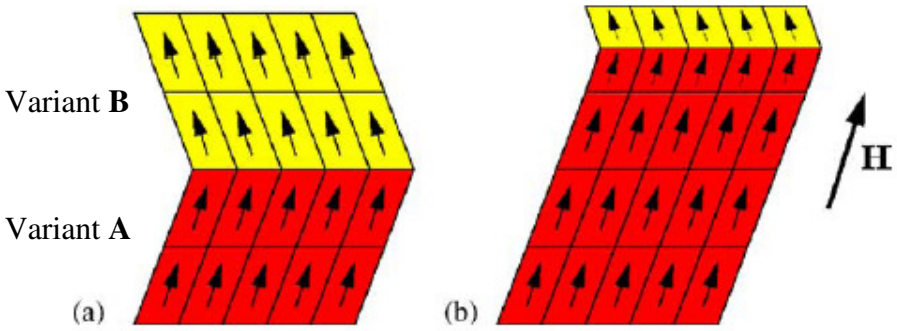

Figure 1. 13 Schematic of strain mechanism in Ni-Mn-Ga FMSAs. (a) Two variants without magnetic field and (b) Redistribution of variants in an applied magnetic as shown [22].

an external magnetic field is applied, variants (Variant **A**) favoured by the applied field increase in size through twin reorientation. This applied field will favour variants with their magnetization of unit cells along its direction. Thus, unit cells along the twin boundary switches their magnetization orientation such that their short c-axis is aligned along the field direction. The global effect is then the growth of favourable variant (Variant **A**) as the expense of unfavourable ones (Variant **B**) through twin boundary motion which in turn results overall axial lengthening of the bulk sample. As the field is increased to the point where no further twin boundary motion is possible, the field energy is sufficiently large to overcome the magnetic anisotropy energy and thus resulting alignment of magnetization vectors along the field direction.

Up on the removal of applied magnetic field, the reorientation of unit cell and change of size of the sample will not occur since there is no driving force for these reverse processes. However, twin boundary motion and reversible strain can be induced by applying perpendicular field, axial compressive stress, or transverse tensile stress, all of which favour the nucleation and growth of the other variants (Variant **B**). In the case of applied external stress, it should be greater than the twinning stress to induce the nucleation and growth of the other variant.

1.2.6 Martensitic and magnetic phase transition in ferromagnetic shape memory Ni-Mn-Ga alloys: $Ni_{2+x}Mn_{1-x}Ga$

From the point of view of most practical applications, shape memory alloys should be in martensite phase at room temperature. In addition to this, for ferromagnetic magnetic

shape memory alloys, the magnetic transition from ferromagnetic state to paramagnetic state must be higher than room temperature. In other words, both martensite transformation (structural) temperature (T_m) and Curie temperature (T_c) should be higher than room temperature. These are the two requirements that need to be achieved in this work for Ni-Mn-Ga thin film on piezoelectric substrate for magnetoelectric effect observation. The first requirement is not stratified by the stoichiometric Ni_2MnGa but the second requirement is satisfied, since T_m=200K and T_c=373K for x=0 [33]. However, both martensite and Curie temperature are composition dependent and thus they can be tailored by varying the value of x (or composition). In this section, a brief review for the dependence of martensite and Curie temperature on composition for bulk Ni-Mn-Ga alloys is presented. For Ni-Mn-Ga alloys thin film, studies are still ongoing and thus there is no well documentation of its dependence of Curie and Martensite temperature on composition like the bulk alloy.

Bulk Ni-Mn-Ga alloys properties are discussed hereafter. A N. Vasiliev et al. have studied the effect of variation of composition on Curie and martensitic temperature for the $Ni_{2+x}Mn_{1-x}Ga$ alloys [33]. In their study, they have identified three distinctive regions from the plot of T_m and T_c versus composition x. Figure 1.14 below shows the plot of martensite and Curie temperature versus composition for $Ni_{2+x}Mn_{1-x}Ga$ alloys.

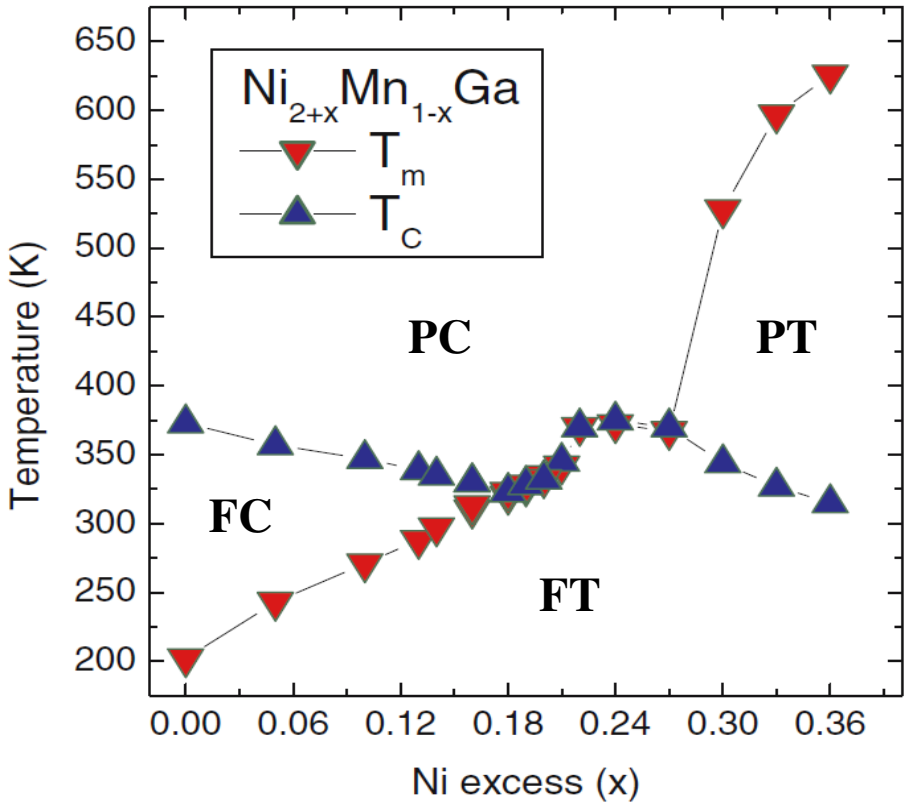

Figure 1. 14 Martensitic and Curie phase transition temperatures determined from DSC and low-field magnetization measurements as function of Ni excess x in $Ni_{2+x}MN_{1-x}Ga$ alloys FT= ferromagnetic tetragonal Martensite, PC= paramagnetic cubic (austenite), PT= paramagnetic tetragonal (martensite), and FC= ferromagnetic cubic (austenite) [33].

As it can be seen clearly from the plot, for $0 \leq x \leq 0.16$, $T_m < T_c$ which implies the transformation from martensite to austenite takes place in ferromagnetic state. Both martensite and austenite phases are ferromagnetic state. For alloys with compositional values in this region, it is possible to change from low ferromagnetic tetragonal martensite phase to ferromagnetic cubic austenite phase and to paramagnetic cubic austenite phase up on heating or in the reverse direction up on cooling. In this region, as the composition x increases the martensitic temperature increases nearly linearly while the Curie temperature linearly decreases as shown in the figure. In the second region, for $0.18 \leq x \leq 0.27$, alloys with these values of x are characterized by a coupled magnetostructural transition, i.e. the two temperatures merge or $T_m \approx T_c$. In this region, the transformation from martensite to austenite is accompanied by a transition from ferromagnetic to paramagnetic state. The temperature in this region has non- monotonous dependence on x. The third

region, for $x \geq 0.30$, the Curie temperature is lower than the martensitic transformation temperature. For alloys with values x in this region, martensite transformation takes place in the paramagnetic state.

The spontaneous magnetization of $Ni_{2+x}Mn_{1-x}Ga$ alloys like martensite and Curie temperature depends on composition. V.V. Khovailo et al. have studied the magnetization dependence for different composition of $Ni_{2+x}Mn_{1-x}Ga$ alloys, Ni atom excess alloys [33] as shown in Figure 1.15 below. As it can be seen from the figure for compositional values of $x < 0.16$, the

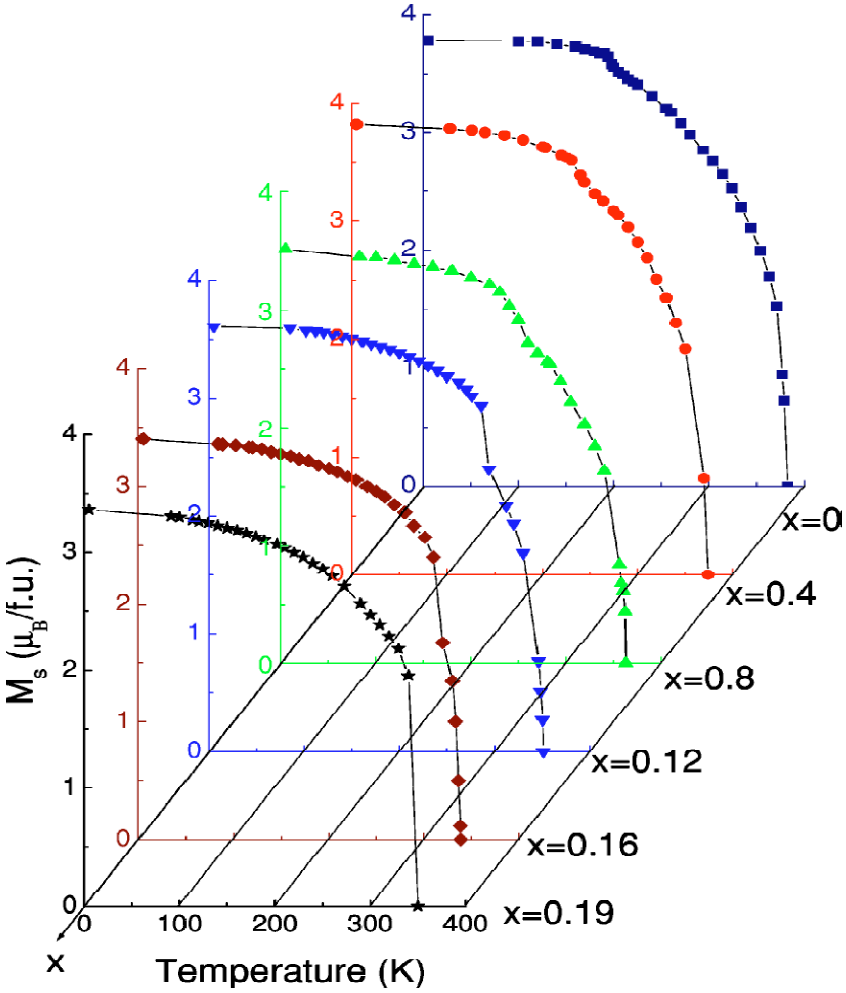

Figure 1. 15 Temperature dependence of spontaneous magnetization of $Ni_{2+x}Mn_{1-x}Ga$ alloys. Ms was determined from the field dependence of magnetization measured up to 10T [33].

magnetization decrease smoothly as temperature increase and then shows a jump when approaching to the structural transition temperature. However, for $x = 0.19$, the

transformation from martensite to austenite is accompanied by a transition from the ferromagnetic to the paramagnetic state. The variation of the structural and Curie temperature on composition which is extracted from the above magnetization curves showed the same behaviour like the previous one from DSC measurement. The magnetic moment of these alloys ($M_s(0)$), determined by extrapolating of $M_s(T)$ to 0K, decreases as x increases like the Curie temperature does as shown in the Figure 1.16 below. The effective magnetic moment decreases with substitution of Mn by Ni atoms.

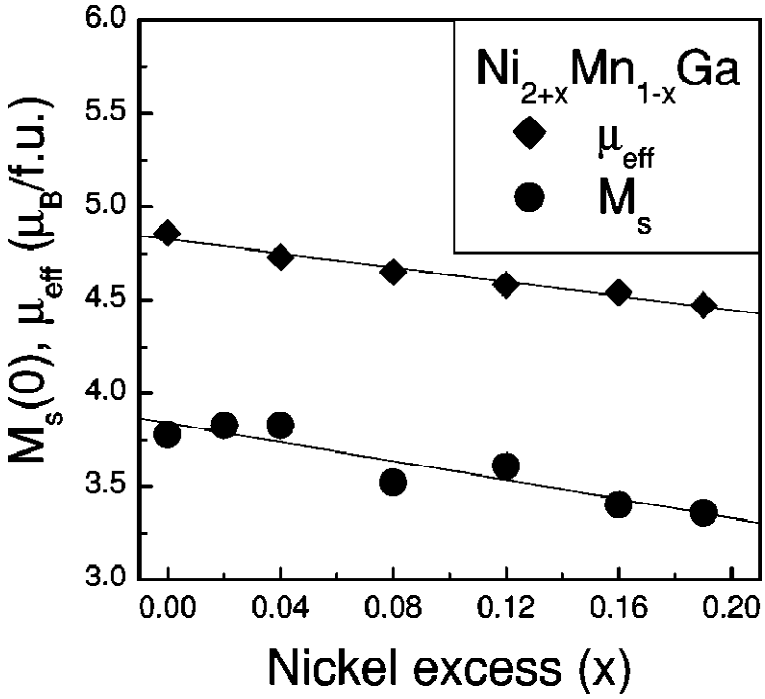

Figure 1. 16 The compositional dependence of saturation magnetic moment $M_s(0)$ and effective magnetic moment μ_{eff} of the $Ni_{2+x}Mn_{1-x}Ga$ alloys [33].

1.3 Multiferroicity

As it is mentioned in the introductory section both ferromagnetic and ferroelectric materials have many applications in modern technology. For instance, ferroelectric materials are widely used as tuneable capacitors and form the basis of ferroelectric random access memory (FRAM) for computers, and ferromagnetic materials used for recording and storing data in hard drive. However, the current technology is following a trend towards device miniaturization, which has led to the interest in combination of these and other properties in a multifunctional materials. The coexistence or combination of several

order parameters will bring out novel physical phenomena and offers possibilities for new device functions. Multiferroic materials are materials that possess two or more of the so called ferroic order parameters (ferromagnetic, ferroelectric, and ferroelastic) that have potential application as multifunctional devices. In this section only ferromagnetic ferroelectric multiferroic materials are addressed. Figure 1.17 depicts different possible couplings present in materials and relationship between Multiferroic and magnetoelectric materials. As shown in the figure only a small subgroup of

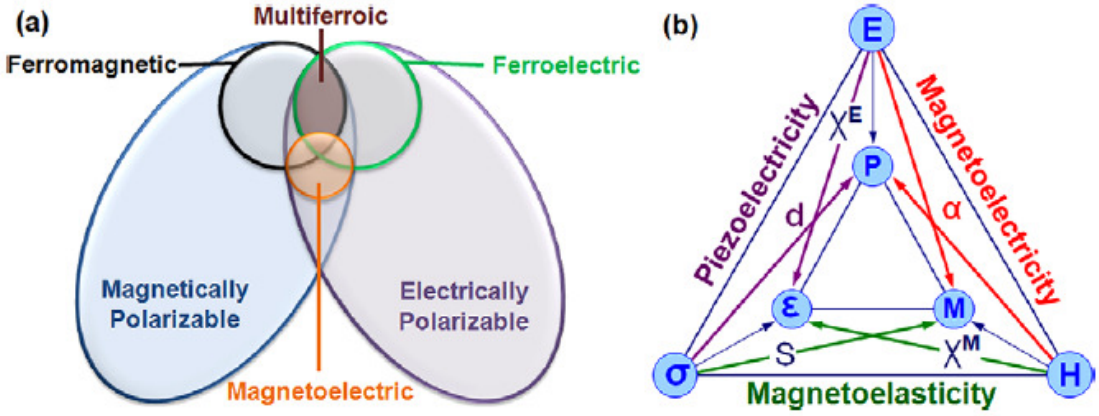

Figure 1. 17 (a) Relationship between Multiferroic and magnetoelectric materials, and (b) schematic illustrating different types of coupling [34].

all magnetically and electrically polarizable materials are either ferromagnetic or ferroelectric and fewer still simultaneously exhibit both order parameters. In this type of multiferroic materials, there is a possibility to control magnetization and/or polarization by an electric field and/or magnetic field. Figure 1.18 below shows the hysteresis loop of these materials. As it is shown in the Figure 1.18, these materials not only have excellent polarization and magnetization hysteresis but also high quality of polarization-magnetic field hysteresis and magnetization-electric field hysteresis.

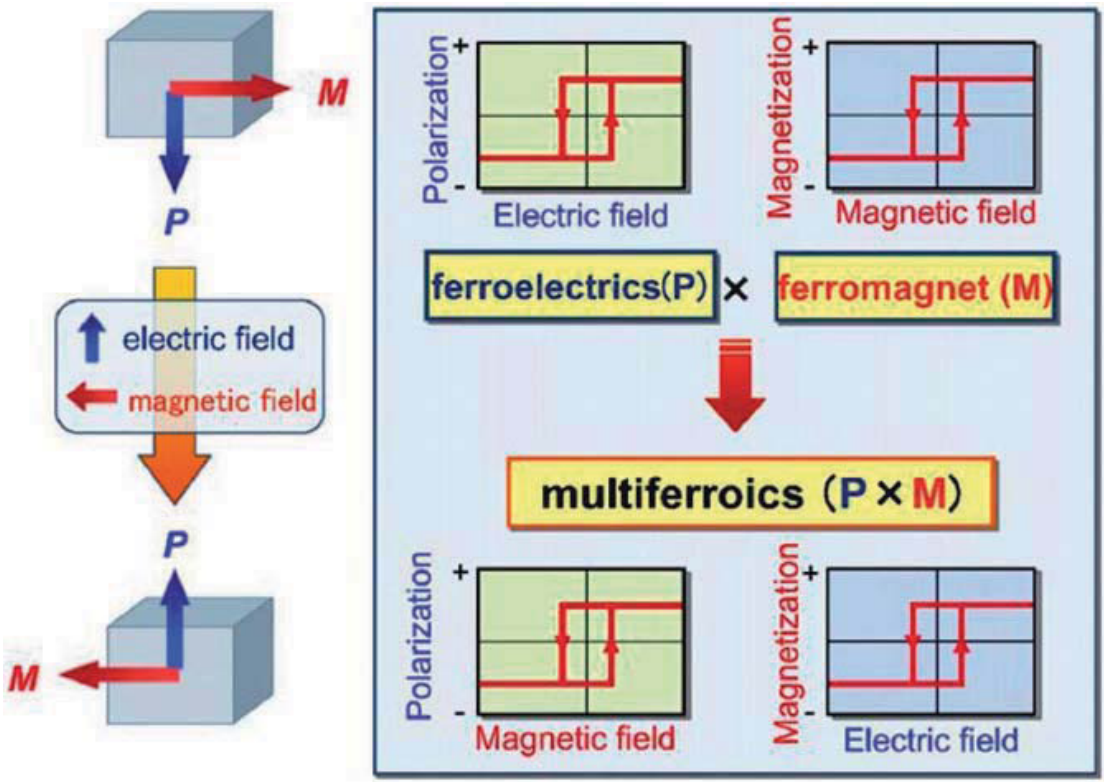

Figure 1. 18 the sketches of ferroelectric and ferromagnetism integration as well as the mutual control between them in multiferroic [1].

The most general definition of the coupling between electric and magnetic fields in mater, i.e. the induction of magnetization (M) by the electric field (E) or polarization (p) generated by a magnetic field (H) is known as magnetoelectric. Magnetoelectricity is an independent phenomenon that can arise in any material with both magnetic and electronic polarizability, regardless of whether it is multiferroic or not as it is shown in Figure 1.17 (a). By definition, a magnetoelectric multiferroic must be simultaneously both ferromagnetic and ferroelectric [5]. Magnetoelectricity has been observed as an intrinsic effect in some materials at low temperatures for example, $TbMnO_3$, $DyMnO_3$, $YMnO_3$, [35-37].

1.3.1 Magnetoelectric Multiferroics

A real interest in magnetoelectric (ME) lies on a strong coupling between the order parameters and the possibility to create new functionalities in materials. This requires better understanding of magnetoelectric coupling. Indeed, the magnetoelectric coupling

can be understood by Landau theory framework, approached by the expansion of free energy for a magnetoelectric system.

The free energy expansion [2] is given by

$$-F(E,H) = F_0 + P_i^s E_i + M_i^s H_i + \frac{1}{2}\varepsilon_0\varepsilon_{ij}E_iE_j + \frac{1}{2}\mu_0\mu_{ij}H_iH_j + \alpha_{ij}E_iH_j + \frac{1}{2}\beta_{ijk}E_iH_jH_k + \frac{1}{2}\gamma_{ijk}H_iE_jE_k + \cdots, \quad (1.9)$$

where $F_0$is the ground state free energy, subscripts (i, j, k) refer to the three components of a variable in spatial coordinate, E_i and H_i are the components of electric and magnetic field, respectively, $P_i^s$and $M_i^s$are the components of the spontaneous polarization and magnetization, $\varepsilon_0$and μ_0 are the dielectric and magnetic susceptibilities of vacuum, ε_{ij} and μ_{ij} are the second-order tensors of dielectric and magnetic susceptibilities, β_{ijk} and γ_{ijk} are the third-order tensor coefficients and $\alpha_{ij}$is the components of the tensor α which is known as linear magnetoelectric coefficients. The linear magnetoelectric coefficient tells us the induction of magnetization by electric field or polarization by the magnetic field. The higher order terms like γ and β tells higher order magnetoelectric effects and they are very small. Using equation (1.9), the polarization is then given by

$$P_i(E,H) = -\frac{\partial F}{\partial E_i} = P_i^s + \varepsilon_0\varepsilon_{ij}E_j + \alpha_{ij}H_j + \frac{1}{2}\beta_{ijk}H_jH_k + \gamma_{ijk}H_iE_j + \cdots, \quad (1.10)$$

and magnetization is given by

$$M_i(E,H) = -\frac{\partial F}{\partial H_i} = M_i^s + \mu_0\mu_{ij}H_j + \alpha_{ij}E_j + \frac{1}{2}\beta_{ijk}H_jE_i + \frac{1}{2}\gamma_{ijk}E_jE_k + \cdots. \quad (1.11)$$

The magnetoelectric effect for intrinsic single phase multiferroic materials is usually small and is limited by $\alpha_{ij}^2 \leq \varepsilon_{ij}\mu_{ij}$. This implies that to observe magnetoelectricity in single phase the large dielectric constant and magnetic susceptibility are important. However, in two phase multiferroic composite there is a possibility that this effect can be large. For instance, in multilayer composite structure composed of piezomagnetic layer (e.g. nickel ferrite) and piezoelectric layer (e.g. lead zirconate titanate), large magnetoelectric effect (1500mV/cm Oe) was observed [38-40]. In composite material, magnetoelectric property is product property, which is originating from cross interaction between two phases. Neither the piezoelectric nor the ferromagnetic phase has the intrinsic ME effects, but the composite of the two phases have remarkable ME effect. Thus the ME effect is a result of

the product of the magnetostrictive effect (magnetic/mechanical effect) in the magnetic phase and the piezoelectric effect (mechanical/electrical) in the piezoelectric phase. One can then write these product properties as

$$\mathrm{ME_E effect} = \left[\frac{\text{Electric}}{\text{Mechanical}}\right] \times \left[\frac{\text{Mechanical}}{\text{Magnetic}}\right] \tag{1.12}$$

and

$$\mathrm{ME_H effect} = \left[\frac{\text{Magnetic}}{\text{Mechanical}}\right] \times \left[\frac{Mechanical}{Electric}\right]. \tag{1.13}$$

As the above two equation can tell, the coupling between electrical and magnetic phenomenon is through elastic interaction. The first equation tells us that when an electric field is applied to the composite, the piezoelectric phase deforms because of piezoelectric effect. The deformation (or strain) is passed to the magnetic phase resulting change in magnetization of magnetic phase. This effect is known as converse magnetoelectric effect (ME_E). The second equation tells us that when magnetic field is applied to the magnetic phase, the magnetic phase deforms magnetostrictivily. The strain is passed along to the piezoelectric phase, resulting in electric polarization in piezoelectric phase. This effect is known as direct magnetoelectric effect (ME_H)

For magnetoelectric effect to be observed in a single phase multiferroic materials (or intrinsic multiferroics), ferroelectric and ferromagnetic property must exist in the single phase simultaneously. It is not only ME effect is small in these materials, but also it is hard (or naturally rare) to find materials that have both of the order parameter simultaneously. The reason is as follows: most ferroelectric are insulators (and 3d transition metals based oxide typically having empty d shells) while itinerant ferromagnets need conduction electrons; even in double exchange ferromagnets such as the manganites, magnetism is mediated by incompletely filled 3d shells. Thus, the weak multiferroic (or ME) response and the paucity of single phase Multiferroic materials is attributed to seemingly contradiction between the conventional mechanism of off-centering in a ferroelectric and the formation of magnetic order in ferromagnetism. Because of this and the technological importance of ME response in multiferroic materials, the focus of many researchers has been in designing and identifying new mechanisms that lead to ME coupling and multiferroic behavior. ME effect on composite (two phase) has been

investigated in different material systems such as (1) bulk ceramics ME composite of piezoelectric ceramics and ferrites, (2) two-phase composite of magnetic alloys and piezoelectric materials, (3) three phase ME composites, and (4) thin films (nanostructure composites) of ferroelectric and magnetic oxides. To get ME effect in two-phase composite, both materials should be integrated or connected in some way. Newnham et. al. have introduced concept that describes the connectivity of these two-phase [41]. Accordingly, the structure of a two-phase composite are described by 0-3, 2-2, 1-3, etc-type, each numbers denote the connectivity of the respective phase. For example, a 0-3-type particulate composite means the one phase particle (denoted by 0) embedded in the matrix another phase (denoted by 3). These structures have been studied for bulk composite magnetoelectric multiferroic materials. Moreover, nanostructured composite of thin films of magnetic materials and ferroelectric oxides have been proposed. It is mentioned in Li Yan et al. that Zheng et. al. reported a pioneering experiment on nanostructured films of the $BaTiO_3/CoFe_2O_4$ system with series of experiments [42].

1.3.2 Thin Film Multiferroics

The new approaches or developments on thin film growth techniques and discovery of ferroelectric oxides with large piezoelectric effect have opened interests on multiferroic thin films. The availability of techniques provides the opportunity to produce high quality multiferroic materials and a path way to discover new multiferroic materials. Among the thin film deposition techniques that have been used to produce multiferroic thin film materials are sputtering, pulsed laser ablation, spin coating, sol-gel processes, metal-organic chemical vapour deposition, molecular beam epitaxy, and so on.

1.3.2.1 Single phase multiferroic thin films

Nowadays there are a number of ways that can be used to create multiferroic materials. However, to date the only single phase multiferroic thin films available are the hexagonal manganites and Bi- and Pb-based perovskites. Some examples of such materials are $YMnO_3$ [43-44], $BiMnO_3$ [45, 46], $BiFeO_3$ [47, 3]. For the reasons mentioned in the previous section, the abundance of single phase multiferroic materials in nature is rare, and the multiferroic property for such materials is observed for low temperatures and high

magnetic field which question their applicability at room temperature (or feasibility for practical application). Moreover, single phase materials involve expensive materials and processing techniques. In the case of magnetoelectric multiferroics, the magnitude of magnetization or polarization is much smaller than in conventional ferromagnets or ferroelectric. The solution to these limitations is offered by shifting to composite of ferromagnets and piezoelectric materials with high magnetic and ferroelectric Curie temperature, respectively, which are favorable candidate at room temperature.

1.3.2.2 Composite Multiferroic thin film materials

A lot of progresses have been shown in the areas of composite magnetoelectric systems. These systems, which are composed of (anti)ferromagnetic and ferroelectric, are promising candidate to show high magnetoelectric effect other than single phase magnetoelectric multiferroics. The systems operate by coupling between a (anti)ferromagnetic material and ferroelectric material through strain. In a composite of ferromagnetic and ferroelectric material, the converse and direct magnetoelectric effect can be achieved in two ways. For example, in converse magnetoelectric effect, an applied electric field on ferroelectric material creates a converse piezoelectric effect (strain) in the ferroelectric material. The strain of the ferroelectric is transferred to the magnetic component with efficiency depending on the geometry of the composite and elastic coupling at their interface between the layers. For the epitaxial grown films, good mechanical coupling may be anticipated, if a small density of defects at the interface is present. The strain transferred to the magnetic materials changes the magnetization or magnetic anisotropy of this material because of piezomagnetic effect. Figure 1.19 below depicts the schematics of multiferroic thin film composite mediated by strain. In such type of configuration magnetoelectric effect does not exist in the separately ferromagnetic or piezoelectric material but it is the property of the composite. In direct magnetoelectric effect, the distortion of ferromagnetic layer is achieved by applying magnetic field on it which can be transferred to piezoelectric layer and results electric response (polarization) in piezoelectric layer. In general, one can say that the two layers can affect each other through (i) mechanical coupling and (ii) electric or magnetic field strays.

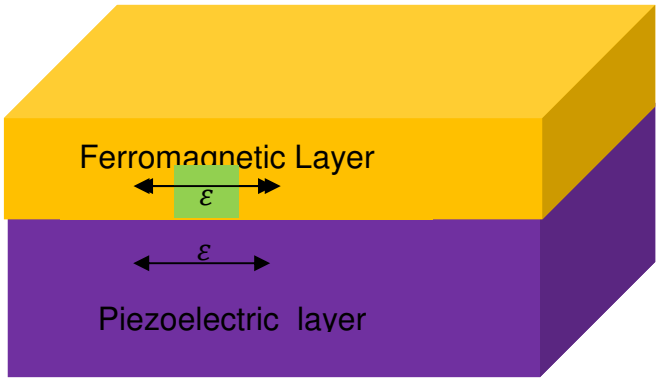

Figure 1. 19 Schematic of a multiferroic composite for stain-mediated magnetoelectric coupling

One way of creation of strain in magnetic films has been introduced by Lee et al. and Dale et al. as it is mentioned K. Dorr et al. [48]. They used piezoelectric monocrystalline substrate of $BaTiO_3$ (001) for magnetic thin film growth. As it is mentioned in K. Dorr et al, Thiele et al. have suggested a replacement of $BaTiO_3$ (001) piezoelectric by $72Pb\left(Mg_{1/3}Nb_{2/3}\right)TiO_3$-$28PbTiO_3(001)$ (PMN-28PT) [48]. This substrate is close to cube ferroelectric with sufficiently uniform substrate lattice parameter to allow quantification of the applied piezoelectric strain. This substrate is also known for having well-defined polarization versus electric field hysteresis and superior piezoelectric properties.

Figure 1.20 below shows more specific sample geometry for magnetic thin film on a piezoelectric substrate as compared to the one shown in Figure 1.19. In this device configuration, voltage is applied between the magnetic film and a counter-electrode on the opposite crystal face which creates strain in piezoelectric substrate. If the magnetic film is

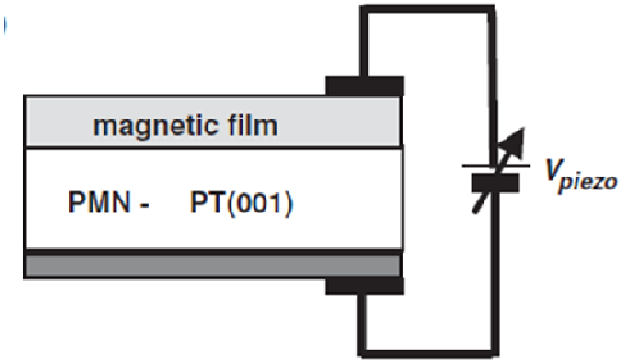

Figure 1. 20 Schematic structure of sample comprising a conducting film on PMN-28PT(001)[48]

insulating, there should be a conducting buffer layer between the film and substrate that function as the upper electrode. In this type of configuration, it is also possible to apply magnetic field on the magnetic thin film and measure voltage across the piezoelectric material (PMN-PT).

The search for combination of materials that can give high ME coefficient is currently hot activity and there are a number of reports in this regard. Some of the materials used as magnetic phase and ferroelectric phase are $CoFe_2O_4$, $NiFeO_3$, Terfenol-D, $La_{1-x}Sr_xMnO3$, $La_{1-x}Ba_xMnO_3$ and $BaTiO_3$, $Pb(Zr, Ti)O_3$ (PZT), $BiFeO_3$, $PbTiO_3$, PMN-PT, respectively [49-55]. Magnetoelectric coefficient ($\alpha_{ME} = \mu_0 \frac{dM}{dE}$) in $La_{0.7}A_{0.3}MnO_3$/PMN-PT (001) (where A=Sr, Ca) composite was found to be as high as 60Oe cm/KV [55]. It is not only metal oxides that are used as magnetic materials but also ferromagnetic shape memory alloys (FSMAs/piezoelectric) [56, 57, 10]. Magnetoelectric coefficient ($\alpha_{ME} = \frac{dP}{dH}$ and $\alpha_{ME} = \mu_0 \frac{dM}{dE}$) in Ni_2MnGa/PZT and Ni_2MnGa/PMN-PT composite was found to be as high as 180mV/cmOe and 41 Oe cm/kV [56, 57].

Among FSMAs, Ni-Mn-Ga alloys have received considerable interest as FSMAs and they are also well studied alloys. Theses alloys are known to have large magnetic-field induced strain (MFIS) in martensitic state which provides a room to be incorporated in multiferroic composite structure where magnetic field induced elastic deformation in the Heusler alloys may result in a large magnetoelectric coupling coefficient. In Ni-Mn-Ga alloys, the MFIS can be considered as an equivalent magnetostrictive effect. The magnetostrictive coefficient (or MFIS), for example in bulk single-crystalline stoichiometric Ni_2MnGa, in martensitic state is more than one order of magnitude that the normal magnetostrictive coefficient. As it is discussed in section 1.2.6, the martensite and ferromagnetic transformation temperatures can be tuned by varying the composition of Ni and Mn atoms. In other words, it is possible to produce off-stoichiometric Ni-Mn-Ga alloy thin film with martensite and ferromagnetic transition temperature above room temperature so that the magnetoelectric coupling of Ni-Mn-Ga FMSA thin film on the piezoelectric substrate (PMN-PT) can operate at room temperature. This work is aimed at producing and

studying magnetoelectric effect of Ni-Mn-Ga/PMN-PT multiferroic thin film composite heterostructure that can function or operate at room temperature.

2 Experimental Methods

2.1 Substrate choice and preparation

It is well know that substrate plays a vital role in controlling and getting a good quality thin film. In general properties of substrate affect the quality of a film in many ways. Thus, to produce a quality thin film, substrate should have smooth and flat surface, high thermal conductivity, good stability, good adhesion property, low cost and ease of handling during processing (or deposition of a film), and others. In this work commercially available different substrates with thickness of 0.5mm and with different crystal orientation as shown in the table 1.1 below were used to deposit Ni-Mn-Ga alloy thin films. Even though different substrates for film deposition were used, this work is mainly concerned to the PMN-PT substrate, and others substrates were used for comparison.

Table 2. 1 Types and orientation of substrate

Substrate	$0.66Pb\left(Mg_{1/3}Nb_{2/3}\right)TiO_3$-$0.33PbTiO_3$) (PMN-PT)	$SrTiO_3$ (STO)	MgO	Al_2O_3
Crystal orientation	(100)	(100)	(100)	(0001)

In addition to good choice of substrates, preparation of substrate is critical to produce quality thin film. Prior to the deposition of Ni-Mn-Ga (NMG) alloy thin film, the substrates should be cleaned, polished, and appropriate size for testing. Firstly, the substrates as they were bought were cut in to a number of small pieces of dimensions $0.5 \times 5 \times 10mm^3$ and $0.5 \times 10 \times 10mm^3$. Different batches (or series) were prepared in this way in which all of them were one sided polished except only one $SrTiO_3$ substrate in the last batch (see the next section). And then after, all substrates were cleaned for 15 minutes with acetone PA and another 15 minutes with ethanol PA in ultrasound bath. The cleaned substrates were dried and ready for deposition.

2.2 Sputtering Deposition

Sputtering deposition is one of the most widely used physical vapour deposition techniques that is used to deposit thin films [58]. It is the ejection of particle species from a solid called target and deposit a thin, firmly bounded film on adjacent surface called substrate. The process involves bombarding the surface of the target with inert gaseous ions by using high voltage acceleration. In the first step to sputter atoms from the target surface, plasma has to be created. This can be done by introducing atoms of inert gases (Ar gas) in a vacuum chamber and holding the target at negative bias while the shield around the target and the chamber are grounded. This potential accelerates electrons in the inert gas environment (Ar) in which they can collide in-elastically with Ar atoms. The collision of an electron with Ar atom creates Ar^+ and second electron. Electrons produced in this way repeat the above process and causing the gas to breakdown the discharge to glow (or form plasma). The second electrons help to sustain the discharge. The created Ar^+ ions in this way are accelerated towards the target and sputter the target. The target atoms that are knocked out from the target will be transported to the substrate due to momentum transfer but not by evaporation. The incident argon ions lose some energy during collision with target atoms. Thus, heating the target should be controlled by water cooling system attached to it.

The basic principle of sputtering as briefly described in the above paragraph is the same for all sputtering technologies. The difference lies on the manner in which the ion bombardment of the target is realized. Thus, based on the type of power used we have different types of sputtering which are called DC or RF sputtering, DC or RF Magnetron sputtering. DC sputtering is used to deposit conducting materials but it cannot be used for depositing

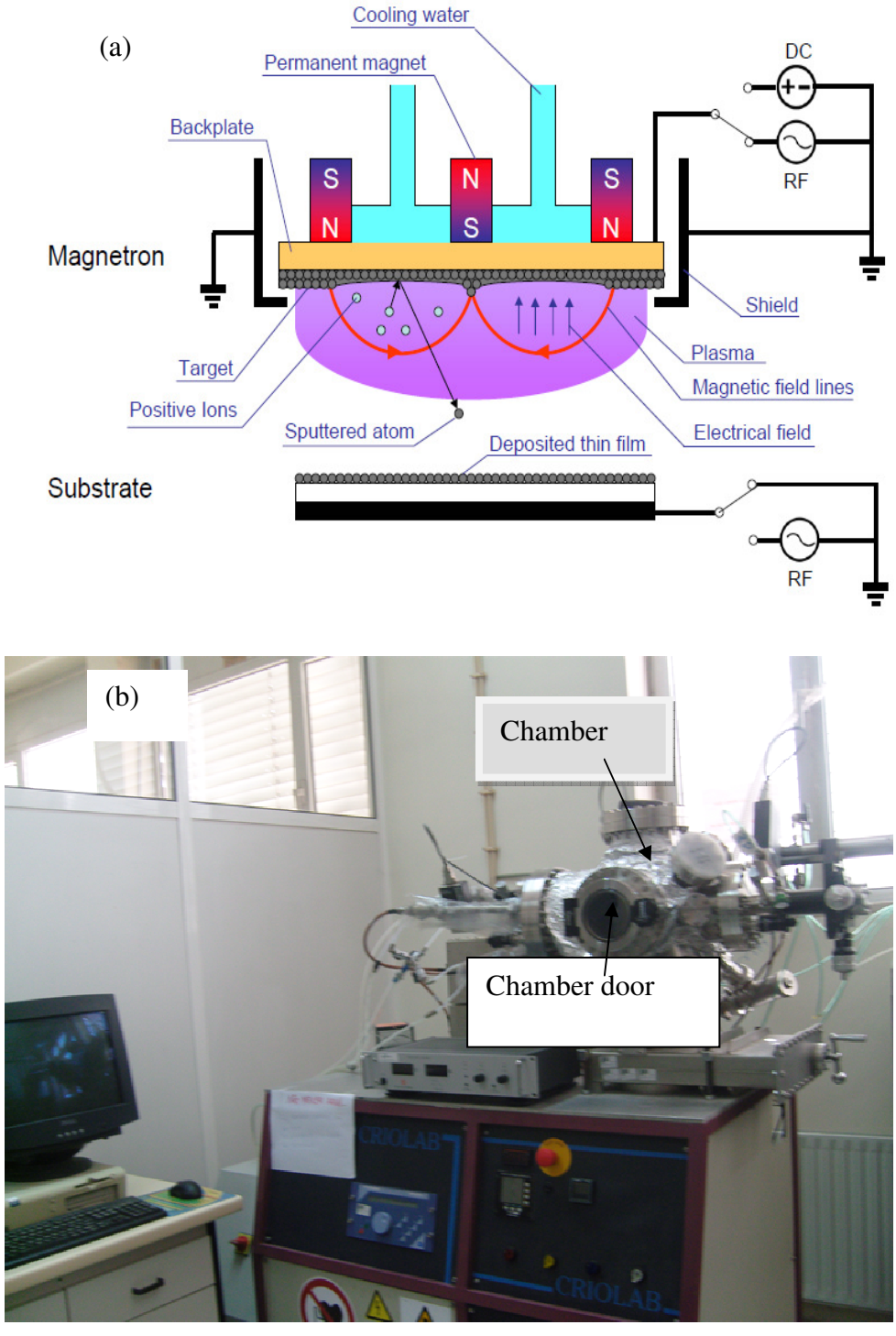

Figure 2. 1 (a) Schematics of Magnetron sputtering system [49] and (b) a photo of Magnetron sputtering deposition system.

insulating materials. The reason is because there will be charge build up during Ar^+ bombarding at the insulating cathode. Thus, to eliminate this problem AC power should be used, that developed the RF Sputtering technique.

Magnetron sputtering is a sputtering deposition system where permanents magnets located behind targets are used to create magnetic field as shown in the Figure 2.1 above. This magnetic field helps the electrons trajectory to be confined immediately to the vicinity of the target as result electrons bombard the target and increase of target temperature. In addition to this, the magnetic field allows the plasma to ignite with less concentration of Ar atoms (lower processing Ar pressure) which intern enables higher deposition rate and improved control of film growth.

Sputtering is usually characterized by sputter yield, S, which is define as the mean number of atoms removed from the target per incident argon ions and is given by

$$S=\frac{\text{Atoms removed}}{\text{Incident ions}}. \quad (2.1)$$

This quantity depends on many factors among which power, gas pressure, target material, and angle of incidence are some of the factors that are addressed here.

The energy of bombarding ion and discharge current strongly depends on the power used which strongly affects the sputter rate. The sputtering yield is proportional to the bombarding argon ion energy. The sputter rate increase as power increases.

Gas pressure is another factor affecting the yield. The collision of sputtered atoms with the gas atoms results deflections of the sputtered atoms, sometimes cause the atom re-deposit on the target, so that the re-deposition rate increases as the gas pressure increase. On the other hand, increasing the working pressure increases the discharge current for constant power due to increasing plasma potential. Thus, there is a working pressure at which the sputtering rate is maximum.

The nature of target material affects the sputter yield. This is because different materials require different amount of energy to sputter or they have different binding energy. The higher binding energy the target material has, the lower sputter yield will be since it requires higher energy to remove the atoms from the target surface. On the other hand, targets with lower binding energy have higher sputter yield.

Sputter yield is also dependent on the angle of incident where angle of incidence is defined as the angle between the trajectory of the incident ion and an imaginary line perpendicular

to the target surface. It was experimentally found that sputter yield increases until around 70^0 and then rapidly decrease with increasing angle of incidence [58].

In general by varying or controlling the deposition conditions, it is possible to control the structural and magnetic property of any magnetic thin film using sputtering deposition systems. In this work, since the fundamental precondition (or requirement) for most technical applications in general and magnetoelectric effect in particular is that the films should be ferromagnetic and martensitic with different variants at room temperature, we tried to control the magnetic and martensitic property of Ni-Mn-Ga alloy thin films on different substrates by small variation of power on targets, varying substrate temperature and keeping gas pressure constant in radio-frequency (RF) sputtering deposition system as shown in the table 2.2 below. In other words, we aimed to find the best condition of deposition that will lead to observe of magnetoelectric effect in Ni-Mn-Ga/PMN-PT thin film multiferroic composite and ferromagnetic martensite in the other films. Prior to deposition the chamber base pressure was maintained below $10^{-7}Torr$ for all series of samples. Different deposition conditions used for different series of samples are shown in the table 2.2 below. To produce the films with these deposition conditions, magnetron RF co-sputtering of two targets with 2inch in diameter and composition of $Ni_{50}Ga_{50}$ and $Ni_{50}Mn_{50}$ which were located at a distance of 150mm from the substrates were used. The final structure of the films on substrates after deposition looks like as shown in Figure 2.2.

Table 2. 2 Deposition condition for each sample

Series	Sample	Power(W)		Ar Pressure(mbar)	Temperature (^{0}C)	Time (minutes)	Ar flow(Sccm)
		$Ni_{50}Ga_{50}$	$Ni_{50}Mn_{50}$				
14	NMG/STO NMG/MgO NMG/ PMN-PT	16	18	6×10^{-3}	320	20	10
15	NMG/Al_2O_3 NMG/MgO NMG/ PMN-PT NMG/STO	9	11	6×10^{-3}	370	150	10
16	NMG/STO NMG/ PMN-PT NMG/Al_2O_3	12	16	6×10^{-3}	400	150	10

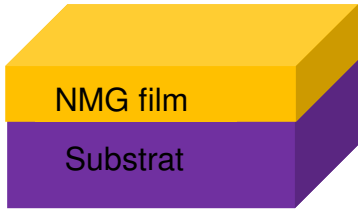

Figure 2. 2 The schematic structure of the device after deposition.

3 Characterization Techniques

3.1 Structural characterization

3.1.1 X-Ray Powder Diffraction

X-ray diffraction technique is a technique often used to study the crystal structure and lattice parameter of materials. The diffraction of the x-ray is the result of interaction between x-rays and periodic array of atoms of a crystal or films. The x-rays are produced by the interaction of electrons with matter such as Copper, Molybdenum and others. In this work XRD system of X´Pert PRO MRD from PANALYTICAL which uses Copper to produce x-rays with characteristics wavelength $Cu_{k\alpha}$ of $\lambda = 1.5406A^0$ were used. The schematic of this system is shown in the Figure 3.1 (a) below. The technique in general includes $\theta/2\theta$ scan, ϕ scan, and rocking curve (ω scan). In this work we used the $\theta/2\theta$ scan were used to identify the phase of the magnetic alloy thin film grown on different substrates.

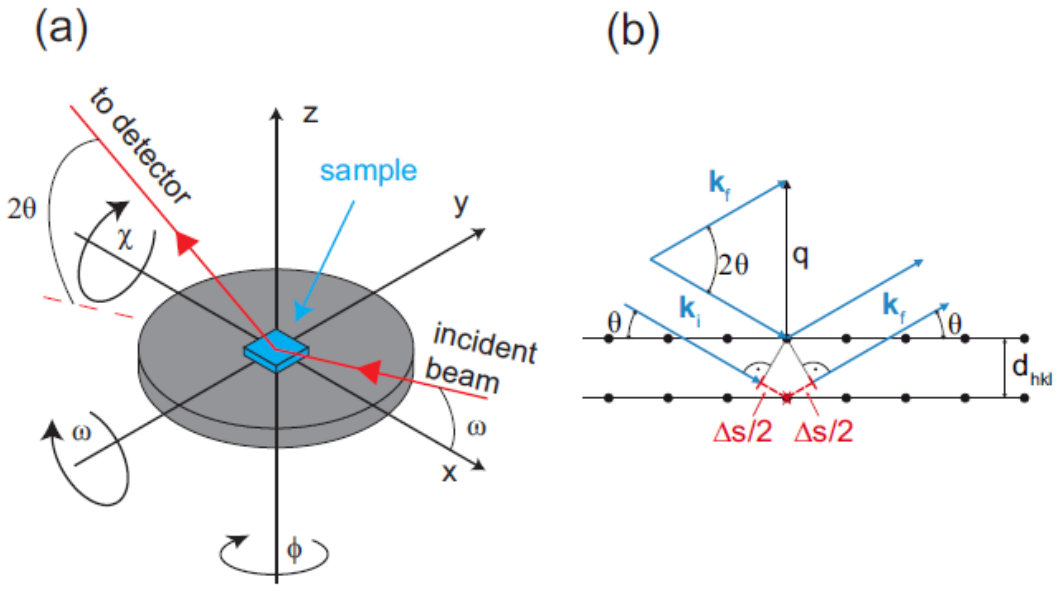

Figure 3. 1 (a) The schematic view of 4-circle diffractometer, (b) the diffraction of x-ray beam by plane of atoms [60].

The basic working principle in simple way can be described as follows. If parallel and monochromatic x-ray beams with wavelength λ and wave vector $\mathbf{k}_i$ are diffracted by atoms in parallel planes with plane distance d_{hkl} then the diffracted beams with wave vector $\mathbf{k}_f$ will interfere constructively or destructively as shown in Figure 3.1 (b). According to Bragg´s law of diffraction, constructive interference occurs when the path difference between two beams shown in the Figure 3.1 b is an integral multiple of λ , that is,

$$\Delta s = 2d_{hkl} sin\theta = n\lambda, \quad (3.1)$$

where θ is the angle between incident rays and the sample surface, hkl are the Miller indices of atomic planes and n is the order of diffraction. The source (θ) and the detector (2θ is the angle between the diffracted beam and the incident beam) angles are synchronized to each other, so that the Brag´s condition is satisfied for planes parallel to the film plane. The angles can be varied generally in two ways: detector and the sample can rotate or detector and the source can rotate. During $\theta/2\theta$ scan as the detector rotates, the detector records the intensity of diffracted beams $I(2\theta)$ as function of 2θ. Thus, from the result one can calculate d_{hkl} for each peaks and lattice parameters.

3.2 Magnetic and Piezoresponse Measurements

3.2.1 Magnetic Force Microscopy and Piezoresponse Force Microscopy

Atomic force microscopy (AFM) is an important characterization technique which can be used to study top surface of thin films or any material with nano-scale resolution. It is so flexible that it can be used to image various forces by changing the tip and scanning mode. In this work, piezoresponse force microscopy (PFM) and magnetic force microscopy (MFM) are used to study ferroelectric and magnetic domains, respectively. MFM technique was used to check whether the deposited magnetic films on different substrates are ferromagnetic (have magnetic response) or not while the PFM technique was used to check whether the ferroelectric property of the PMN-PT substrate is maintained after deposition or not.

The basic working principles of these techniques are similar except the interaction between the tip and the sample are different. Basic components of AFM are a tip, a cantilever, and a laser beam, a photodetector, feedback electronic system, a display system that converts

the measured data in to an image, and mechanical scanning system. A tip which interacts with the sample by either repelled or attracted to the sample surface is mounted on one end of a cantilever and used to scan the sample. The cantilever is critical part of AFM device in which one of its ends is attached to the tip and the other end is attached to a rigid substrate that can be held fixed. Because of attractive or repulsive interaction of the tip with the sample surface, there will be a positive or negative bending of the cantilever. The deflection of the cantilever caused by the interaction between the tip and the sample should be detected in some way. It is detected by photodetector as shown in Figure 3.2 below. The photodetector detects the relative position of the laser on photodiode. The photodetector has four compartments which are divided by vertical and horizontal line and are used to detect the lateral and vertical deflection of the cantilever. The controlled movement of the cantilever is done by expanding and contracting piezocrystal due to applied voltage on it.

Magnetic force microscopy is a variation of AFM which is used to study magnetic materials equipped with a special tip coated with magnetic layer. As the tip scans on the sample surface, it interacts with magnetic domains on the surface of the sample that results to the deflection of a cantilever. MFM measures these influences using the principle of force gradient detection. The force gradient contains information from both surface structure and surface magnetization ($F = F_{surface} + F_{magnetic}$where $F_{surface}$is the surface component of the gradient and $F_{magnetic}$is the magnetic component of the gradient). Signals from the surface dominate at a distance close to the surface while at a distance further away from the sample the magnetic signals dominate. Thus, depending on the distance between the tip and the sample surface, MFM images may contain both topographic image and magnetic image. In other words, information about the sample can be obtained by using lift (or non contact mode) and tapping mode. Figure 3.3 below depicts the measurement method of MFM. Indeed, the magnetic information depends on the nature or strength of magnetic interaction

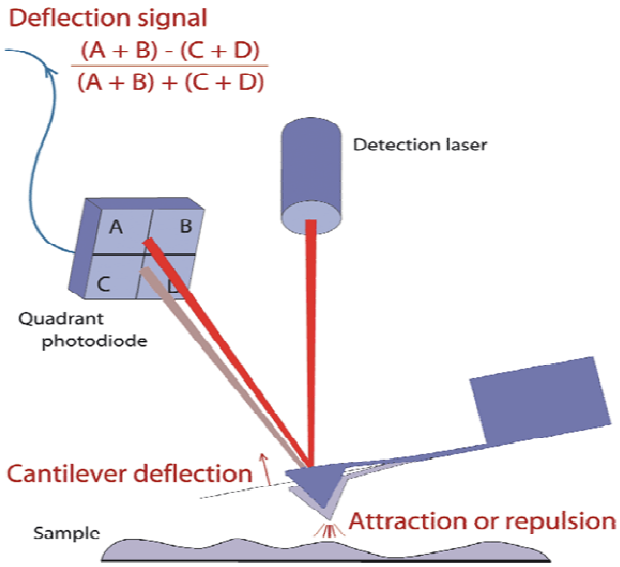

Figure 3. 2 Block diagram of Atomic Force Microscope [61]

between the tip and the sample. Thus a cantilever should be coated with a magnetic material having small magnetic signal.

The vertical gradient force on the tip shifts the resonance frequency (f_0) by some small amount,Δf, where f_0 is the resonance frequency of the tip in the absence of magnetic field.

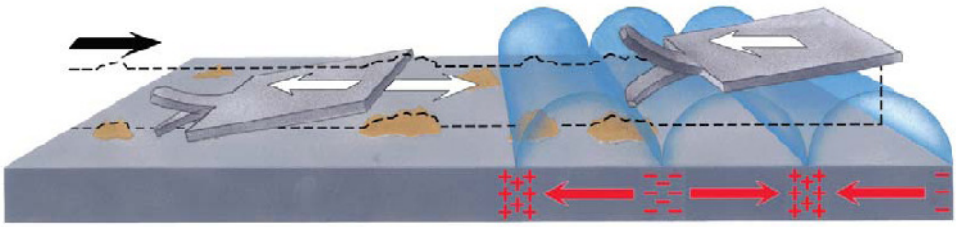

Figure 3. 3 Schematic illustration of magnetic force microscopy: Red arrows show the direction of spontaneous magnetization direction in each domain and the white arrows show the directions of motion of the cantilever [62].

This frequency shift can be detected by three ways: phase detection which measures or detects the cantilever´s phase of oscillation relative to the Piezo drive, amplitude detection which tracks the variation in oscillation of amplitude, and frequency modulation which directly tracks the shift in resonance frequency. In this work MFM phase image was used to study the magnetic property of the thin film on top of piezoelectric substrate and other substrates.

Since our aim is to make a device composed of composite of piezoelectric and magnetic film, we should maintain ferroelectric property of the substrates. Thus, PFM was used to check the piezoresponse of the substrates. Its working principle is as follows. The PFM measurement works in contact mode. When an AC or DC electric field is applied between a conductive tip (top electrode) and the sample (bottom electrode), the Piezo material generate strain because of converse piezoelectric effect. The response depends on sign of the applied field and the orientation of local electric polarization of the sample under study. When the positive voltage is applied on the domains with vertically upward polarization, then the sample will expand locally. If the polarization is vertically downward polarization, sample contracts locally. Figure 3.4 below demonstrates this situation. The phase of electromechanical response of the surface yields information about the orientation of polarization. For upward orientation of polarization, the phase is zero and for the downward orientation the phase is 180^0

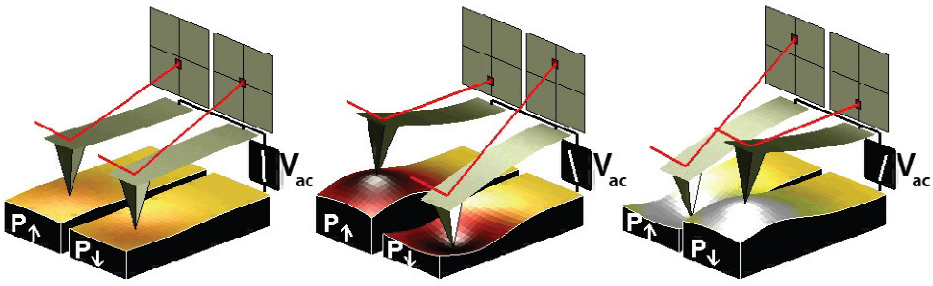

Figure 3. 4 Sign dependence of piezoresponse of piezoelectric material [63]

3.2.2 Vibrating Sample Magnetometer (VSM)

Vibrating Sample Magnetometer (VSM) was used to measure the magnetic properties of the Ni-Mn-Ga thin film deposited on different substrates using sputtering deposition. The working principle of this instrument is based on the Faraday´s law of induction. The

sample to be measured is suspended by non magnetic rod that is attached to a vibrating head in a homogenous magnetic field where maximum signal can be detected. The sample in this field is made to undergo mechanical vibration by the vibrator which is attached at the other end of the rod. The photo of VSM magnetometer used in this work is shown in the Figure 3.5 below. As a result of the vibration of sample in the field, there are magnetic flux changes which are converted to electrical signal (or voltage) by picking up coils. According to Faradays law of induction, the induced voltage is proportional to the rate of change of flux ($V = \frac{d\varphi}{dt}$). Thus, it is possible to extract the magnetic moment of the sample as a function of magnetic field. The VSM instrument used in this work is capable of producing magnetic fields up to$\pm 10T$ using a superconducting magnet. From this measurement one can get the magnetization versus magnetic field M(H) or temperature M(T) in the range of 2 to 320K. From both curves magnetic parameters like saturation magnetization, coercive field and others can be extracted. To avoid the movement of the samples inside a plastic tube, the samples were fixed by a plastic plaster to the tube in which both the plaster and the tube have weak diamagnetic signal. However, there is one difficulty with VSM measurement, that is, it has low resolution$10^{-6}emu\ or\ 10^{-5}emu$.

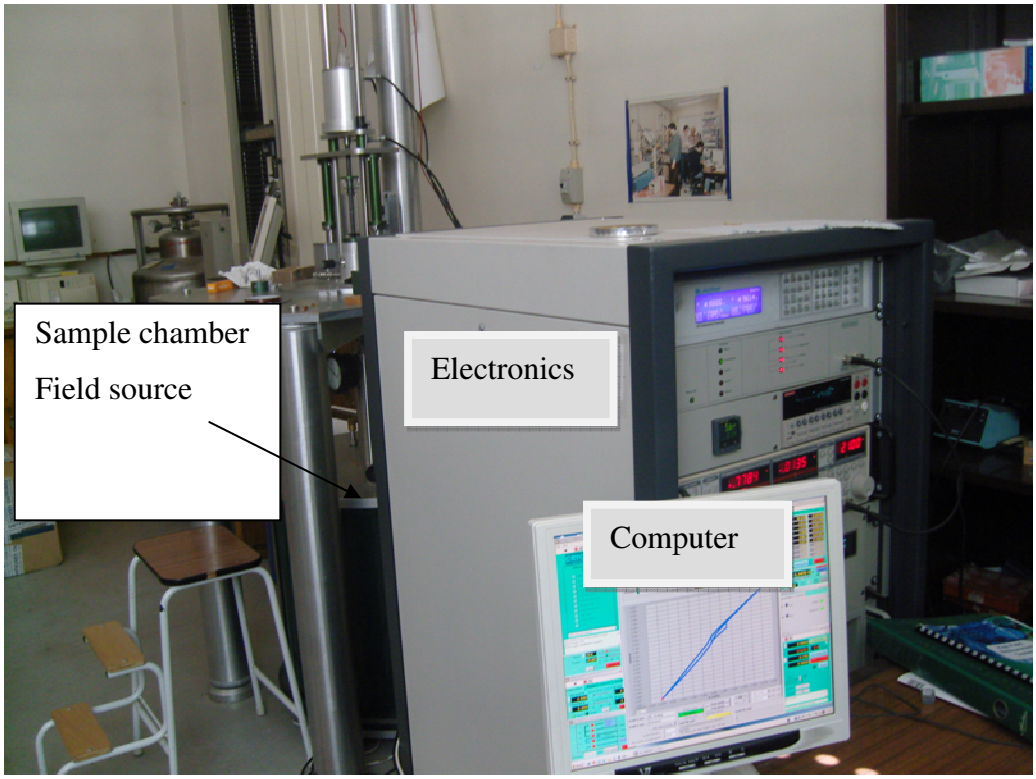

Figure 3. 5 Photo of VSM.

For thin films with small signals lower than this resolution, the VSM is not preferred for magnetic measurement since it will not detect the hysteresis loop, because of diamagnetic properties of substrates. The presence of the diamagnetic substrates give the measured magnetization curves from VSM or SQUID magnetometer a negative slope like the one shown in the Figure 3.6 (a) below. For further analysis of the magnetization hysteresis curves, the substrate contribution should be removed from the curve. This was done by subtracting the substrate contribution from the original data, that is, $M_{corrected} = M_{measured} - \chi_{dia}H$, where χ_{dia} is the high field slope after saturation. The corrected M(H) hysteresis loop show horizontal curve after saturation as shown in the Figure 3.6 (b) below. Some of Ni-Mn-Ga alloy thin films on some substrates we produced were so thin that they did not give enough magnetic signals using VSM. Thus, for these films Superconductor Quantum Interference Device Magnetometer (SQUID) at the University of Porto were used to obtain their hysteresis loops and magnetization versus temperature curves.

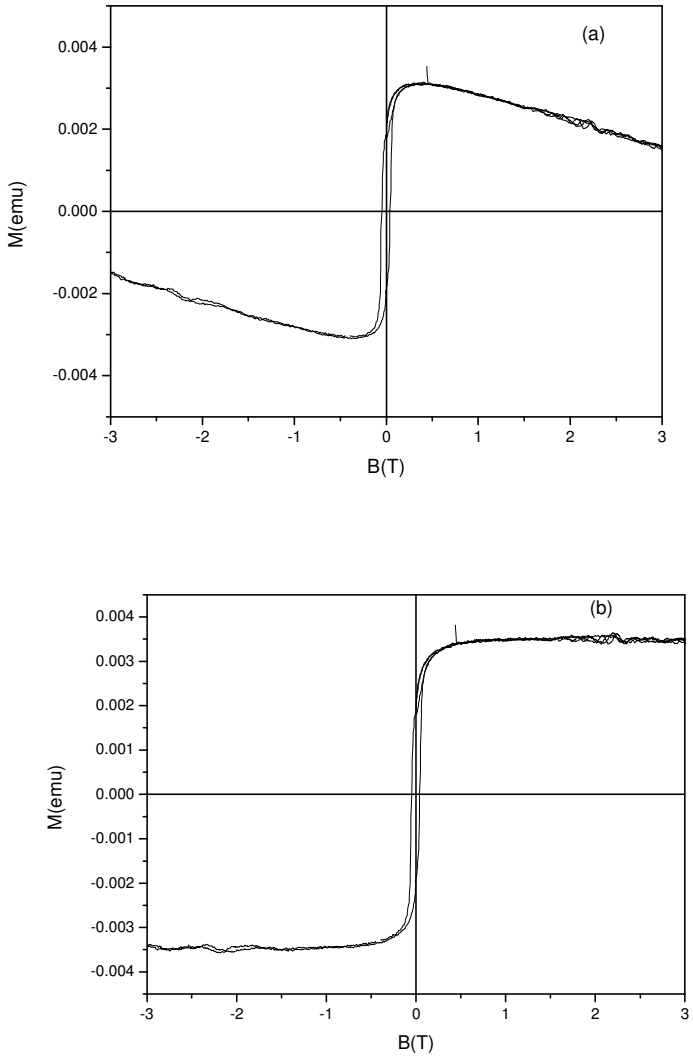

Figure 3. 6 M(H) hysteresis loop (a) from the original data and (b) after removing substrate contribution for the sample of Ni-Mn-Ga/Al_2O_3.

3.2.3 Superconducting Quantum Interference Device (SQUID) Magnetometer

Superconductor Quantum Interference Device (SQUID) Magnetometer can be used to measure a magnetization (M) of a sample with high precision as a function of parameters such as external magnetic field (H) or temperature (T). This system is equipped with SQUID which is a very sensitive device that can detect magnetic flux as small as $\sim 10^{-14}\ Tesla$ by superconducting loops containing Josephson junctions. In fact, SQUID

magnetometer consists of the following basic components: a superconducting magnet, a superconducting detection coil (pick-up coil), a SQUID and a superconducting magnetic shield. The magnetic sensitivity the SQUID magnetometer is about$10^{-7} - 10^{-8} emu$. A schematic of a SQUID magnetometer is shown in the Figure 3.7 below. The sample to be measured is inserted inside the pick-up coils. When this sample moves it produce an alternating magnetic flux in the pick-up coils which leads to an alternating output voltage in the SQUID. The output signal is then amplified and read out by the magnetometer electronic. The output signal is proportional to the magnetic moment of the sample which can be magnetized by a magnetic field produced by the superconducting magnet.

The Quantum Design MPMS Magnetometer which was used to measure some Ni-Mn-Ga/ substrate thin films in this work can operate in temperature range between 2 and 400K and magnetic fields up to 5.5T. However, magnetic fields used for M(H) measurement were up to $\pm 2T$ and for M(T) measurement was at 0.1T. Its picture is shown in Figure 3.7 below. As in VSM, to avoid the movement of the samples inside a plastic tube, the samples were fixed by a plastic plaster to the tube in which both the plaster and the tube have weak diamagnetic signal.

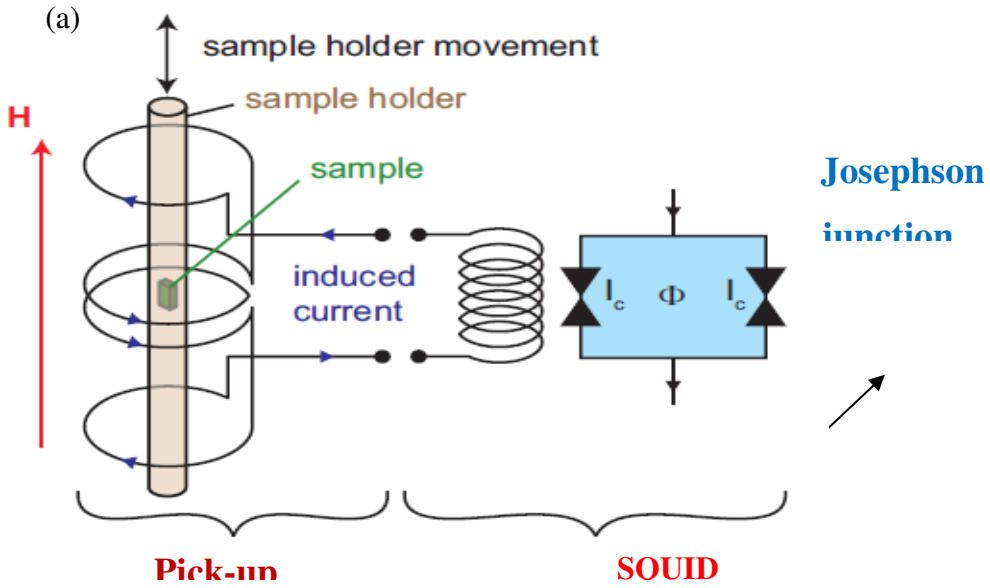

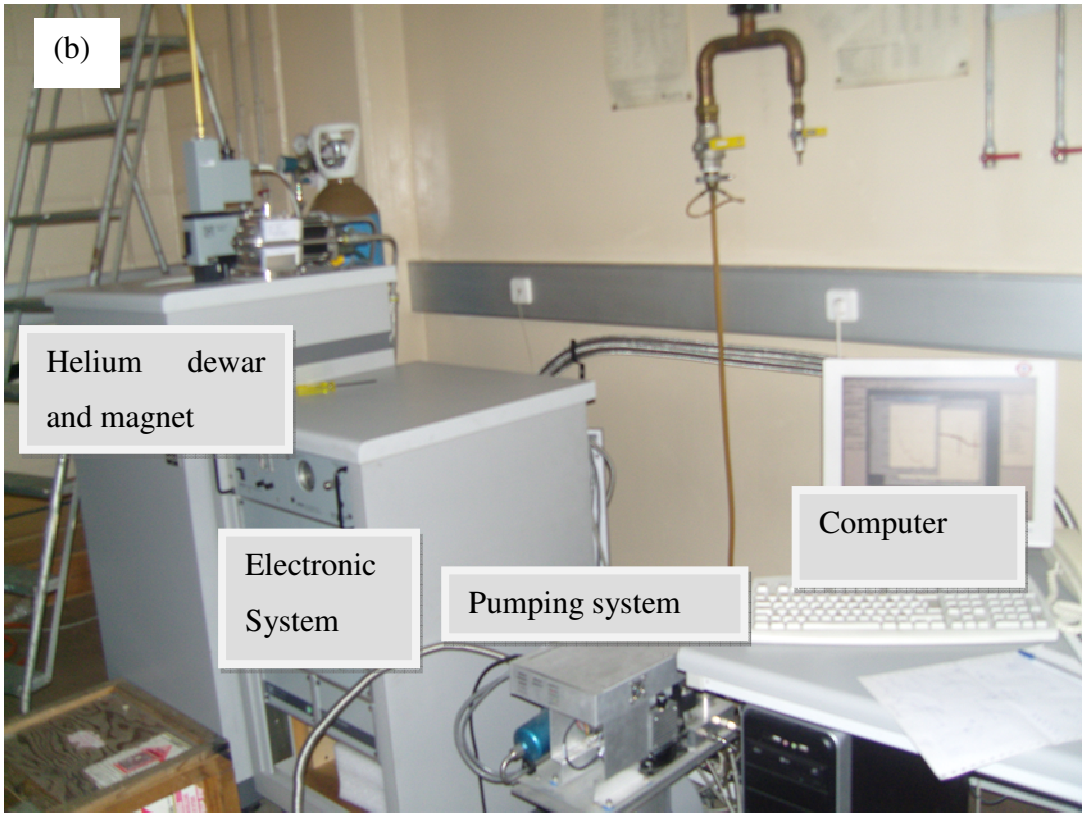

Figure 3. 7 (a) A Schematic illustration of SQUID magnetometer [64] and (b) Photo of SQUID.

3.3 Magnetoelectric (ME) Measurement

To study magnetoelectric effect different measurement methods (techniques) by many researcher groups have been used such as using SQUID, VSM, AFM and Lock-in technique. As a result of using these different techniques, results may differ even for the same materials. In this work, a lock-in technique was used to study the magnetoelectric effect in composite of FMSAs, Ni-Mn-Ga film and piezoelectric substrate PMN-PT. The detailed description about the experiment can be found in paper written by G.V. Duong et al. [65]. The schematic of experimental set up and the photo of the equipment are shown in the Figure 3.8 (a) and (b), respectively, below. A power supply provides current to coils in the electromagnets. The electromagnetic in the set up is used to produce a DC magnetic field up to 15kOe. Near to this electromagnet, Helmholtz coils are used to produce AC magnetic field which is superimposed with the DC field. The frequency of the AC signal can be changed up to 100 kHz and its amplitude can be up to 10Oe. In such kind of experimental set up, the direct magnetoelectric effect is observed very easily, that is

measuring voltage or electric field by applying magnetic field. The sample to be measured is placed in the field with its surface perpendicular or parallel to the field direction, according to the longitudinal and transverse measurement, respectively. The DC field between the electromagnets is measured by using Hall probe. The magnetoelectric voltage can be measured by the lock-in amplifier which has an input resistance of 100MΩ. The measured signal is processed by transferred the signal to a computer interfaced with Labview program.

When the magnetoelectric material is exposed to an external magnetic field, the voltage V appears in these materials and this voltage can be written as

$$V(H) = f(H) = const. + \alpha H + \beta H^2 + \gamma H^3 + \delta H^4 +$$

$$\Rightarrow \frac{dV}{dH} = \alpha + 2\beta H + 3\gamma H^2 + 4\delta H^3 + \cdots. \quad (3.2)$$

If the external magnetic field is filed due to bias DC field from electromagnet and a small AC field ($h = h_0 sin\omega t$) from Helmholtz coils, then the total field can be written as

$$H_{total} = H + h_0 sin\omega t. \quad (3.3)$$

Up on substituting H_{total} in the V expression, we can obtain

$$V = const. + \alpha(H + h_0 sin\omega t) + \beta(H + h_0 sin\omega t)^2 + \gamma(H + h_0 sin\omega t)^3 + \delta(H + h_0 sin\omega t)^4 + \cdots. \quad (3.4)$$

After expanding the powers, simplified form of equation 3.4 is given by

$$V = \{(const. + 4\beta h_0^2 + 3\delta h_0^4 + 8\alpha H + 12\gamma h_0^2 H + 8\beta H^2 + 24\delta h_0^2 H^2 + 8\gamma H^3 + 8\delta H^4) (8\alpha h_0 + 6\gamma h_0^3 + 16\beta H h_0 + 24\delta H + 24\gamma h_0 h_0^3 H^2 + 32\delta h_0 H^3 sin\omega t) + (-4\beta h_0^2 - 4\delta h_0^4 - 12\gamma h_0^2 H - 24\delta h_0^2 H^2) cos2\omega t + \cdots\} \quad (3.5)$$

The output Voltage from the lock-in amplifier is then given by

$$V_{out} = \frac{1}{8}(8\alpha h_0 + 6\gamma h_0^3 + 16\beta h_0 H + 24\delta h_0^3 H + 24\gamma h_0 H^2 + 32\delta h_0 H^2)$$

$$V_{out} = \frac{H^4}{8}\left[\frac{8\alpha}{H^3}\left(\frac{h_0}{H}\right) + \frac{6\gamma}{H}\left(\frac{h_0}{H}\right)^3 + \frac{16\beta}{H^2}\left(\frac{h_0}{H}\right) + 24\delta\left(\frac{h_0}{H}\right)^3 + \frac{24\gamma}{H}\left(\frac{h_0}{H}\right) + 32\delta\left(\frac{h_0}{H}\right)\right]. \quad (3.6)$$

When $h_0 \ll H$, higher order terms can be neglected and the voltage output can be written as

$$V_{out} = h_0(\alpha + 2\beta H + 3\gamma H^2 + 4\delta H^3) = h_0\left(\frac{dV}{dH}\right). \quad (3.7)$$

Therefore, the magnetoelectric voltage coefficient is given by

$$ME\ coefficient = \alpha_{ME} = \frac{dE}{dH} = \frac{1}{d}\left(\frac{dV}{dH}\right) = \frac{V_{out}}{h_0 d}, \quad (3.8)$$

where d is the effective thickness of the piezoelectric phase. This technique allows us to measure voltage (V_{out}) that appear across the sample as a function of DC bias field.

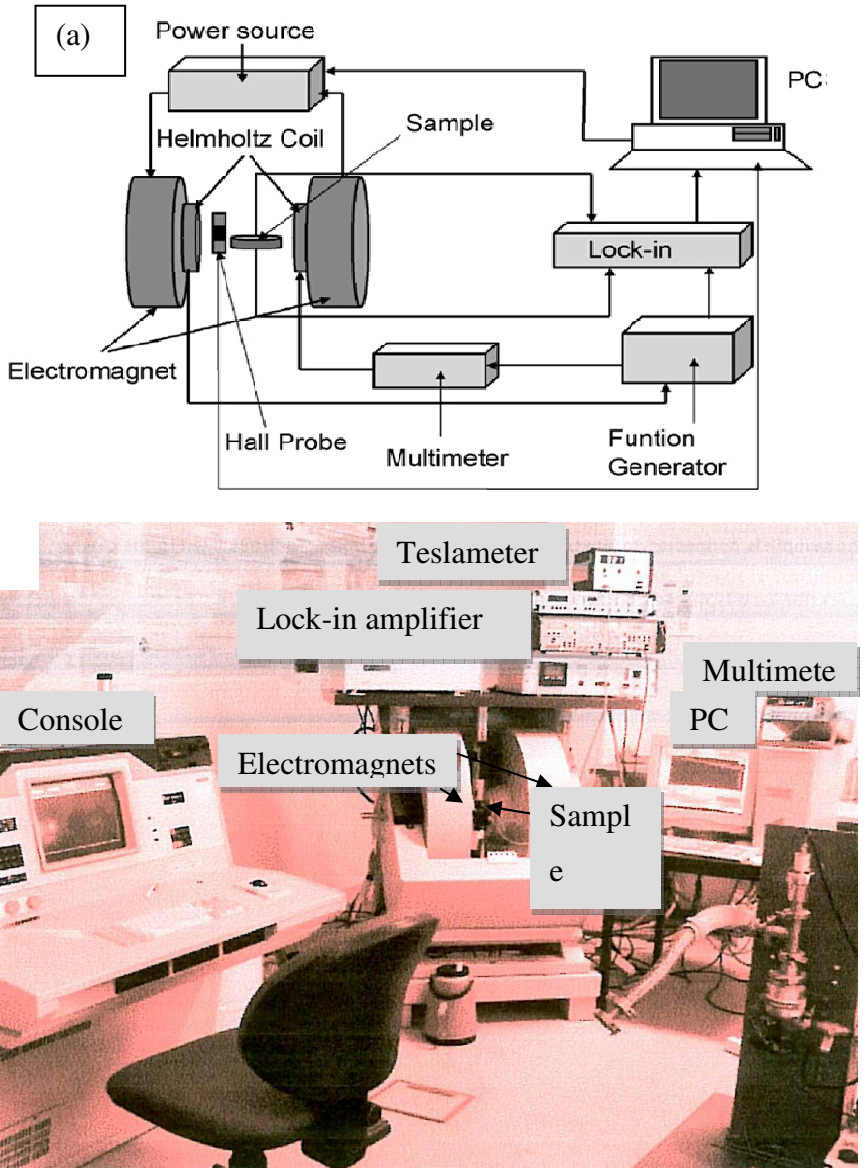

Figure 3. 8 (a) Schematic [65] and (b) Photo of Experimental set up.

4 Results and Discussion

In the present work, Ni-Mn-Ga alloy thin films were deposited on different substrates as mentioned in the experimental part of this report using different deposition conditions by means of RF magnetron co-sputtering of two targets namely $Ni_{50}Ga_{50}$ and $Ni_{50}Mn_{50}$. Knowing the calibrated deposition rates, thicknesses of Ni-Mn-Ga thin films are calculated as 35nm, 70nm, and 210nm for the films deposited at deposition temperature of 320^0C, 370^0C, and 400^0C, respectively. The area of all samples was measured by scanning the samples using scanner. The area and thickness later are used to calculate the volume of the films and magnetization in emu per unit volume. The samples structural properties were characterized by XRD and magnetic properties were characterized by VSM, SQUID, and MFM. Moreover, ME measurements on samples with PMN-PT substrate were done to see the coupling between the film of Ni-Mn-Ga FSMA and piezoelectric substrate PMN-PT. The results of these measurements are presented and discussed as follows.

4.1 Structure

4.1.1 XRD Result for Ni-Mn-Ga/Al_2O_3(0001) film

Figure 4.1 shows the XRD $\theta - 2\theta$ scan from bare Al_2O_3 (0001) substrate and other two Ni-Mn-Ga/Al_2O_3(0001) films deposited at substrate temperatures of 370^0C and 400^0C. As it can be seen from the figure, strong reflection from the Al_2O_3 substrate was obtained at $2\theta \approx 43.38^0$, indicating that this single crystal substrate is highly (000l) oriented. The film deposited at substrate temperature of 370^0C exhibits peak at $2\theta \approx 44.13^0$ which can be indexed as $(220)_c$ cubic which correspond to austenite phase of the alloy [66]. A small peak at the shoulder of this peak at $2\theta \approx 44.21^0$ with smaller intensity is observed for the film which can be indexed as $(202)_t$ of martensite phase of the alloy [67]. Two phases coexist in the film. The film deposited at substrate temperate of 400^0C has also two peaks at the angle of diffraction of $2\theta \approx 43.38^0$ and $2\theta \approx 44.13^0$ but with different values of intensities which implies that the amount of martensite phase of the alloy in this case is more than that of the austenite phase. Though, it is very difficult to determine the amount of each phase present in the films, we can roughly speak the amount of phases present by assuming that only these two phases exist. Indeed, the x-ray showed that the films are

partially crystalline but from the two phases we can have rough estimation about the amount of the two phases present by neglecting the amorphous part. In the first case the amount of austenite phase (72.8%) is roughly two and half times the martensitic phase (27.2%) and in the second case the austenite phase (34.7%) is almost half of the martensite phase (65.3%). Thus, one can say that the increase of substrate temperature increase the amount of martensite phase.

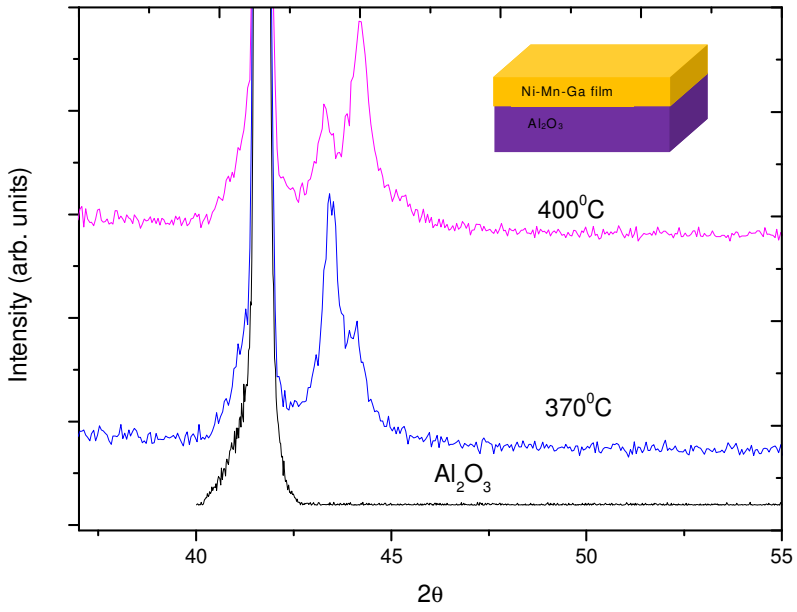

Figure 4. 1 XRD $\theta - 2\theta$ scan of bare Al_2O_3 substrate and Ni-Mn-Ga films deposited at substrate temperature of 370^{0}C and 400^{0}C.

4.1.2 XRD Result for Ni-Mn-Ga/PMN-PT thin film

Figure 4.2 depicts the XRD $\theta - 2\theta$ from bare PMN-PT(100) substrate and from thin films of Ni-Mn-Ga/PMN-PT(100) deposited at substrate temperatures of 320^{0}C, 370^{0}C, and 400^{0}C. Three very pronounced and sharp peaks as shown in the measured x-ray diffraction originates from the single crystalline PMN-PT (l00) (for l=1, 2, 3) substrate. Because of the high intensities of the peaks from the substrate, it is very difficult to identify peaks from the film unambiguously. In spite of this difficulty peaks from the film at the shoulder of the middle high peak of the substrate are observed with angle of diffraction $2\theta \approx 43.24^0$ for films deposited at substrate temperatures of 320^{0}C and 370^{0}C which can be

indexed as $(220)_c$ cubic austenite phase of the alloy [68] or as $(112)_t$ martensite phase of the alloy [68, 10] , see part b in the figure. Moreover, for the film deposited at the substrate temperature of 400^0C another peak appears at the angle of $2\theta \approx 50.58^0$ which cannot be assigned unambiguously.

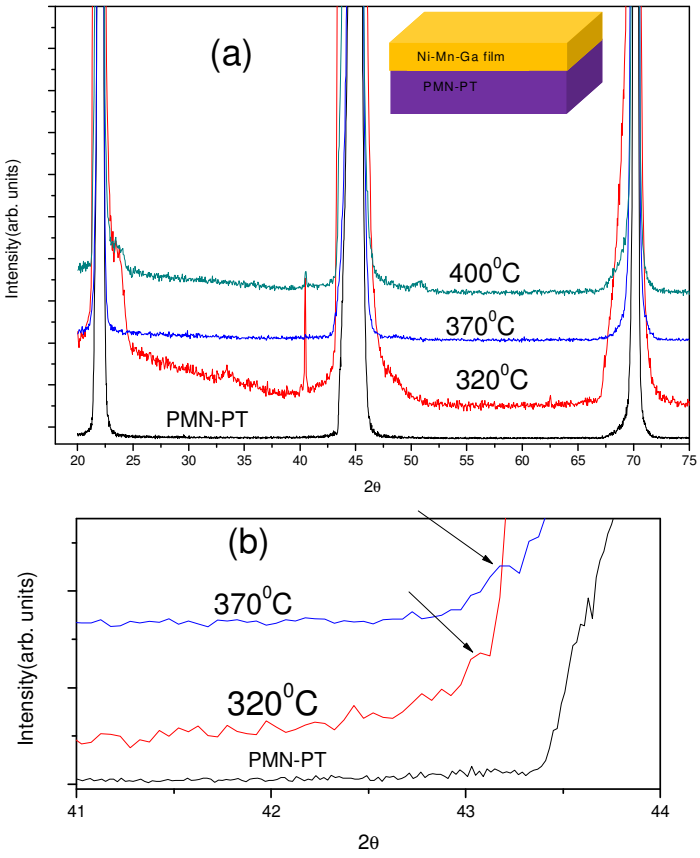

Figure 4. 2 XRD $\theta - 2\theta$ scan of bare PMN-PT substrate and Ni-Mn-Ga/PMN-PT films deposited at substrate temperature of 320^0C, 370^0C and 400^0C.

4.1.3 XRD Results for Ni-Mn-Ga/MgO thin film

Figure 4.3 depicts the XRD $\theta - 2\theta$ from bare MgO (100) substrate and from thin films of Ni-Mn-Ga/MgO (100) deposited at substrate temperatures of 320^0C and 370^0C. Strong peak from the substrate at $2\theta \approx 42.72^0$ is observed. For the film deposited at substrate temperature of 320^0C two distinctive convolutions of peaks close to $(200)_c$ austenite lines are observed. These peaks are due to martensite phase. However, a peak observed at $2\theta \approx 66.78^0$ which close to $(400)_c$ austenite phase line does not show convolution of

peaks [69, 66]. The film deposited at substrate temperature of 370^{0}C exhibits more additional peaks. Peaks observed at $2\theta \approx 38.55$ for the two films correspond to k_β-radiation. The films showed broad diffraction peaks which indicate partially crystalline nature of the films. Because of the broadness of the peaks at $2\theta \approx 66.78^0$, it is difficult to associate a phase to this peak unambiguously. However, if the peak is due to austenite phase, then the film posses mixed phases of martensite and austenite.

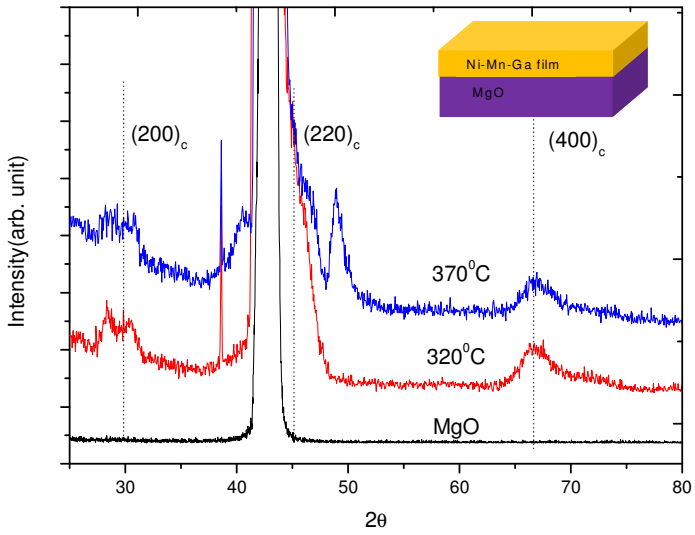

Figure 4. 3 XRD $\theta - 2\theta$ scan of bare MgO substrate and Ni-Mn-Ga/MgO thin films deposited at substrate temperatures of 320^{0}C and 370^{0}C.

4.1.4 XRD Results for Ni-Mn-Ga/STO thin film

The XRD pattern of bare STO substrate and Ni-Mn-Ga/STO thin films deposited at substrate temperatures of 320^{0}C, 370^{0}C, and 400^{0}C are show in the Figure 4.4 below. As it can be seen from the figure strong reflections from the bare substrate is observed at $2\theta \approx 46.23^0$. For the film deposited at substrate temperature of 320^{0}C, there is no peak observed. But for the film deposited at substrate temperature of 370^{0}C very small peaks $2\theta \approx 44.19^0$ from the film are observed which can be indexed as $(202)_m$ or $(112)_t$ martensite phase of the alloy or (220)c austenite phase of the alloy [68, 70]. This peak is dominated by the peak from the substrate. Moreover, the intensity of this peak is very

small which may indicate that small amount of crystalline phase exits or the film is dominantly amorphous phase.

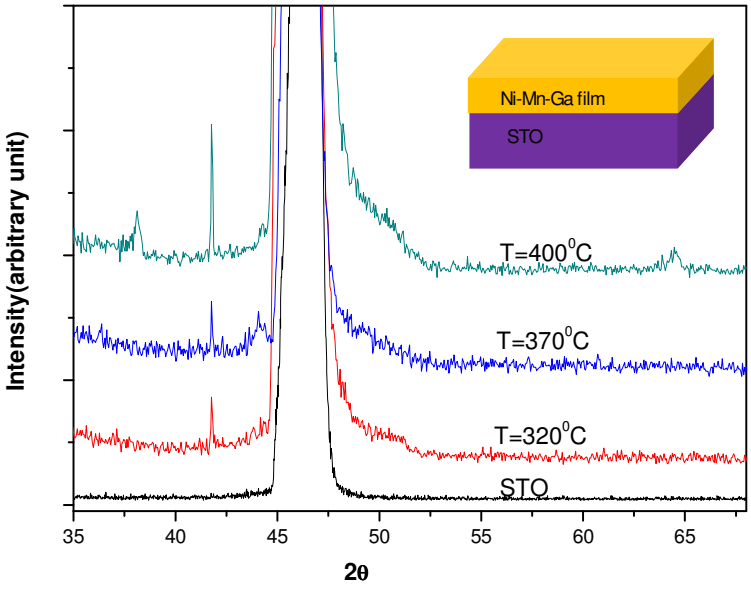

Figure 4. 4 XRD $\theta - 2\theta$ scan of bare STO substrate and Ni-Mn-Ga/STO thin films deposited at substrate temperatures of 320^{0}C, 370^{0}C and 400^{0}C.

However, if we compare crystalline phase (or amorphous phase) between the two films, the film deposited at substrate temperature of 370^{0}C has more crystalline phase. For the film deposited at 400^{0}C peaks at $2\theta \approx 38.21^0$ and $2\theta \approx 64.44^0$ are observed. Peaks observed at $2\theta \approx 41.81^0$ corresponds to k_β-radiation. The XRD data showed that degree of crystalline increases as the substrate temperature increases.

In general, the above XRD data from all the films showed that the films deposited on different substrates at different substrate temperatures are partially crystalline. The angular position of peaks for different substrates are different which may indicate that an influence of the substrates on the films microstructure. Moreover, overall results suggest that the phases present in the films vary with substrate and its deposition temperature. However, reasonable interpretation of the crystallographic state of the films at room temperature can be suggested taking into account the whole set of experimental results obtained in this work. In any case, one or two peaks in XRD pattern are not enough for rigorous crystallographic analysis. Thus, it is hard to identify unambiguously the martensite

structure in these films and additional characterizations (or measurements) such as magnetization versus temperature, electrical resistivity versus temperature are needed to indentify clearly the phases present at room temperature in the films.

4.2 Magnetic and Piezoresponse Measurements

4.2.1 Vibrating Sample Magnetometer and Superconducting Quantum Interference Device Magnetometer

The magnetization versus magnetic field hysteresis loops of all films as-deposited were measured by using Vibrating Sample Magnetometer (VSM) and superconducting quantum interference device (SQUID) magnetometer. All the hysteresis loops were obtained for magnetic field applied parallel to plane of direction of films. The magnetization curves for some films were measured by using SQUID since it was very difficult to get measurable signals by VSM. The measured hysteresis loops at room temperature and 5K are presented as follows according to substrate deposition temperature.

The magnetizations versus magnetic field curves for films deposited at substrate deposition temperature of 320^0C at room temperature are shown in the Figure 4.5 below. At this substrate deposition temperature all the films showed ferromagnetic behavior except the film with STO substrate. For this group of films, magnetization values are very small as compared to other batches, see table 4.1. The substrate temperature was not enough to get crystalline films; instead films are dominantly amorphous as it is confirmed by the XRD results.

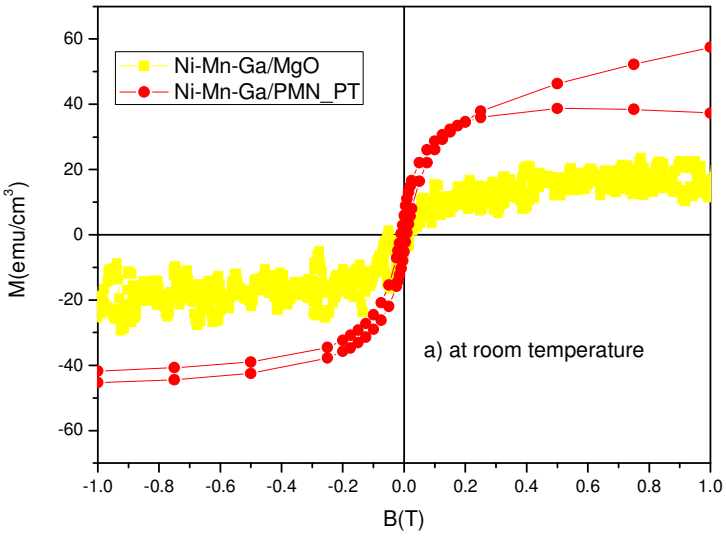

Figure 4. 5 M-H loops of Ni-Mn-Ga thin film measured at room temperature and deposited on different substrates at substrate temperature of 320^{0}C.

The hysteresis M(H) loops for films deposited at substrate temperature of 370^{0}C are shown in the Figure 4.6 below. These magnetization curves have been obtained at 5K and room

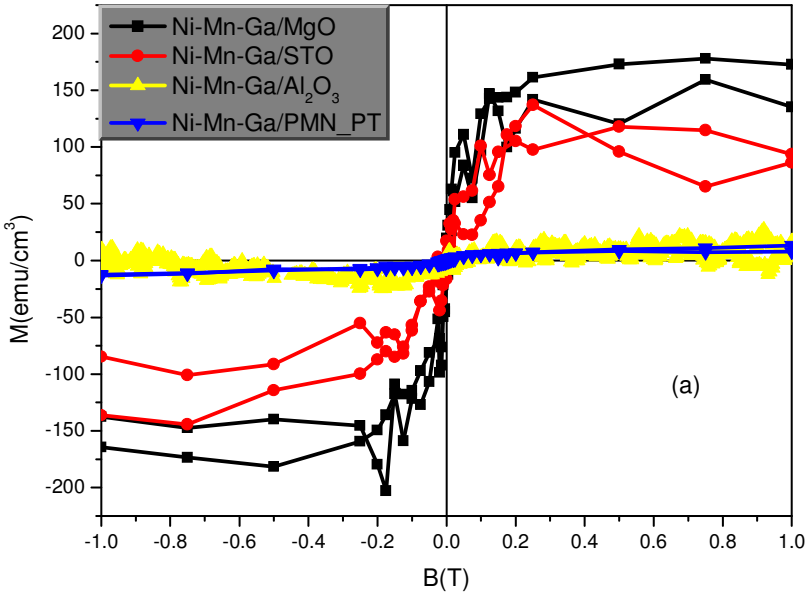

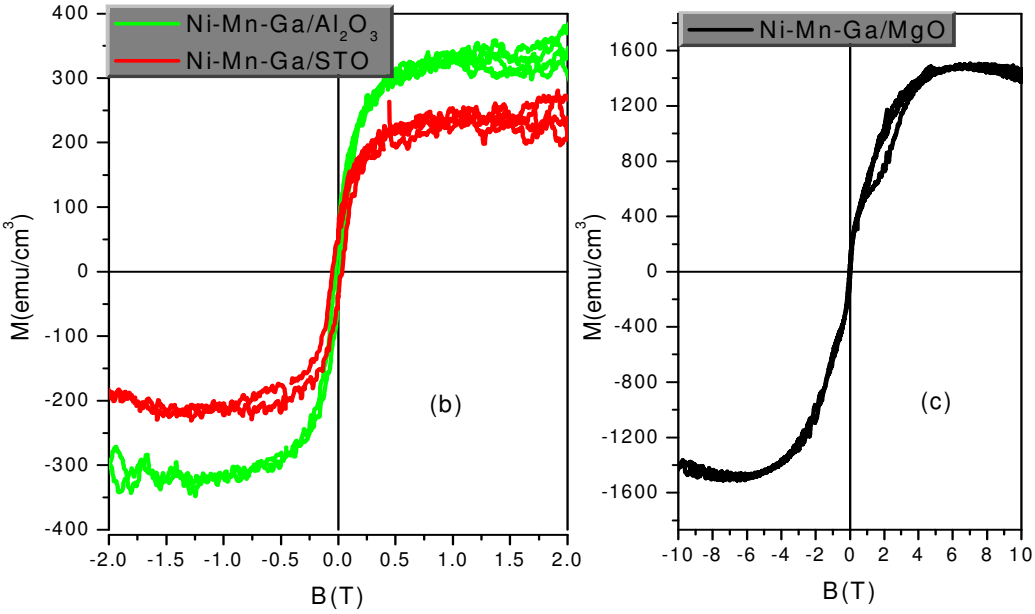

Figure 4. 6 M(H) hysteresis loops for films deposited at substrate temperature of 370^{0}C: (a) for all films measured at room temperature, (b) for Ni-Mn-Ga/STO and Ni-Mn-Ga/Al_2O_3 films measured at 5K and, (c) for Ni-Mn-Ga/MgO film measured at 5K.

temperature. As it can be seen in the Figure 4.6 (a), all films are ferromagnetic at room temperature. However, the saturation magnetization values obtained from all the curves in the above figure for these films at room temperature and at 5K are different as shown in table 4.1. Moreover, as shown in the Figure 4.6 b and c the behaviors of M(H) hysteresis curves at 5k for the films are different. In the case of Ni-Mn-Ga/MgO thin film, close inspection of its M(H) curve showed hysteresis loop and the magnetization saturates at higher fields. When the magnetic field reaches 0.99T the change in magnetization becomes less and a steeper jump like magnetization occurs. When the field decreases from saturation, the magnetization does not follow the previous path but a jump like decrease occurs at lower field, resulting in increased hysteresis in the first quadrant of magnetization loop. The same type of behavior is observed in the fourth quadrant with small hysteresis. The jump like behavior may be associated to the reorientation or redistribution of martensite variants, which occurs at fields sufficiently high to move twin boundaries. The differences in magnetization curves clearly show that the magnetic characteristics of Ni-Mn-Ga films depend on nature of substrate which may affect the crystallography, substructure, and residual stress of the films. The saturation magnetization value and

saturation magnetic field for the film with MgO substrate as shown in the Figure 4.6 c are strange values. Because of these strange values the measurement was done two times and the results were more or less the same. The saturation magnetization value is four times greater than the magnetization value of other Ni-Mn-Ga films in the same batch. This happens probably due to the composition of the film may be different or due to contamination of the film. There is no any clear experimental evidence that justifies the strange values (high saturation magnetization and saturation field) so far done in this work. The measured hysteresis loops for samples deposited at substrate temperature of 400^0C are shown in the Figure 4.7 below. The measurements of the magnetization curves were done at room temperature and 5K. As it can be seen from the curves and their analysis,

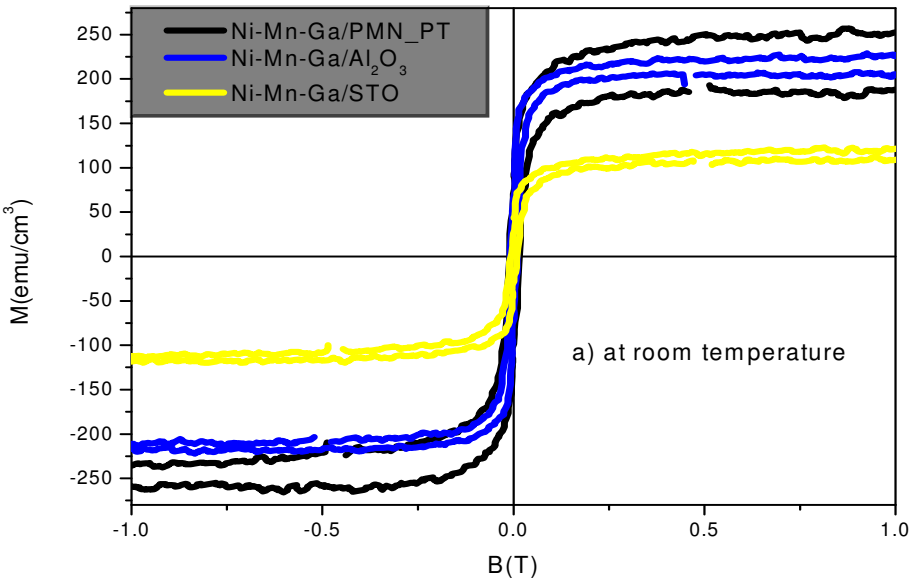

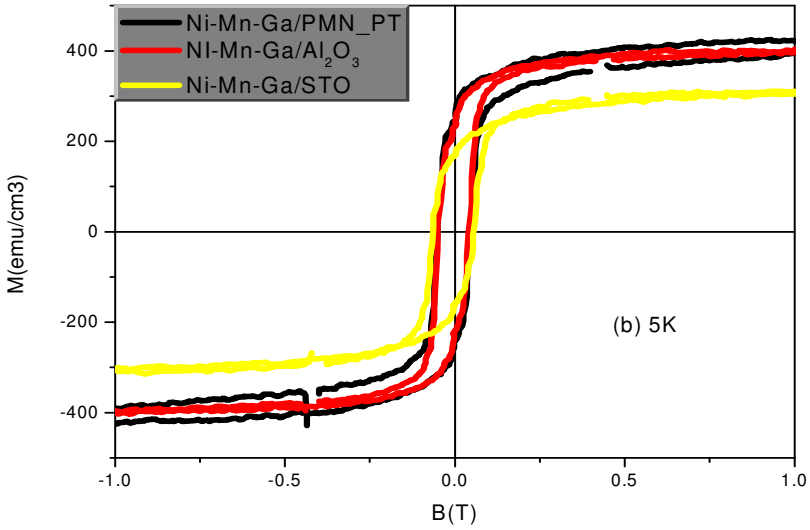

Figure 4. 7 M-H loops of Ni-Mn-Ga thin film measured at temperature of a) 304K and b) 5K on different substrates deposited at substrate temperature of 400^{0}C

Table 4. 1 Curie temperature, saturation magnetization and coercive fields at 300K and 5K of Ni-Mn-Ga on different substrates.

Deposition temperature (^{0}C)	Sample	Magnetization (emu/cm^3)		Coercive field(Oe)		Tc(K)
		@5K	@300K	@5K	@300K	
320^{0}C	Ni-Mn-Ga/MgO	--------	17	--------	--------	--------
	Ni-Mn-Ga/PMN-PT	--------	40	--------	103	--------
370^{0}C	Ni-Mn-Ga/Al_2O_3	327	10	158	--------	--------
	Ni-Mn-Ga/MgO	1490	170	347	66	--------
	Ni-Mn-Ga/PMN-PT	--------	10	--------	99	--------
	Ni-Mn-Ga/STO	200	120	354	63	--------
400^{0}C	Ni-Mn-Ga/STO	340	120	584	88	345
	Ni-Mn-Ga/PMN-PT	400	250	479	154	337
	Ni-Mn-Ga/Al_2O_3	405	225	400	96	348

films deposited at different substrates exhibit soft ferromagnetic properties which is characterized by low coercive fields and narrow hysteresis loops. The soft magnetic property may be an indication that magnetic property comes from a single phase. The value of coercive fields and saturation magnetizations for these samples are tabulated as shown in table 4.1 above. The saturation magnetization values vary from 120emu/cm^3 to 250emu/cm^3 which shows the role of substrate type on the magnetic property of the Ni-Mn-Ga thin films. Even though the difference is not very exaggerated, film with $SrTiO_3$ substrate showed the least saturation magnetization value among all the films while films with PMN-PT and Al_2O_3 substrate showed more or less the same value. The saturation magnetization of Ni-Mn-Ga film on STO(100) substrate has showed value of 120emu/cm^3 at room temperature. The saturation magnetization values obtained for the film with STO substrate is less than the others may be due to its roughness. The STO substrate was used on the non-polished side during sample preparation as it also confirmed by the AFM measurement presented in the next section. Hence, the film microstructure and its magnetic properties are affected accordingly. The magnetization of the film with PMN-PT substrate at room temperature attains 30emu/g while the bulk Ni-Mn-Ga alloy has magnetization of 65emu/g at room temperature [71]. The saturation magnetization values 30emu/g and 65emu/g were obtained by using density $\rho = 8.16 g/cm^3$. Not only of difference in magnetization of films on different substrates is observed but also some differences in coercive field of films which are 154Oe for STO, 88Oe PMN-PT substrate and 96Oe Oe for Al_2O_3 substrate is observed.

The M-H hysteresis loops for the same set of samples measured at temperature of 5K are shown in the Figure 4.5 b) above. Magnetic parameters (saturation magnetization and coercive field) for these films are extracted from these curves and are listed in table 4.1. As one can see from the table and the graph, film with PMN-PT and Al_2O_3 substrate showed highest and almost the same saturation magnetization while film with $SrTiO_3$ showed the lowest value saturation magnetization among the samples. But the saturation magnetization values for these films at this temperature are higher as compared to its value at room temperature as expected. Magnetization value varies from 340emu/cm^3 to 405emu/cm^3, which shows that the saturation magnetization at this temperature is also

dependent on the nature of substrate like the above case. But for films with substrate PMN-PT and Al_2O_3, the saturation magnetization has almost the same value. Not only the magnetization values at 5K with respect to magnetization at room temperature are increased but also the coercive fields for all of these films are increased.

In general from the observation of M(H) hysteresis measurement, the magnetic (or ferromagnetic) properties of the films dependence on the nature of substrate and growth (or substrate) temperature. Interestingly, the saturation magnetization per unit volume for all the films increases significantly on increasing the substrate temperature with some minor inconsistency that may be due to measurement problems, see table 4.1. The nature of substrate and substrate deposition temperature are seemingly main factors determining the degree of crystalline state of the films.

The temperature dependence of magnetization measurements, M(T), for the films deposited at substrate temperature of 400^0C were carried out with SQUID magnetometer. This measurement was done to identify the structural (martensite to austenite if possible) and magnetic transition (Curie) temperature. These magnetization curves are shown in the Figure 4.8 below. The magnetization curves can provide signature of structural transition (T_m) by showing an anomaly (a sudden increase or decrease) in magnetization and magnetic transition (T_c) by showing a drop in magnetization upon heating. However, the observation of magnetization curves reveals that they reflect only magnetic transition and no separate signature of structural transition was noticed in contrast to stoichiometric Ni_2MnGa, where $T_c = 373K$ and $T_m = 200K$[33]. The Curie temperature is very clear to observe in the curves and it is extracted from the curves in the following way.

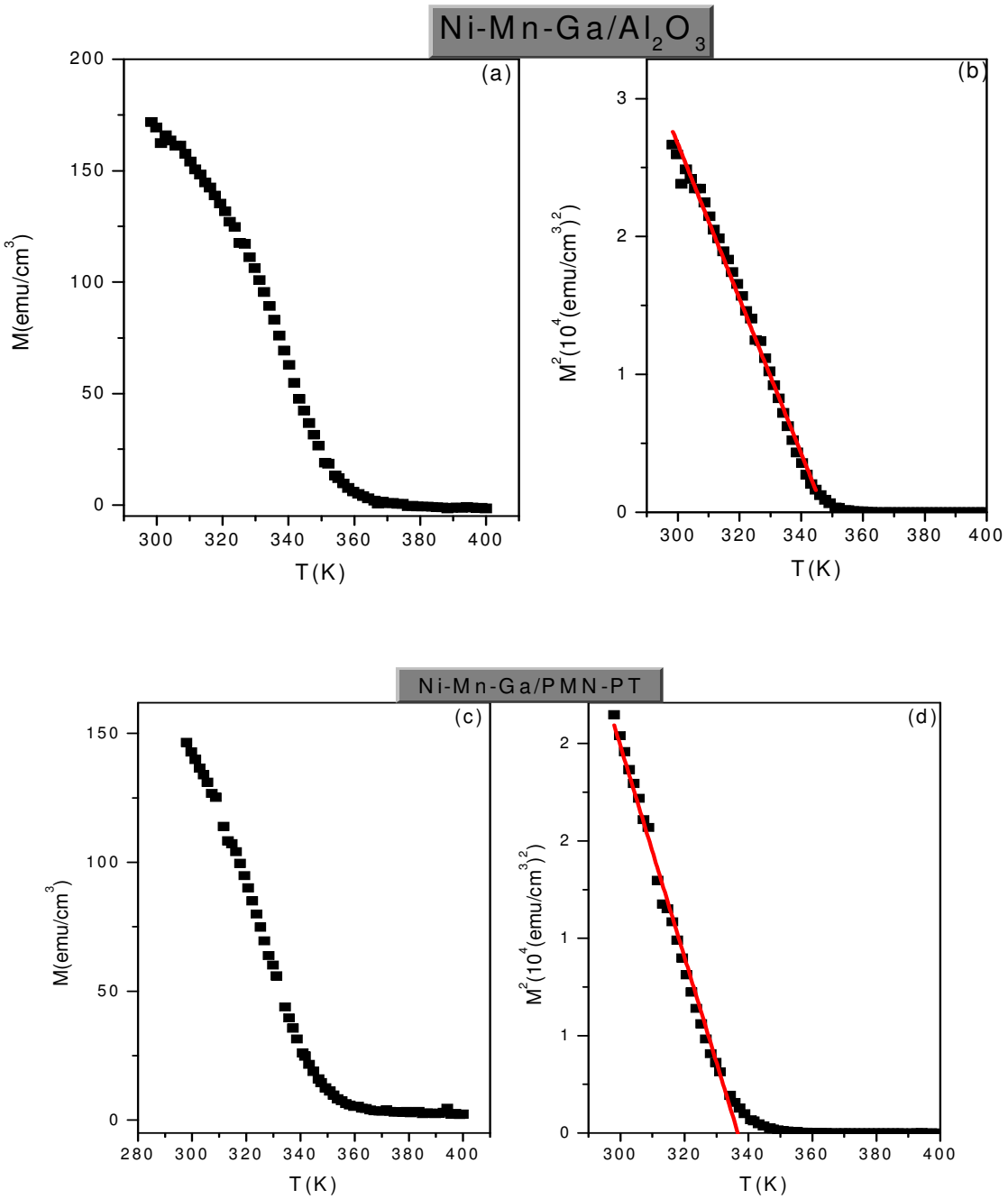
Ni-Mn-Ga/Al2O3
(a)
(b)
M(emu/cm3)
M2(10^4(emu/cm3)2)
T(K)
Ni-Mn-Ga/PMN-PT
(c)
(d)
M(emu/cm3)
M2(10^4(emu/cm3)2)
T(K)

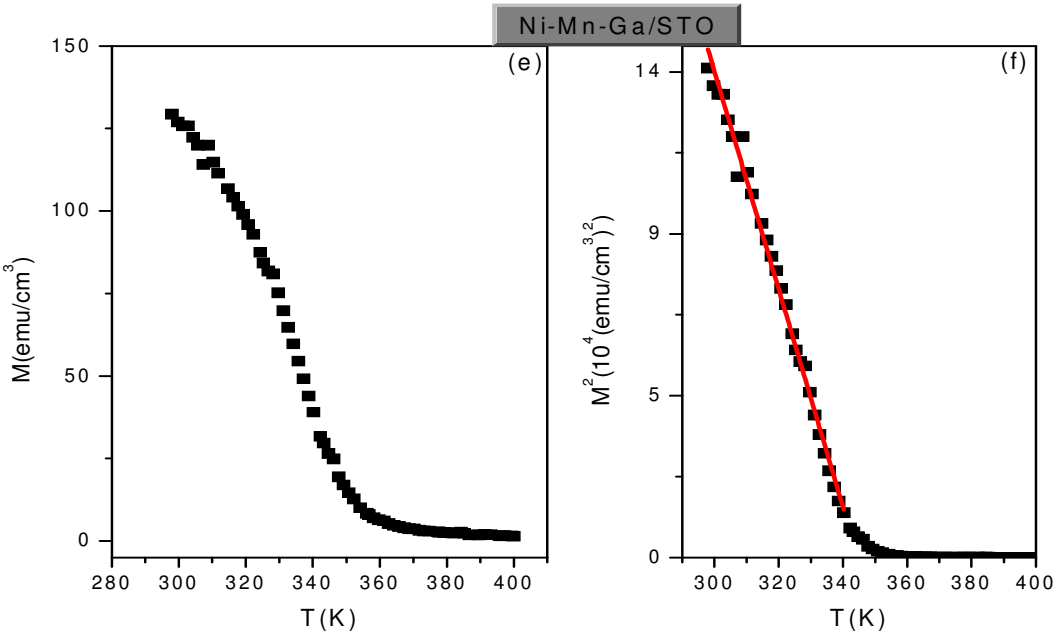

Figure 4. 8 The temperature dependence of magnetization for Ni-Mn-Ga/Al_2O_3 (a), Ni-Mn-Ga/PMN-PT (c), and Ni-Mn-Ga/STO films. Straight line fitted to the linear range of M^2(T) for Ni-Mn-Ga/Al_2O_3 (b), Ni-Mn-Ga/PMN-PT (e), and Ni-Mn-Ga/STO (f) films.

For these films, following the mean field approximation the square of magnetization $M^2(T)$ is approximately linear in temperature range near below T_c. Thus, the value of T_c has been determined by extrapolating the linear part of $M^2(T)$ to $M = 0$. The values of the Curie temperature for these films are found to be above room temperature and the values are 337K, 345K, and 348K. Even though, the ferromagnetic to paramagnetic curie transition was clearly observed for these films, the absence of a separate observation of martensite transition in the magnetization curves may be due to the small change in the magnetization value during the occurrence of martensitic transition in the films or may be due to occurrence of magneto-structural transition. Indeed, this needs further study to understand the structural transition.

4.2.2 Magnetic Force Microscopy (MFM)

The magnetic property of three batches of samples deposited at different substrate temperatures was also characterized by magnetic force microscopy (MFM). This characterization technique is more sensitive for samples with magnetic moments which are oriented along the perpendicular direction to the surface (out-of-plane direction). The

results of this measurement are organized in to three groups in the following sections based on the deposition substrate temperature.

4.2.2.1 The MFM Result for films deposited at substrate temperature of 320^0C

The AFM topography and MFM image of Ni-Mn-Ga thin films deposited on different substrates at substrate temperature of 320^0C are depicted in the Figures 4.7-4.9 below. The thickness of the films for this batch is calculated to be 35nm. The topography image of the Ni-Mn-Ga thin film on the PMN-PT shows smooth surface with peak-to-valley roughness of 2nm and RMS roughness of 0.49nm. On the other hand, the Ni-Mn-Ga/MgO and Ni-Mn-Ga/STO films have roughness of 10nm and 17nm, respectively, and their RMS roughness is almost the same that is 2.89nm. The MFM image for Ni-Mn-Ga/MgO thin film show magnetic contrast which testifies very small magnetic signals. However, Ni-Mn-Ga/PMN-PT and Ni-Mn-Ga/STO thin films do not show observable magnetic contrast. Lack of clear observable magnetic contrast (or domains) in these films may be due the in-plane alignment of magnetic moments because of film thickness [72]. The two films showed ferromagnetic properties as it is also confirmed by VSM and SQUID measurement except Ni-Mn-Ga/STO film.

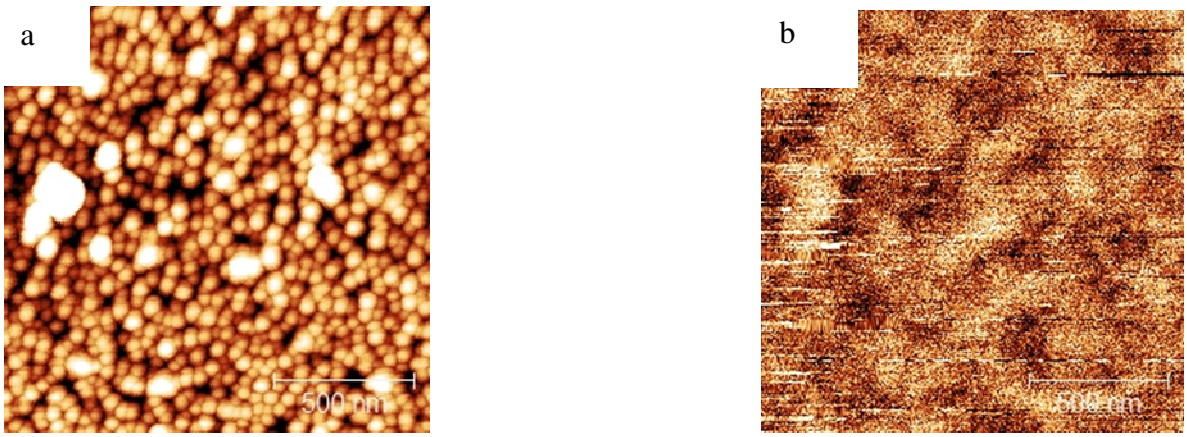

Figure 4. 9 a) AFM topographic image and b) MFM phase image of Ni-Mn-Ga/MgO film deposited at 320^0C substrate temperature

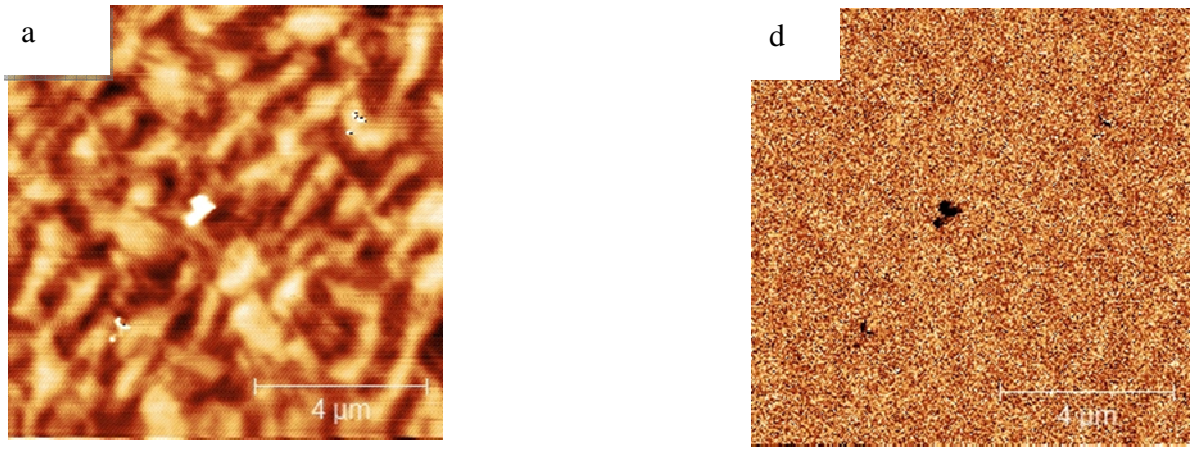

Figure 4. 10 a) AFM topographic image and b) MFM phase image of Ni-Mn-Ga/PMN-PT film deposited at 320^{0}C substrate temperature

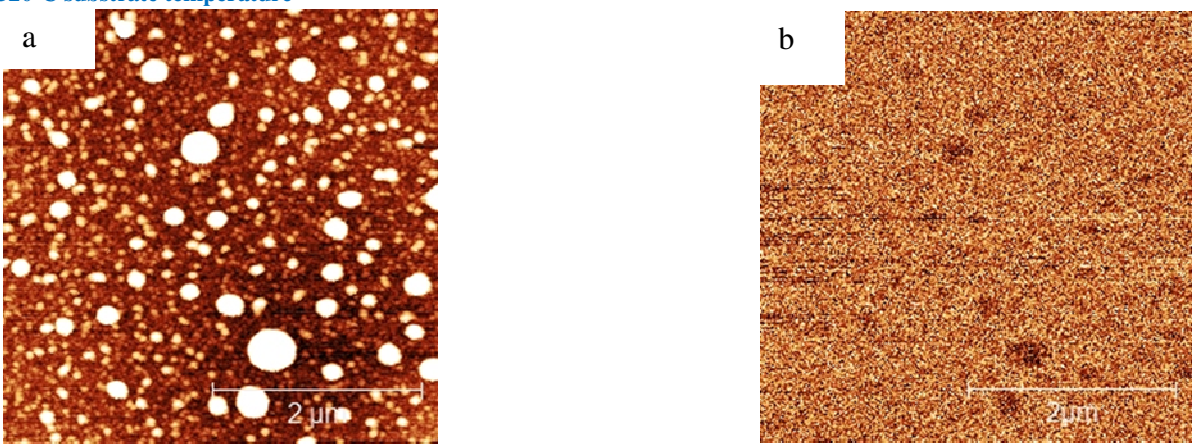

Figure 4. 11 a) AFM topographic image and b) MFM phase image of Ni-Mn-Ga/STO film deposited at 320^{0}C substrate temperature

4.2.2.2 The MFM Result for films deposited at substrate temperature of 370^{0}C

The AFM topographic and MFM images of Ni-Mn-Ga thin films deposited at substrate temperature of 370^{0}C on different substrates are depicted below in the Figure 4.12-4.16. The thickness of the films for this batch is calculated to be 70nm. For the films Ni-Mn-Ga/Al_2O_3, Ni-Mn-Ga/MgO, Ni-Mn-Ga/PMN-PT, Ni-Mn-Ga/STO the roughness is 6nm, 2nm, 7nm, 10nm, respectively and the RMS is 1nm, 0.33nm, 1.38nm, and 2.23nm, respectively. Among the films, Ni-Mn-Ga/MgO has the smoothest surface. From the MFM images for these films, there is no observed color contrast. However, from the SQIUD measurement these films have showed ferromagnetic,

Figure 4. 12 a) AFM topographic image and b) MFM phase image of Ni-Mn-Ga/Al_2O_3 film deposited at 370^{0}C substrate temperature

behavior. Thus, absence of color contrast may be again due to smallness of magnetic signal from the films to interact with the magnetic tip.

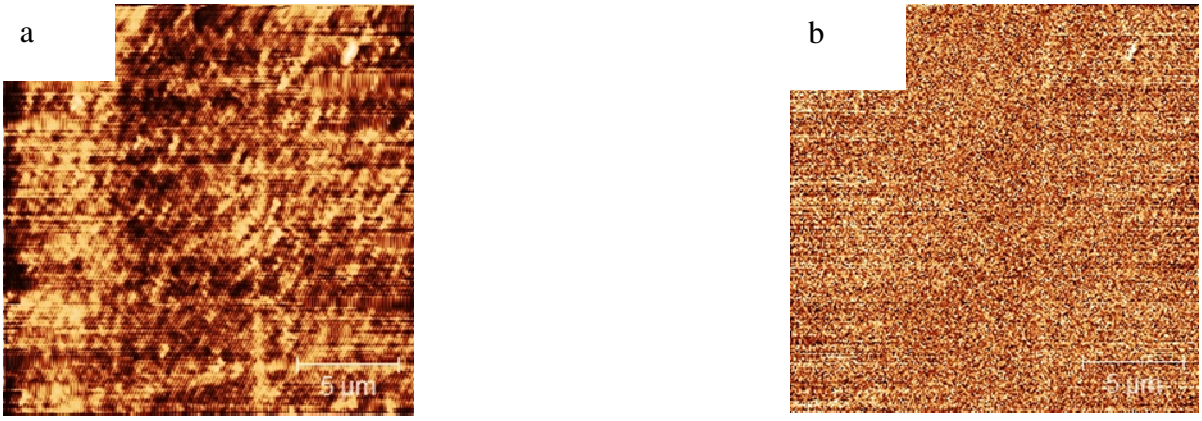

Figure 4. 13 a) AFM topographic image and b) MFM phase image of Ni-Mn-Ga/MgO film deposited at 370^{0}C substrate temperature

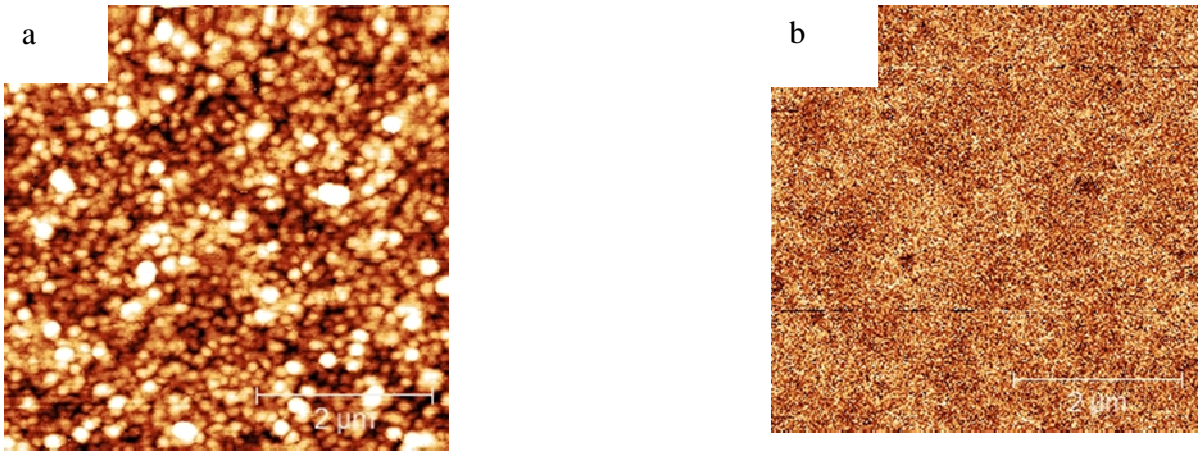

Figure 4. 14 a) AFM topographic image and b) MFM phase image of Ni-Mn-Ga/PMN-PT film deposited at 370^{0}C substrate temperature

Figure 4. 15 a) AFM topographic image and b) MFM phase image of Ni-Mn-Ga/STO film deposited at 370^{0}C substrate temperature

4.2.2.3 The MFM Result for films deposited at substrate temperature of 400^{0}C

Figure 4.16-4.18 show the AFM topography and MFM phase images of the films under zero applied magnetic field. As it can be seen from figures the AFM images show different

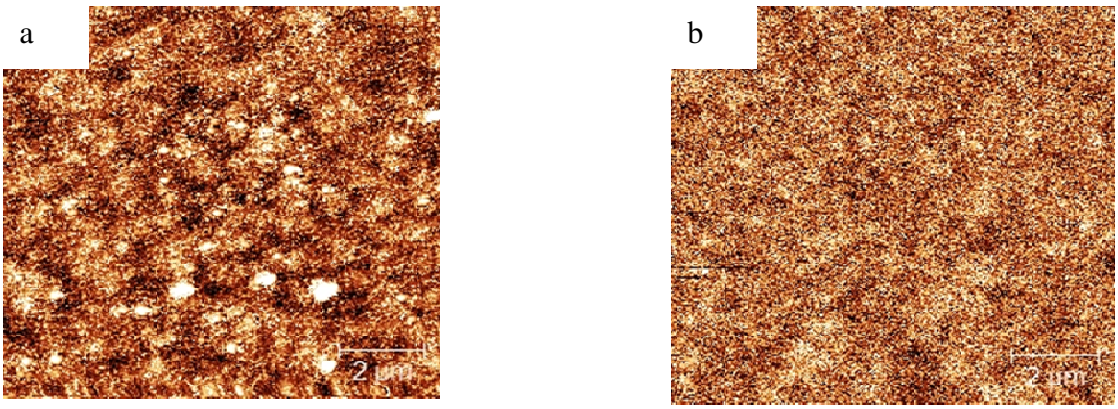

Figure 4. 16 a) AFM topographic image and b) MFM phase image of Ni-Mn-Ga/PMN-PT film deposited at 400^{0}C substrate temperature

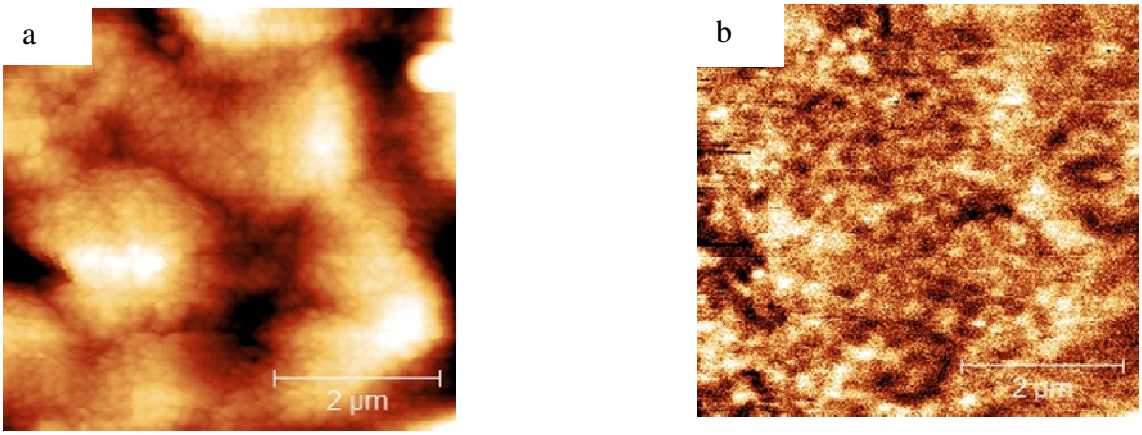

Figure 4. 17 a) AFM topographic image and b) MFM phase image of Ni-Mn-Ga/STO film deposited at 400^{0}C substrate temperature

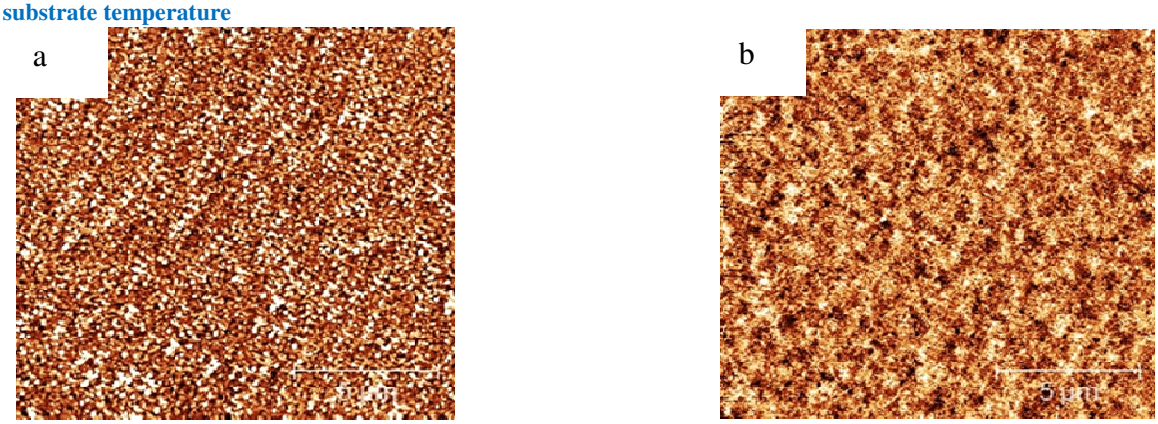

Figure 4. 18 a) AFM topographic image and b) MFM phase image of Ni-Mn-Ga/Al_2O_3 film deposited at 400^{0}C substrate temperature

microstructure for films with different substrates. The thickness of the films for this batch is calculated to be 210nm. In the case of Ni-Mn-Ga/PMN-PT and Ni-Mn-Ga/Al_2O_3 films, the RMS roughness and the maximum peak- to-valley range have almost similar values which are 2nm and 10nm, respectively. However, for the film Ni-Mn-Ga/STO, the RMS roughness and the maximum peak-to-valley are 4.5nm and 20nm, respectively. The film with STO substrate shows the higher roughness while the other films show almost the same and lower roughness. High roughness of film with STO substrate is due to the unpolished surface of the substrate STO used. Thus, small value of roughness of the substrate used in this work could contribute to more perfect microstructural state of the film which in turn affects the properties of the films. All MFM images reveal a magnetic contrast produced by magnetic domains forming a complex type of pattern. The magnetic domains represent regions of uniform magnetization. The bright and dark regions in the MFM images are associated with the magnetization being parallel and antiparallel to the

in- plane direction which, in general, can be along to in plane of the film or tilted position to it. Comparing the MFM images, one can say that there is a dependence of magnetic properties on microstructure of (roughness) the films or nature of substrate.

4.2.3 Piezoresponse Force Microscopy (PFM)

To observe magnetoelectric effect, the ferromagnetic thin film in the thin film multiferroic composite should be in ferromagnetic state and the piezoelectric substrate should be in piezoelectric state at room temperature. Thus, the state of the piezoelectric substrate should be checked after the deposition of the ferromagnetic film. The piezoresponse (or ferroelectric state) of the substrate was studied by piezoresponse force microscopy (PFM). The PFM mode was made with External Lock-in SR830, ac voltage of amplitude 10V and $f = 50kHz$. Tip was used as top electrode and silver paste under the PMN-PT substrate was used as lower electrode. Figure 4.19 below shows the topographic, the phase image and hysteresis loops of the PMN-PT substrate. The measurement was at room temperature done on the samples of Ni-Mn-Ga/PMN-PT which was deposited at substrate temperature of 400^0C.

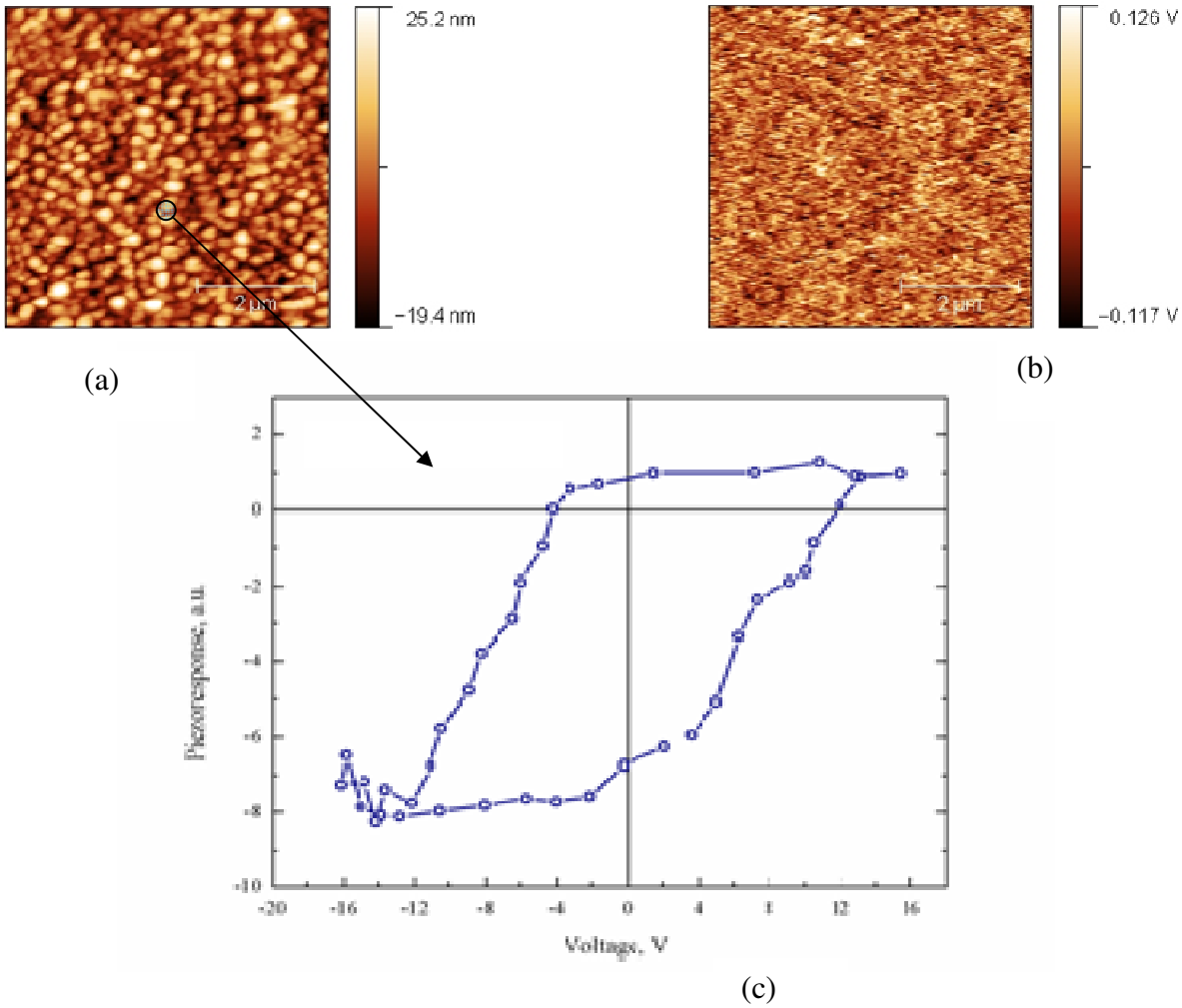

Figure 4. 19 a) topography, b) PFM amplitude, and c) hysteresis loop of PMN-PT substrate under Ni-Mn-Ga film deposited at substrate temperature of 400^{0}C

Because of the presence of Ni-Mn-Ga film on PMN-PT substrate, the PFM contrast seems unclear. However, the piezoresponse was distinguished and confirmed by the hysteresis loop as shown in the Figure 4.19 (c). Therefore, the piezoelectric property of the PMN-PT substrate at substrate deposition temperature of 400^{0}C was maintained.

4.3 Magnetoelectric Effect

The ferroelectric behaviors and ferromagnetic behaviors are basic requirements for a composite to exhibit ME voltage output. The characterization of substrate PMN-PT in the composite showed ferroelectric behaviors, and the characterization of the thin films of Ni-Mn-Ga alloy in the composite showed ferromagnetic behaviors. To see ME effect in the

composite of Ni-Mn-Ga/PMN-PT multiferroics, the experimental set up discussed in the experimental part was used. In the experiment for this composite, DC magnetic field was superimposed with AC magnetic field. An increasing DC bias magnetic field in the range between $50Oe \leq H \leq 10kOe$ was applied. The applied AC magnetic field had small amplitude of 10Oe and its frequency was chosen to be 100 kHz. This frequency was chosen to optimize the maximum output voltage. All measurements were done at room temperature. The multiferroic composite explored here was allowed to operate in the L-T ME coupling mode, i.e. longitudinal magnetized (field direction is along the surface direction) /voltage is measured in the transverse direction as it is mentioned in section 1.3.2.2.

Figure 4.20 shows the ME output voltage as a function of DC bias magnetic field for Ni-Mn-Ga/PMN-PT composite heterostructures deposited at substrate temperature of 370^0C and

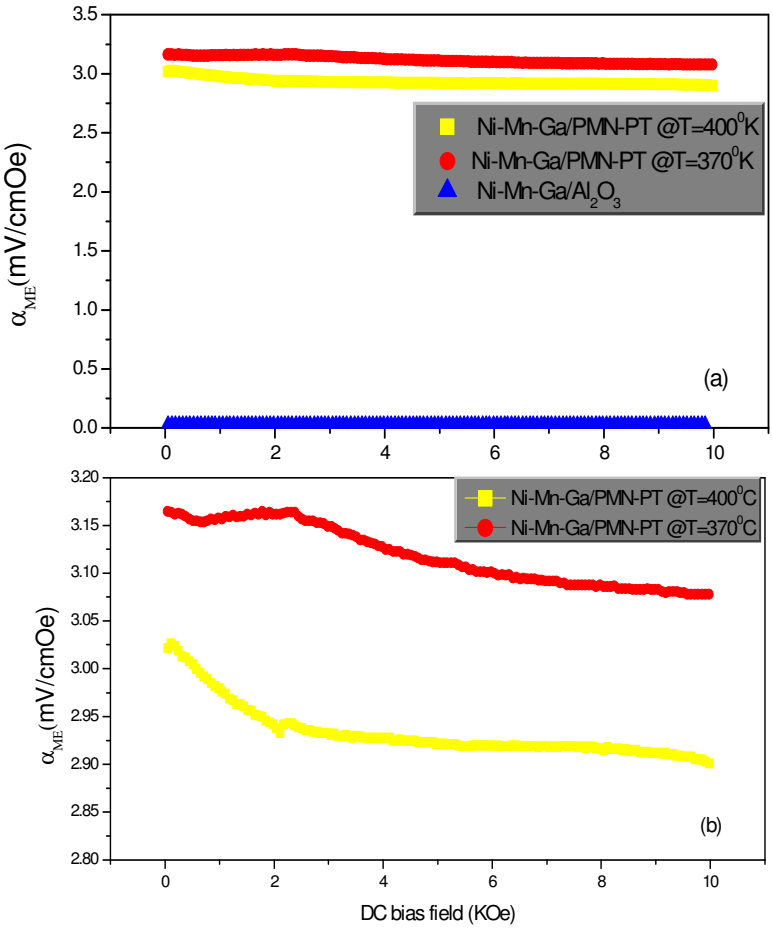

Figure 4. 20 Variation of output Voltage as function of DC bias field for Ni-Mn-Ga/PMN-PT composite multiferroic deposited at a temperature of 370^{0}C and 400^{0}C (a) including none active substrate Al_2O_3 and (b) with only active substrate.

400^{0}C. The ME output voltage for non active substrate (Al_2O_3) was measured and is used as a reference level as shown in the Figure 4.20 (a). As we expected the ME output voltage for the sample with active (piezoelectric) substrate is much higher as compared to the ME output voltage of the sample with non-active (non-piezoelectric) substrate ($\sim 3 \times 10^{-2}$ mV/cm Oe).

The thickness of the films deposited at substrate temperature of 370^{0}C and 400^{0}C are 70nm and 210nm, respectively. For the composite heterostructure deposited at 370^{0}C, the maximum ME voltage output is found to be 3.16mV/cmOe while for the composite heterostructure deposited at 400^{0}C the maximum ME voltage output is 3.02mV/cmOe.

The ME output shows a slight decrease with increase in DC magnetic field. Its value decreases up to 2.9mV/cmOe for the film deposited at the temperature of 400^0C and up to 3.08mV/cmOe for the film deposited at the temperature of 370^0C. The appearance of ME output voltage is due to the change in magnetization of the film which resulted in magnetostriction and development of electric polarization owing to piezoelectric effect, when stress applied by film over ferroelectric phase(PMN-PT). Beyond a certain magnetic field bias field, the magnetostriction gets saturated, and hence would produce a constant electric field in the piezoelectric phase. This leads to a decrease in the ME output at higher magnetic fields. As it is shown in the plot, the composite deposited at 370^0C is observed to have higher ME Voltage than the composite deposited at 400^0C. This difference may be due to large amount magnetic phase in film deposited at substrate temperature of 400^0C than the one deposited at 370^0C which may lead to result discharge process or leakage current.

Different groups use different measuring techniques to study the ME effect. Thus, it is difficult to compare results obtained by different research groups, even on similar materials. Even though, the comparison is not on the same materials, measuring technique, and processing technique, some results for different structures are shown in the table 4.2 below. As it can be seen from the table, the value of ME output voltage obtained in this work is less than by a factor of ten from some of the results but still it is better result than some other results. The most probable reason for this low value is the Ni-Mn-Ga films are partially crystalline. W. H. Wang et al. have reported that single crystal Ni-Mn-Ga sample has very large MFIS [73]. Two orders of magnitude larger than the traditional magnetostrictive materials have been reported. Since the samples produced here are partially crystalline, the MFIS is much smaller than single crystal samples. Thus, the value of ME output voltage is affected accordingly. However, significant ME coefficient enhancement may be achieved by improving the degree of crystallinity of Ni-Mn-Ga alloy, for example, using polycrystalline or single crystal sample. Moreover, the thickness ratio (thickness of the Ni-Mn-Ga thin to the thickness of PMN-PT) must be also taken into account to make the comparison since ME output voltage is dependent on this ratio. The effect of thickness ratio on ME output voltage needs further investigation. The magnetoelectric measurement was done at room temperature. But, it is known that the

crystal structure of Ni-Mn-Ga alloys depends on its temperature and then the MFIS and ME output voltage are affected accordingly. This implies that good ME coupling may be possible at other temperature values. Thus, higher ME output voltage may be obtained.

Table 4. 2 Summery of magnetoelectric coupling coefficient for some structures

Structure	Materials	Magnetoelectric Coefficient (Oe cm/kV or mV/cm Oe)	Temperature	Reference
Laminated Composite heterostructure	Thick film of $La_{0.7}Sr_{0.3}MnO_3$ on PZT	60 mV/cm Oe	RT	[74]
Composite heterostructure	Thin film of Fe_3O_4 on PMN-PT	67 Oe cm/kV	RT	[75]
Composite Heterostructure	Ni_2MnGa/PMN-PT	41 Oe cm/kV	RT	[57]
composite	$BaTiO_3$ and $CoFe_2O_4$	50 mV/cm Oe	RT	[76]
2-2 horizontal heterostructure	CFO and BTO matrix	66 mV/cm Oe	RT	[77]
Composite	$CoFe_2O_4$-$BaTiO_3$	0.1 to 2.23mV/cm Oe	RT	[78]
Composite heterostructure	Thin film of Ni-Mn-Ga on PMN-PT	3.2 mV/cm Oe	RT	Present

5 Conclusion and Outlook

Series of Ni-Mn-Ga thin films deposited on different substrates using three different deposition conditions have been fabricated using Magnetron sputtering deposition system. The main varying parameter of the deposition condition was the substrate deposition temperature which ranges from 320^0C to 400^0C. The substrates used to deposit the films were Al_2O_3, MgO, STO, and PMN-PT. Structural and magnetic properties of these films were studied. In addition, magnetoelectric effect for multiferroic composite structure of Ni-Mn-Ga/PMN-PT was studied.

The structural measurements on Ni-MN-Ga thin films using XRD diffraction have showed that as-deposited films are partially crystalline or they are composed of amorphous and crystalline phase. Moreover, the degree of crystallinity and the phases present vary with substrate deposition temperature. It is known that increasing substrate temperature promotes the growth of coarser (or larger grain) microstructure or single crystal. Thus, increasing the substrate temperature of the films from 320^0C to 400^0C have shown an increase of grain size or improved the degree of crystallinity. Moreover, the XRD measurements for some films have shown that the martensite and austenite phases coexist in the films. An increase of substrate temperature for these films promoted formation or evolution of martensite phase.

The magnetic measurements done using VSM, SQUID, and MFM have shown that the films deposited on different substrates under different deposition conditions are ferromagnetic at room temperature. On increasing the substrate temperature from 320^0C to 400^0C, the magnetization values from the magnetization versus magnetic field measurements have show an increment from the least value 10emu/cm^3 to the maximum value 250 emu/cm^3. Even though, the magnetization has shown an increase in value with substrate temperature, the increase differs from substrate to substrate. The magnetic properties of the films depend not only on the growth temperature but also on the nature of substrate. The magnetization versus temperature or (thermo-magnetic) measurements for the films deposited at the substrate temperature of 400^0C, which have showed best ferromagnetic properties among the produced sample under different conditions, reflect only magnetic transition. The value of Curie temperatures for batch of films is found to be

337K for Ni-Mg-Ga/PMN-PT, 345K for Ni-Mn-Ga/STO and 348K for Ni-Mn-Ga/Al_2O_3 which are all above room temperature. No signature of structural transition temperature was observed in the measured range of temperature. The values of Curie temperature extracted from M(T) curves for the films did not show significant differences.

The magnetoelectric measurement using lock-in technique was done on a heterostructure Ni-Mn-Ga/PMN-PT multiferroic composite. It was found that Ni-Mn-Ga alloy films deposited at substrate temperature of 370^0C and 400^0C have shown ferromagnetic behaviour and the PMN-PT has shown piezoelectric behaviour or response, which are the basic requirements to see magnetoelectric effect in the composite. By changing the applied DC magnetic field on Ni-Mn-Ga alloy thin film to change films magnetization, we measured an induced voltage across the surface of PMN-PT. The maximum induced ME voltages for films deposited at substrate temperature of 370^0C and 400^0C are 3.16mV/cmOe and 3.02mV/cmOe, respectively. This investigation demonstrates that Ni-Mn-Ga/PMN-PT multiferroic composite are found to exhibit magnetoelectric coupling or effect at room temperature.

Future out Look

1. The structural analysis from XRD data have shown that the Ni-Mn-Ga alloy thin films deposited using different deposition conditions on different substrates are partially crystalline. Moreover, the results have also shown that austenite and martensite phase on some substrate coexist. Thus, to crystallize the films fully, either post heat treatment (annealing) of films or higher growth temperatures should be used. In addition to crystallizing the film, post heat treatment can also help to understand the evolution of phases with annealing temperature. However, either the annealing temperature or the growth temperature should not be large enough to allow reaction of the substrate with the film.
2. The thermo-magnetic (magnetization versus temperature) measurements didn´t show noticeable signature on the structural transition. Thus, further study, for example electrical resistivity versus temperature measurements on the films, should be conducted to understand the structural transition.
3. In the view of exhibiting magnetoelectric coupling between ferromagnetic Ni-Mn-Ga alloy thin film and the piezoelectric PMN-PT substrate, further investigation to

improve the magnetoelectric coupling should be done. The improvement can be done in many ways:

- Fully crystallize the films as it mentioned in number one. The structural transition temperature is easily noticeable in crystalline state that in partially crystalline state. This helps to us check whether the films are in martensite state at room temperature or not. Moreover, crystalline films have large strain than partially crystalline films under external magnetic field because of twin boundary motion. Thus, higher magnetoelectric voltage output is expected.
- The magnetoelectric out voltage dependence on the thickness ratio between the magnetic and piezoelectric phase. Thus, investigation of effect of thickness ratio on the magnetoelectric output voltage should be done to find the thickness ratio that will give maximum voltage output.
- The magnetoelectric output voltage dependence on temperature should be also done.

6 Reference

1. K. F. Wang, J.-M. Liu, Z. F. Ren, Adv. in Phys. **58**, 321 (2009).
2. M. Fiebig, J. Phys. D **38**, R123 (2005).
3. C. W. Nan, M. I. Bichurin, S. X. Dong. Viehland, G. Srinivasan, J. appl. Phys. **103**, 031101(2008).
4. Yao Wang, Jiamaian Hu, Yuanhua Lin and Ce-Wen Nan, npg asia mater. **2**(2) 61-68(2010).
5. EerensteinW, Mathur N. D. and Scott J F, Nature **442**, 759(2006).
6. J. Van den Boomegaard, D.R. Terrell, R.A.J. Born, H. F. J.I. Giller, J. Mater. Sci. **9**,1705 (1974).
7. S.N. Babu, K. Srinivas, T. Bhimasankaram, Journal of Magnetism and Magnetic Materials, **321**, 3764-3770 (2009).
8. K. Srininas, G. Prasad, T. Bhimasankaram, S. V. Suryanarayana, C. Prakash, S. N. Chatatarfee, Proc. SPIE **3903**, 266 (1999).
9. S. Dong, J. Zhai, J.-F Li, D. Viehland, Appl. Phys. Lett. **83**, 2265 (2003).
10. F. Figueiras, E. Rauwa, S. Amaral, N. Vyshatko, A. L. Kholkin, V.V Shartsman, P. Borisov, and W. Kleemann, J. Vac. Sci. Technol. A, Vol. 28 (2010).
11. Sang-Wook Cheong, and Maxim Mostovy, Nature materials **6**, 2007
12. E. T. Jaynes, Ferroelectricity, Princeton University Press, 1953.
13. P. M. Vilarihno, Lecture Notes on Dielectric and Ferroelectric, http://e-learning.ua.pt
14. A. L. Kholkin, D. A. Kiselev, L. A. Kholkin and A. Safari, Smart Materials: Ferroelectric Ceramics for Transducer Applications, Taylor and Francis, pp 9-1, 2009.
15. A. J. Moulson, and J. M. Herbert, Electroceramics, Materials, Properties, and Applications, Chapman and Hall, London, 1990.
16. H. F. Kay and P. Vousden, Philos. Mag. **40**, 1019 (1949).
17. P. M. Vilarinho, Functional Materials: Properties, Processing and Applications, in Scanning Probe Microscopy: Characterization, Nanofabrication and Device Application of Functional Materials, NATO Science Series, II. Vol. **186**, Kluwer Academic Publishers, 2005.

18. M. H. Lente, A. L. Zanin, S. B. Assis, I. A. Santos, D. Garcia, and J. A. Eiras, Ferroelectrics, **296**:149-155(2003).
19. D. Gignoux and M. Schlenker, Magnetism Vol.1, Fundamentals, Springer, pp. 169(2005).
20. Charles P. Poole Jr. and Frank J. Owens, Introduction to Nanotechnology, John Wiley & Sons, pp. 165(2003).
21. Mel Schwartz, Encyclopedia of Smart Materials Vol. 1 and 2, John Wiley & Sons, pp. 601 (2002).
22. J. Enkovaara, A. Ayuela, A. T. Zayak, P. Entel, L. Nordstrom, M. Dude, J. Jalkanen, J. Impola, R. M. Nieminen, Materials Science and Engineering A **378** , 52-60, 2004.
23. Schuichi Miyazaki, Yong Qing Fu, and Wei Min Huang, Thin Film shape Memory alloys: Fundamentals and Device Applications, Cambridge University Press, 2009.
24. Ralph C. Smith, Smart materials Systems Model development, Society for Industrial and Applied Mathematics, pp. 21-27, 2005.
25. A. N. Vasilév, V. D. Buche´nikov, T. Takagi, V. V. Khovailo, E. I. Estrin, Cond-matl-sci 0311433v1, 2003.
26. K. Ullakko, J. K. Huang, C. Kantner, V. V. Kokorin, and R. C. O'Handley., Appl. Phys. Lett. **69**(13):1966-1968 (1996).
27. G. Jakob, T. Eichhorn, M. Kallmayer, and H. J. Elmers, Phys. Rev. B 76, 174407(2007).
28. R. Tickle, R. D. James, T. Shield, M. Wuttig, and V. V. Kokorin, IEEE Transactions on Magnetics **35**, 5(1999).
29. P. J. Webster. Heusler Alloys, Contemp. Phys., **10**:559-577, 1969.
30. A. D. Boshko, A. N. Vasilév, V. V. Khovailo, I. E. Dikshetein, V. V. Koledov, S. M. Seleteski, A. A. Tulaikova, A. A. Cherechukin, V. G. Shavrov and V. D. Bushel´nikov, J. Exp. and Theor. Phys., **88**:954-962, 1999.
31. N. Lanska, O. Soderberg, A Sozinov, Y. Ge, and K. Ullakko, J. Appl. Phys. 95(12):8074, 2004.
32. Dimitris C. Lagoudas, Shape Memory Alloy: Modeling and Engineering Applications, Springer, pp. 328(2008).

33. A. N. Vasiliev, R. Z. Levitin and V. V. Khovaylo, Smart Materials for Ranging Systems, Springer, pp. 223-243(2006).

34. L. W. Martin, S. P. Crane, Y. H. Chu, M. B. Holcomb, M. Gajek, M. Huijben, C. H. Yang, N. Balke and R. Ramesh, J. Phys.:Condens. Mater **20**, 434220 (2008).

35. T. Goto, T. Kimura, G. Lawes, A. P. Ramirez, and Y. Tokura, Phys. Rev. Lett. **92**, 257201 (2004).

36. W. Prellier, M. P. Singh, and P. Murugavel, J. Phys.: Condens. Matter **17**, R803 (2005).

37. N. A. Hill, J. Phys. Chem. B **104**, 6694 (2000).

38. G. Srinivasan, E. T. Rasmussen, J. Gallegos, R. Srinivasan, Y. I. Bokhan, and V. M. Laletin, Phys. Rev. B **64**, 214408 (2001).

39. K. K. Patankar, R. P. Nipankar, V. L. Mathe, R. P. Mahajan, and S. A. Patil, Ceram. Int. **27**, 853 (2001).

40. V. L. Mathe, K. K. Patankar, U. V. Jadhav, A. N. Patil, S. D. Lotake, and S. A. Patil, Ceram. Int. **27**, 531 (2000).

41. R. E. Newnham, D. P. Skinner, and L. E. Cross, Mater. Res. Bull. **13**, 525(1978).

42. Li Yan, Zengping Xing, Zhiguang Wang, Tao Wang, Guangyin Lei, Jiefang Li, and D. Viehland, Appl. Phys. Lett. **94**, 192902(2009).

43. Imada S, Shouriki S, Tokumitsu E and Ishiwara H, Japan. J. Appl. Phys. **37** 6497(1998).

44. Imada S, Kuraoka T, Tokumitsu E and Ishiwara H, Japan. J. Appl. Phys. **40** 666(2001)**.**

45. Sharan A, An I, Chen C, Collins R W, Lettieri J, Jia Y, Schlom D G and Gopalan V Appl. Phys. Lett. **83** 5169(2003).

46. Sharan A, Lettieri J, Jia Y, Tian W, Pan X, Schlom D G and Gopalan V Phys. Rev. B **69** 214109(2004).

47. Palkar V R, John J and Pinto R Appl. Phys. Lett. **80** 1628(2002).

48. K. Dorr, C. Thiele, J.,-W. Kim, O. Bilani, K. Nenkov, and L. Schultz, Pholosophical Magazine Letters, Vol. **87**, 269-278 (2007).

49. R. K. Zheng, J. Wang, X. Y. Zhou, Y. Wang, H. L. W. Chan, and C. L. Choy, and H. S. Luo, J. Appl. Phys. **99**, 123714(2006).

50. A. Hanumaiah, T. Bhimasakaran, S. V. Suryanaryana, and G. S. Kumar, Bull Mater. Sci. **17**, 405(1994).
51. J. Van Den Boomgaard, A. M. J. G. Van Run, and J. Van Suchtelen, Ferroelctrics **14**, 727 (1976).
52. W. E. Kramer, R. H. Hopkins, and M. R. Daniel, J. Mater. Sci. Lett. **12**, 409(1977).
53. M. Avellaneda and G. Harshe, J. Intell. Mater. Syst. Struct. **5**, 501 (1994).
54. D. N. Astrov, Sov. Phys. JETP **11**, 708–709 (1960).
55. C. Thiele, K. Dorr, O. Bilani, J. Rodel, L. Schultz, Phys. Rev. B **75**, 054408(2007).
56. K. Zhao, K. Chen, Y. R. Dai, J. G. Wan, and J. S. Zhu, Appl. Phys. Lett. **87**, 162901(2005).
57. Yajile Chen, Jingmin Wang, Ming Liu, Jing Lou, Nian X. Sun, Carmine Vittoria, and Vicent G. Harris, Appl. Phys. Lett. **93**, 112502(2008).
58. M. Ohring,Material Science of Thin Films, Academic Press, Inc., San Diego, CA, 1991.
59. Ricardo Ferreira, Ion Beam Deposited Magnetic spin tunnel Junctions targeted HDD Read Heads, Non Volatile Memories and magnetic field sensor application, PhD Thesis, Instituto Superior Tecnico, Lisbon, Portugal, April 2008.
60. B. D. Cullity, Elements of x-ray Diffraction, Addison- Wesley, Inc., 1956.
61. JPK Instruments, The NanoWizard AFN handbook Version 1.3, 2005
62. Dimension^{TM} 3100 Scanning Probe Microscope, Manual by Veeco.
63. Asylum research, Atomic Force Microscopy, PFM App. Note 10.
64. R. Gross and A. Marx, Applied Superconductivity, 2006.
65. G. V. Duong, R. Groessinger, M. Schoenhart, D. Bueno-Basques, Journal of Magnetism and Magnetic Materials **316,** 390(2007).
66. PDF File No. 04-008-1269.
67. V. Chernenko, M. Kohl, S. Doyle, P. Mullner, and M. Ohtsuk, Scr. Mater. **54**, 1287(2006).
68. PDF File No. 04-008-1270.
69. M. Thomas, O. Heczcko, J. Buschbeck, U. K Robler, J. McCord, N. Scheerbaum, L. Scultz, and S. Fahler, New Journal of Physics **10**, 023040(2008).
70. PDF File No. 01-076-2630.

71. V. A. Chernenko, V. A. L´vov, V. V. Khovailo, T. Takagi, T. Kanomata, T. Suzuki, and R. Kainuma, J. Phys.: Condens. Matter **16**, 8345(2004).
72. V. A. Chernenko, R. Lopez Anton, M. Kohl, J.M. Barandiaran, M. Ohtsuka, I. Orue, S. Besseghini, Acta Materialia **54,** 5461–5467(2006).
73. W. H. Wang, G. H. Wu, J. L. Chen, C. H. Yu, S. X. Gao, W. S. Zhan, Z. Wang, Z. Y. Gao, Y. F. Zheng, and L. C. Zhao, Appl. Phys. Lett. **77**, 3245(200).
74. Srinivasan G, Rasmussen E T, Levin B J and Hayes R Phys. Rev. B **65** 134402(2002).
75. Ming Liu, Ogheneyunume Obi, Zhuhua Cai, Jing Lou, Guomin Yang, Katherine S. Ziemer, and Nian X. Sun, J. Appl. Phys. **107,** 073916(2010).
76. Van Run, A. M. J. G., Terrell, D. R. & Scholing, J. Mater. Sci. **9**, 1710–-1714 (1974).
77. Y. Zhang, C. Deng, J. Ma, Y. Lin, C. W. Nan, Appl. Phys. Lett. **92**, 062911 (2008).
78. G. V. Duong, R. Groessinger, Journal of Magnetism and Magnetic Materials **316** (2007) e624–e627.